BLENDS OF ACETIC ACID-MODIFIED EPOXIDIZED NATURAL RUBBER WITH POLY(ETHYLENE OXIDE)

NG JIN GUAN

FACULTY OF SCIENCE
UNIVERSITY OF MALAYA
KUALA LUMPUR

2013

BLENDS OF ACETIC ACID-MODIFIED EPOXIDIZED NATURAL RUBBER WITH POLY(ETHYLENE OXIDE)

NG JIN GUAN

DISSERTATION SUBMITTED IN FULFILLMENT OF THE REQUIREMENTS FOR THE DEGREE OF MASTER OF SCIENCE

DEPARTMENT OF CHEMISTRY
FACULTY OF SCIENCE
UNIVERSITY OF MALAYA
KUALA LUMPUR

2013

ABSTRACT

BLENDS OF ACETIC ACID-MODIFIED EPOXIDIZED NATURAL RUBBER WITH POLY(ETHYLENE OXIDE)

This dissertation describes a study of using acetic acid to modify epoxidized natural rubber with 50% epoxidation level (ENR50) to form acetic acid-modified ENR50 which was blended with poly(ethylene oxide) (PEO). The study is divided into two sections: (i) Synthesis of modified ENR50 and (ii) Compatibility study on polymer blends comprising of acetic acid-modified ENR50 and PEO. In the first section, ENR50 was dissolved in toluene and reacted with acetic acid. Acetic acid-modified ENR50 formed was precipitated in methanol. Fourier-transform infrared (FTIR) spectroscopy and nuclear magnetic resonance (NMR) spectroscopy were used to investigate the chemical structure while thermal gravimetric analysis (TGA) and differential scanning calorimetry (DSC) were used to study the thermal properties. Presence of ester and hydroxyl functional groups in acetic acid-modified ENR50 was confirmed. Acetic acid-modified ENR50 possess a higher glass transition temperature (T_g) at 10 ^oC as compared to ENR50 with T_g at -29 ^oC. Reaction of 1 mol% of epoxy group leads to an increase in T_g by 0.8 ^oC. Polymer blends comprising of acetic acid-modified ENR50 and PEO were prepared by solution casting method. Incompatibility of acetic acid-modified ENR50 and PEO is revealed using FTIR analysis. No significant shifting of the major bands observed and there are no obvious changes on the shape of the major bands in FTIR spectra. T_g analysis by DSC shows that acetic acid-modified ENR50/PEO blends are immiscible. Radial growth rate (G) of PEO in acetic acid-modified ENR50/PEO blends decrease with ascending acetic acid-modified ENR50 content and lower G values were observed for acetic acid-modified ENR50/PEO blends compared to

ENR50/PEO blends. The fine fibrillar texture of PEO becomes slightly irregular and coarse in acetic acid-modified ENR50/PEO blends. ENR50/PEO blends doped with 12 wt % lithium perchlorate ($LiClO_4$) exhibit ionic conductivities in the range of 10^{-7} to 10^{-5} S cm^{-1} at 30 ℃. Acetic acid-modified ENR50/PEO blends with same amount of lithium salt show improved conductivity measurements in the range of 10^{-6} to 10^{-4} S cm^{-1} at 30 ^{o}C.

ABSTRAK

ADUNAN GETAH ASLI TEREPOKSIDA YANG TELAH DIUBAHSUAIKAN DENGAN ASID ASETIK DENGAN POLI(ETILENA OKSIDA)

Disertasi ini menerangkan kajian penggunaan asid asetik untuk mengubah suai getah asli terepoksida yang mempunyai 50% tahap epoksida (ENR50) kepada getah asli terepoksida yang telah diubahsuaikan dengan asid asetik yang akan diadunkan dengan poli(etilena oksida) (PEO). Kajian ini dibahagikan kepada dua bahagian: (i) Sintesis ENR50 yang diubahsuai dan (ii) Penyelidikan keserasian bagi adunan polimer yang terdiri daripada ENR50 yang telah diubahsuaikan dengan asid asetik dan PEO. Bagi seksyen pertama, ENR50 dilarutkan dalam toluena dan bertindak balas dengan asid asetik. Hasil ENR50 yang telah diubahsuaikan dengan asid asetik dimendakkan dalam larutan metanol. Spektroskopi jelmaan Fourier infra merah (FTIR) dan spektroskopi resonans magnet nuklear (NMR) digunakan untuk menyiasat struktur kimia manakala analisis termal gravimetri (TGA) dan kalorimeter pengimbasan pembezaan (DSC) digunakan untuk mengkaji sifat-sifat haba. Kehadiran kumpulan berfungsi ester dan hidroksil dalam ENR50 yang telah diubahsuaikan dengan asid asetik telah dikenalpasti. ENR50 yang telah diubahsuaikan dengan asid asetik mempunyai suhu peralihan kaca (T_g) yang lebih tinggi iaitu 10 ^oC berbanding ENR50 dengan T_g sebanyak -29 ^oC. Setiap mol% kumpulan epoksida yang bertindak balas mendorong kenaikan suhu T_g sebanyak 0.8 ^oC. Adunan polimer yang terdiri daripada ENR50 yang telah diubahsuaikan dengan asid asetik dan PEO disediakan dengan kaedah pelarutan. Ketidakserasian antara ENR50 yang telah diubahsuaikan dengan asid asetik dengan PEO didedahkan oleh analisis FTIR. Tiada anjakan signifikan pada jalur-jalur utama yang diperhatikan dan tiada perubahan ketara pada bentuk jalur-jalur utama dalam spektrum FTIR. Analisis T_g

oleh DSC menunjukkan ketidakgaulan adunan ENR50 yang telah diubahsuaikan dengan asid asetik/PEO. Kadar pertumbuhan jejari sferulit (*G*) PEO untuk adunan polimer berkurangan dengan kandungan ENR50 yang telah diubahsuaikan dengan asid asetik yang meningkat dan nilai-nilai *G* yang lebih rendah telah diperhatikan bagi adunan ENR50 yang telah diubahsuaikan dengan asid asetik/PEO jika dibandingkan dengan adunan ENR50/PEO. Tekstur halus berserabut bagi PEO menjadi tidak teratur dan kasar bagi adunan ENR50 yang telah diubahsuaikan dengan asid asetik/PEO. Adunan ENR50/PEO yang didopkan dengan 12% jisim litium perklorat ($LiClO_4$) menunjukkan kekonduksian elektrik dalam julat 10^{-7} hingga 10^{-5} S cm^{-1} pada suhu 30 ^{o}C. Adunan ENR50 yang telah diubahsuaikan dengan asid asetik/PEO yang digabungkan dengan jumlah litium garam yang sama menunjukkan kekonduksian elektrik yang lebih memuaskan dalam julat 10^{-6} hingga 10^{-4} S cm^{-1} pada suhu 30 ^{o}C.

ACKNOWLEDGEMENTS

First and foremost, I would like to express my gratitude to both of my supervisors, Professor Dr. Gan Seng Neon from University of Malaya, Kuala Lumpur and Dr. Chan Chin Han from Universiti Teknologi MARA, Shah Alam for their guidance and advice throughout my research study. I am very grateful for given a chance to participate in this collaboration.

Secondly, I would like to thank Professor Hans-Werner Kammer from University of Halle, Germany for his stimulating ideas and suggestions during my work. I would like to express my appreciation to University of Malaya for supporting my candidature under University of Malaya Fellowship Scheme.

Last but not least, I would like to thank all of the laboratory technicians from both of the universities for their kind assistance and advice in the equipments' techniques during my bench work. Not to forget, to all my friends and family for their generous in sharing their knowledge, understanding and encouragement during my candidature.

TABLE OF CONTENTS

LIST OF FIGURES

LIST OF TABLES

LIST OF EQUATIONS

LIST OF SYMBOLS AND ABBREVIATIONS

A	Absorbance
$\lvert \bar{b} - b \rvert$	Errors for b
c	Correlation coefficient
$CDCl_3$	Deuterated chloroform
d	Diameter for growing PEO spherulite
$\bar{d}$	Mean of diameter for growing PEO spherulite
DA	Dodecanedioic acid
DSC	Differential Scanning Calorimetry
EC	Ethylene carbonate
ENR	Epoxidized natural rubber
ENR10	Epoxidized natural rubber with 10 mol% epoxidation level
ENR25	Epoxidized natural rubber with 25 mol% epoxidation level
ENR50	Epoxidized natural rubber with 50 mol% epoxidation level
FESEM	Field Emission Scanning Electron Microscopy
FTIR	Fourier-Transform Infrared
G	Radial growth rate
GPC	Gel Permeation Chromatography
KBr	Potassium bromide
L	Thickness of polymer electrolyte film
$LiCF_3SO_3$	Lithium triflate
$LiClO_4$	Lithium perchlorate
M_n	Number average molecular mass
M_w	Weight average molecular mass

M_η	Viscosity average molecular mass
n	Number of micrograph captured
n_{ep} (0)	Initial number of moles of epoxy
n_{ep} (t)	Number of moles of epoxy at time t
NMR	Nuclear Magnetic Resonance
NR	Natural rubber
$Pb(OAc)_4$	Lead tetraacetate
PC	Propylene carbonate
PCL	Poly(ε-caprolactone)
PCM	Phase Contrast Microscopy
PEO	Poly(ethylene oxide)
PET	Poly(ethylene terephthalate)
PHB	Poly(3-hydroxybutyrate)
PHBV	Poly(3-hydroxybutyrate-*co*-3-hydroxyvalerate)
PMMA	Poly(methyl methacrylate)
PnBMA	Poly(n-butyl methacrylate)
POM	Polarizing Optical Microscope
PVC	Poly(vinyl chloride)
PVPh	Poly(vinyl phenol)
Q	Matching ratio
r	Mass ratio
R	Radius of growing spherulite
R_b	Bulk electrolyte resistance
rpm	rotations per minute
s	Standard deviation

S_a	Surface area
SEM	Scanning Electron Microscope
s_x	Standard deviation for *x* value
s_y	Standard deviation for *y* value
t	Reaction time
$t_{0.95\ ,\ n-2}$	Measure of student's t-test distribution that the experimental values are situated in a confidence interval of 95%
$T°_m$	Equilibrium melting temperature
T_c	Crystallization temperature
$T_{d,\ 5\%\ wt\ loss}$	Decomposition temperature for 5% weight loss
$T_{d,\ inflection}$	Maximum rate of decomposition temperature
$T_{d,\ onset}$	Onset temperature
T_g	Glass transition temperature
TGA	Thermal Gravimetric Analysis
THF	Tetrahydrofuran
T_m	Melting temperature
TMS	Tetramethylsilane
w/v	weight/volume
w/w	weight/weight
wt %	weight percent
W_{PEO}	Weight fraction of PEO
X_{PEO}	Degree of crystallinity for PEO
XRD	X-ray Diffraction
α	Degree of conversion
σ	Ionic conductivity
δC_p	Delta heat capacity

ΔH_c	Crystallization enthalpy
ΔH_m	Melting enthalpy
$\Delta H_{m\,ref}$	Melting enthalpy of 100% crystalline PEO

CHAPTER 1

INTRODUCTION AND LITERATURE REVIEW

The introduction of polymers into the market has made great contributions to enhance the standard of living and lifestyle. Polymers are widely used for exterior automotive applications, electric and electronic applications, medical applications, building and constructions applications.

1.1 Epoxidized natural rubber (ENR)

There has been a growing interest of developing more environmental friendly polymeric materials from natural and renewable resources. Natural rubber (NR) as an ecological friendly crop contributes primarily to soil conservation, soil fertility, biomass generation, nutrient cycling and as an alternate source to traditional timber (Prabhakaran, 2010). Latex is obtained from the *Hevea brasiliensis* trees which are the only important commercial source of NR. NR latex is one of the major commodities in Malaysia. Most importantly, Malaysia is also one of the leading countries in producing NR besides countries like Thailand and Indonesia.

Epoxidized natural rubber (ENR) is very useful and commercially important semi-synthetic rubber. This modification transfers slightly polar NR to highly polar rubber. Thus, the polarity changes along with the properties of ENR. ENR possess soft elastomeric properties at room temperature and moderate ionic conductivity which is served as a desirable material for polymer electrolyte. Baker *et al.*, (1986) have reported that ENR exhibits strain-induced crystallization as seen in NR and oil resistance similar to medium acrylonitrile rubber, with high damping and good wet grip characteristics and low rolling resistance.

1.1.1 Epoxidation of ENR

There are several methods to synthesis ENR from NR latex. One of the methods is through *in situ* epoxidation by using peroxycarboxylic acids. ENR is prepared by partial epoxidation of natural rubber latex with performic acid formed *in situ* by the reaction of formic acid and hydrogen peroxide where a portion of the carbon-carbon double bonds have been converted to epoxide groups (Gelling & Smith, 1979; Okwu *et al.*, 2001; Tanrattanakul *et al.*, 2003). This is a commonly used method for commercial ENR.

$$HCOOH + H_2O_2 \leftrightarrow HCOOOH + H_2O$$

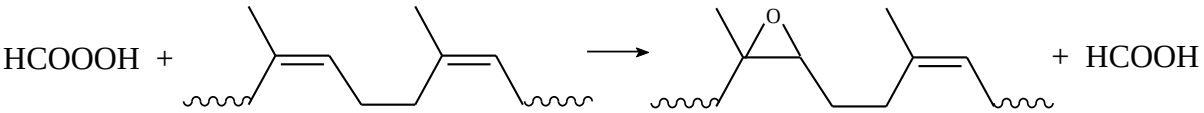

The epoxidation reaction is a random process and therefore epoxide units are randomly distributed along the polymer backbone. This observation is proven by ^{13}C nuclear magnetic resonance (NMR) spectroscopy and ^{1}H NMR studies (Davey & Loadman, 1984).

Any level of epoxidation may be achieved but commercially used ENR is only up to 50 mol%. The effect of epoxidation is to increase the polarity of the polymer, and enhance its glass transition temperature (T_g) as well as resistance to swelling in non-polar organic liquids. As the level of epoxidation is increased, T_g is raised by approximately 1 ℃ per mol percent epoxidation for ENR studied by Baker *et al.*, 1985.

1.1.2 Applications of ENR

1.1.2.1 Tires

ENR is used to prepare radial tire tread and it shows improved wet traction compared to the tread synthesized by unmodified natural rubber. ENR is also suitable for applications such as tire inner liner because of its reduction in gas permeability properties after epoxidation process (Sommer, 2009).

1.1.2.2 Mechanical goods

ENR is used in synthesis of a large variety of products such as rubber linings, seals, gasket, conveyor belts, hose and rubberized fabrics (Sommer, 2009). The choice of elastomer is made on the compromise between price and performance. Thus, ENR is used only in some products due to its certain properties that cannot be replaced by any other type of rubbers.

1.1.2.3 Engineering products

ENR is a unique engineering material because of its high elastic deformability and almost theoretical value for Poisson's ratio of 0.5 (Subramaniam, 1987). Good strength, high fatigue resistance and durability are the advantages of ENR which are favored in dynamic applications such as springs, anti-vibration mountings and bushings.

1.2 Poly(ethylene oxide) (PEO)

Poly(ethylene oxide) (PEO) is a clear, colourless and odourless substance. It is soluble in water and stable to heat. Besides that, PEO is inert to many chemical agents, non-toxic and environmental friendly. PEO is considered to be bio-compatible which enable it to coexist with living tissues or organisms without causing harm.

1.2.1 PEO synthesis

PEO can be synthesized by ring-opening polymerization of the three-membered ring, ethylene oxide, with anionic (e.g., with alcoholates or organometallic compounds), cationic (e.g., with Lewis acid) propagating species by Stevens, (1990) and Hoogenboom, (2009). Anionic mechanism is preferred for the preparation of well-defined PEO structures as it proceeds without side reactions if stringent purification methods are applied for the reagents used.

In contrast, the cationic ring-opening polymerization of ethylene oxide is performed via a cationic activated monomer approach instead of a chain-end activation approach. This is used to reduce the back-biting process that result in the formation of cyclic oligomers. Due to the relatively high nucleophilicity of the oxygen atoms in the polymer chain that could react with the cationic chain end, rather than with the free monomer in solution causes the occurrence of significant back-biting reactions. Usage of an activated monomer approach can significantly reduce the occurrence of back-biting by reducing the amount of cationic chain-ends.

Anionic polymerization method is preferred for the preparation of well-defined polymers whereas cationic polymerization is not often used nowadays. The different ring-opening polymerization mechanisms for the polymerization of ethylene oxide are depicted in Figure 1.1.

Anionic polymerization

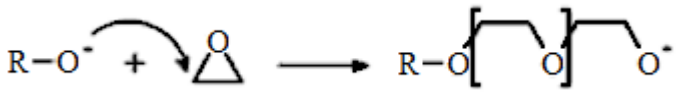

Cationic chain-end polymerization

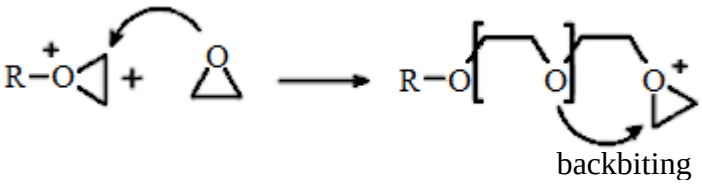

Cationic-activated monomer polymerization

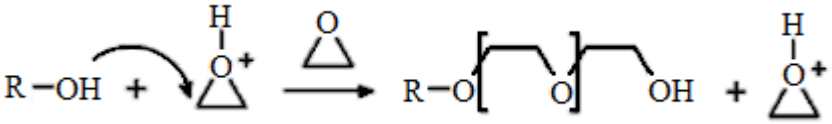

Figure 1.1: Anionic, cationic chain-end and cationic activated-monomer ring-opening polymerization mechanisms for ethylene oxide.

1.2.2 PEO applications

PEO is commonly used in personal, home and health care applications, due to its water solubility in combination with a very low toxicity. These attractive properties of PEO can be ascribed to the distance between the alternating oxygen atoms in the chains that is in agreement with the hydrogen distances in liquid water allowing formation of an extensive hydrogen-bonding network with water (Hoogenboom, 2009). Some applications of PEO are listed in Table 1.1.

Table 1.1: Applications of PEO.

Use	Application
Adhesive	Papers, denture fixative
Flocculation	Water cleaning
Thickener	Paints, oil field applications, cosmetics
Binder	Ceramic applications
Dispersant	Additive for polymerization processes
Lubricant	Soaps, personal care

Source: Fink, J. K. (2011). *Handbook of Engineering and Specialty Thermoplastics, Water Soluble Polymers*. Salem, Massachusetts: Scrivener.

PEO is used as binders for pigments, fillers and ceramics with application in battery electrodes, cathode ray tubes and fluorescent lamps. Strong hydrogen bonding affinity of PEO accounts for its association with various polar compounds such as phenolic resins, mineral acids, halogens, ureas and polycarboxylic acids. These complexes have unique properties with their application in batteries, microencapsulated inks, slow-release bacteriostatic agents or water-soluble adhesives (Blanton *et al.*, 2003). High molecular weight PEO is utilized in paper making applications (Mazzarella *et al*., 1977).

PEO may forms water retention gels and these gels can be used as absorbent pads and diapers. PEO is also used as emollient in cosmetic and hair products (Hossel *et al.*, 2001). Besides that, PEO can also be formed into flexible films by casting techniques or thermoplastic processing. High strength materials can be produced by arranging sheets and films of PEO in order. PEO films are inherently flexible, tough and resistant to most oils and greases. PEO can be used to provide heat sealability and hot melt adhesion in packaging industry (Blanton *et al.*, 2003).

1.2.2.1 Ink jet printing media

Water-soluble PEO is used as a binder component for coatings of ink jet printing media. Usage of poly(vinyl alcohol-ethylene oxide) copolymer in the ink receiving layer provides a number of functional benefits including control of ink-coalescence, improved humid-fastness and gives superior image quality and long-term stability. This copolymer shows better compatibility with the ink receiving layer and the colorants in the ink (Niu *et al.*, 2006).

1.2.2.2 Laundry detergents

Surfactants and builders are the essential ingredients for washing process but detergent generally comprise further constituents which include foam regulators, graying inhibitors, bleaching agents and soil-releasing properties substances. This soil-releasing properties substances support the soil-release capability of the formulation. Due to the chemical similarity to polyester fibers which particularly effective soil-release agents for fabrics made of such materials are copolyesters containing alkylene glycol and poly(alkylene glycol) units. Active polyester soil-release polymers include copolyesters of dicarboxylic acids such as adipic acid or terephthalic acid and with diols such as ethylene glycol or PEO (Moyse *et al.*, 1969).

1.2.2.3 Superabsorbents

PEO is used as a crosslinking agent for polysaccharides and used as superabsorbents (Fink, 2011). Superabsorbent polysaccharides show water absorption range of 700 – 5300 g g^{-1} for deionized water and for saline solutions are up to 140 g g^{-1}.

1.2.2.4 Pharmaceutical compositions

PEO is used as a component of medicaments in tablet form designed to be administered by oral route. Surface coating is employed to improve the appearance of tablet, thus making the drug more readily acceptable to the patient. Conventional coating is used because it is safe to be consumed and surface coating can be achieved by using a quick dissolving film.

1.3 Polymer blending

Polymer blending is one of the fastest growing branches of polymer technology. This is because blending of two polymers together makes possible tailoring of properties not obtained with a single polymer (Kammer *et al.*, 1993). Blending of different polymers for desired purposes serves as an alternative solution to reduce cost and time consuming problems to synthesized new monomers (Cowie, 1973; Kienzle, 1988; Haldar *et al*., 1997). These polymer blends system can be develop rapidly and able to respond efficiently to the requirements of new market.

The main purpose to study polymer blend is to understand the nature and strength of the chemical and physical interactions that promote or impede miscibility and compatibility. Better understanding of the miscibility of a blend may enhance the development of useful blends (Boon & Aczue, 1968). Precise control of mechanical properties of the blends can be easily achieved by compositional changes.

1.3.1 Amorphous and semicrystalline polymers

Amorphous polymer usually possesses bulky side groups or short-chain branches which attached to its macromolecular backbone. Amorphous polymers are difficult to crystallize due to its polymeric chains cannot be made to line regularly with ease. Amorphous polymer does not possess sharp melting temperature (T_m) and fully

amorphous polymer does not possess T_m (Lee *et al*., 2005). Amorphous polymers are normally softer, less rigid, transparent and penetrated more by solvents. One of the advantageous of amorphous polymer is the amorphous region ascribes toughness and flexibility to the macromolecular chain which allow the polymer to bend without breaking. The most used amorphous polymer in blends such as ENR, polycarbonate, polysulfone and polyarylate are generally good in dimensional stability, war page resistance and impact strength (Silvestre *et al*., 1991).

Semicrystalline polymer has both crystalline and amorphous composition. Semicrystalline polymer possesses the properties which are intermediate between those of elastomers and glassy polymers. Highly crystalline polymer is rigid, possess high melting point and less affected by solvent penetration. Crystallinity makes a polymer strong but lowers its impact resistance. For a semicrystalline polymer the toughness and ability to bend without breaking depends very much on its degree of crystallinity. Examples of semicrystalline polymer are PEO and poly(ε-caprolactone) (PCL) (Billmeyer, 1971).

The mechanical properties of polymer blends depend mainly on the crystallinity of the semicrystalline polymer. It is a common practice to blend an amorphous polymer with a semicrystalline polymer. Combination of crystalline and amorphous polymer may show good dimensional stability, ease of processing, chemical resistance, significant flexural tensile strength, good in heat distortion and mechanical properties for specific application (Silvestre *et al*., 1991). These combination properties usually cannot be achieved by single polymer.

1.3.2 Applications of polymer blends

Polymer blends are used as electrochemical devices such as sensors, electrochromic windows, display devices, supercapacitors and batteries (Glasse *et al*.,

2002). Polymer blend is also important for the application of automotive industry such as car-body panel, which gives chemical resistance and impact resistance to automotive components. Polymer blends are used as materials in textile fiber industry, plastics and protective coating such as protective mask and bullet proof vest.

Polymer electrolyte is also one of the applications for polymer blends. Thin polymer films consisting of ionic salts dissolve in an appropriate polymer and exhibit ionic conductivity at room temperature are termed as polymer electrolytes (Linford, 1991). Studies of polymer electrolyte consist of PEO as the main component has been intensively investigated (Acosta & Morales, 1996; Rocco *et al.,* 2002; Rocco *et al.,* 2003). Polymer gel electrolyte systems have been used in solid polymer batteries which have shown an improvement in ionic conductivity. A major merit of the lithium polymer battery is its inherent safety over the liquid electrolyte type lithium-ion battery (Murata *et al.,* 2000). Improvement in ionic conductivity was observed for lithium polymer battery over previous conventional solid polymer electrolyte systems. The main drawback for these systems is their dimensional instability with high plasticizer concentration. Mechanical properties of solid polymer electrolyte may be improved by modifying polymer and plasticizer ratio (Glasse *et al.,* 2002). Thin flat batteries fabricated from polymer electrolyte-based systems are used in cellular telephone devices.

1.4 Chemical modification on ENR using various carboxylic acids

ENR is obtained by replacing some double bonds with epoxide units. Epoxide unit on ENR is the reactive site for chemical modification with various carboxylic acids. Chemical modified ENR have shown improved physical and chemical properties after the reaction with carboxylic acids.

Study of curing behaviour and mechanical properties of ENR with dodecanedioic acid (DA) self-vulcanized blends was done by Pire *et al*., (2010). Crosslinking reaction at 180 ^{o}C of reactive functional rubber containing 10 and 25 mol% epoxide groups was followed by rheology. The properties of the cured materials were studied by dynamic mechanical analysis, stress-strain experiments and Differential Scanning Calorimetry (DSC) measurements. At 180 ^{o}C, the increase of elastic modulus shows that the crosslinking reaction becomes effective. The increasing of elastic modulus with decreasing number of epoxide sites for one diacid molecule indicates the reaction proceeds faster with increasing amount of diacid. The final elastic modulus increases with decreasing number of epoxide sites for one diacid molecule, which indicates a higher crosslinking density with increasing quantity of diacid. The kinetics of DA/ENR with 10 mol% epoxidation level (ENR10) reaction is slower than the one of DA/ENR with 25 mol% epoxidation level (ENR25) for the same proportion of DA, probably because of a lower meeting probability between carboxylic acid functions and epoxide sites in the ENR10 case. However, cured ENR10 exhibits promising mechanical properties. But, when more diacid is incorporated to the rubber, the resulted material becomes brittle. It breaks at low deformation rate, and the curve does not show hyper-elastic behaviour. After 3 h of curing at 180 ^{o}C, the melting peak is no longer observed in DSC spectrum, meaning that most of the DA was consumed or at least there is not enough free diacid to be detected. For all samples, cured materials exhibit a higher T_g than raw ENR25, meaning that reaction with diacids decreases the mobility of elastomer matrix. This phenomenon can be explained by crosslinking formation, as well as main-chain modifications due to the ring-opening of the oxirane groups. This effect was attributed to the polar hydroxyl group present on the main-chain after ring-opening, introducing intermolecular and intramolecular hydrogen bonding.

DSC studies of the reaction between ENR and benzoic acid were done by Gan and Burfield, (1989). The investigation was carried out at elevated temperatures of range 398 - 433 K, a significance increase in T_g of material proportional to the amount of acid added. The reaction is found to be first order with respect to benzoic acid and to have an overall activation of 70 kJ mol^{-1}. ^{13}C NMR studies employing ^{13}C-enriched benzoic acid showed that the benzoic acid was rapidly incorporated into the polymer main chain with the formation of ester linkages. The incorporation of benzoic acid leads to a T_g elevation of about 3.7 K $mol\%^{-1}$ modification suggests that such reactions might prove useful in changing the physical properties of such rubbers. The significant elevation of T_g associated with ENR vulcanized by dibasic acids is probably predominantly due to the modified main chain structure rather than the crosslinking network.

Crosslinking of ENR with dibasic acids was investigated by Loo, (1985). Crosslinking of ENR with dibasic acids takes place via the ring opening of the epoxide by the diacid with subsequent formation of a diester linkage. The formation of hard crumbs during mixing in the cases of oxalic and malonic acids is most probably related to high acid strength of the diacids. Thus, they could cause furanization in ENR during mixing. No T_g from -100 ^oC to 100 ^oC was observed. This absence of T_g implies that complete furanization has occurred in ENR with 50 mol% epoxidation level (ENR50) because ENR50 has varying block length of epoxide units situated randomly along the rubber chain. The furanized ENR50 would be expected to produce a whole range of very weak transitions which would appear as a broad gentle slope and hence no T_g was observed. It was found that the processibility and curing behaviour depended on hydrocarbon chain length of diacid, the dosage of diacid and the epoxidation level. The acids vulcanisates of ENR had very low resilience and compression set in combination with excellent retention of tensile strength after ageing. Compared to a semi-efficient

sulphur recipe, the diacid cure system produced ENR vulcanisates with higher air impermeability and lower oil swell. Further, it was found that vulcanisate resilience decreased with increasing state of crosslinking. This suggests that inter-chain crosslinking and intramolecular modifications could occur simultaneously.

Loo, (1988) studied on the enhancing oil resistance of ENR by carboxylic acid modification. Oil resistance properties of ENR could be enhance by using suitable carboxylic acids such as benzoic acid or its derivatives. Carboxylic acid modification is achieved *in situ* during normal crosslinking of ENR. The carboxylic acid-modified ENR was found to possess better resistance to oil swell than the unmodified ENR. Increase in oil-swell resistance is attributed to a combined effect of rubber chain modifications and formation of ether crosslinks. The ether crosslinking also contributes to lower compression set in the ENR vulcanisate as well as better resistance to overcure reversion. From infra-red spectra, ENR heated with benzoic acid has a strong peak at 1713 cm^{-1} which corresponding to the stretching frequency of the carboxyl of an ester group which indicates the carboxyl group has been grafted onto ENR. Other groups such as diol and furan were formed as well depending on the acidity of acid and epoxide level. Carboxylic acid modification increases the T_g of ENR and also introduces ether crosslinking, the oil resistance of modified ENR is enhanced. Several benefits could be derived from this *in situ* acid modification for ENR applications. Firstly, the oil resistance of ENR25 can be further enhanced as an alternative to the use of ENR of a higher epoxide level. Secondly, the oil resistance of ENR50 can be further improved to compete with nitrile rubbers with higher acrylonitrile content. Thirdly, a combination of lower compression set and increased oil resistance makes ENR more useful in oil-seal applications.

Gan and Hamid, (1997) studied partial conversion of epoxide groups to diols in ENR. In this study, when latex was boiled under mildly acidic or alkaline pH, only a

small amount of epoxide groups in ENR latex were converted to diols. ^{1}H NMR was unable to determine accurately the small amount of diols. But the present of this small amount of diols could be demonstrated by degradation reaction using lead tetraacetate, $Pb(OAc)_4$. Hydroxyl and carbonyl groups formed after the degradation process could be observed in infra-red spectra. Higher level of diols could be introduced and controlled by reacting ENR50 dissolved in toluene with a mixture of water and acetic acid in tetrahydrofuran (THF) at 60 ^{o}C. Amount of conversion of epoxide to diol increases with reaction time, and up to 23 mol% of diol in the rubber chain could be achieved after 24 h of reaction. ^{1}H NMR is able to determine the extent of conversion from NMR spectra of samples. One of the advantageous is that ENR containing diols in the main chain could serve as a good intermediate for further chemical modifications.

1.5 Miscibility

Mixtures of polymers may form miscible or immiscible blend systems. Miscibility refers to mixing of the components down to molecular level that leads to a single phase. A miscible blend is homogeneous on a macroscopic scale when exist as a single phase of mixed segments of the two components at equilibrium whereas a heterogeneous blend on the macroscopic scale is where a mixture of two polymers separates into two distinct phases consisting of individual components. This heterogeneous blend is considered to be immiscible in the thermodynamic sense (Olabisi *et al*., 1979).

1.5.1 Miscible PEO-based blend

Properties of PEO-based blends are strongly influenced by blend compositions, crystallinity, thermal behaviour and morphologies (Zhong & Guo, 2000; Chan *et al*., 2011; Pereira *et al*., 2011).

The behaviour of semicrystalline PEO and amorphous poly(vinyl phenol) (PVPh) mixture was studied by Sotele *et al*., (1997). Transmission microscopy with crossed polarizers was employed to evaluate the crystallization of semi-crystalline blend component at different compositions. Infra-red data, thermal analyses and determination of the Flory-Huggins parameter indicate both that the hydroxyl groups of PVPh are hydrogen bonded to the ethereal oxygen of PEO and that the system is miscible.

Phase diagram, crystallization and melting behaviour of PEO/poly(n-butyl methacrylate) (PnBMA) blends have been investigated using DSC and optical microscopy by Shafee and Ueda, (2002). The blends are miscible up to 85 ℃ and show a lower critical solution temperature-type demixing at higher temperature. The isothermal crystallization studies of the blends indicate a reduction in the overall rate of crystallization. Isothermal crystallization analysis by means of Avrami equation leads to average values of the Avrami index of 2.5 for pure PEO and 3.0 for the different blend compositions.

Crystallization kinetics of poly(3-hydroxybutyrate-*co*-3-hydroxyvalerate) (PHBV) and PEO have been studied by Tan *et al*., (2006) using DSC and Polarizing Optical Microscope (POM). This study reveals that the constituents are miscible in the amorphous state. Crystallization behaviour of the blends was studied under isothermal and non-isothermal conditions. Degree of crystallinity in the blends stays constant for PHBV and decreases slightly for PEO with ascending PHBV content. The rate of crystallization of PHBV decreases in blends as compared to the neat polymer whereas the opposite behaviour is observed for PEO. Non-isothermal crystallization is discussed in terms of a quasi-isothermal approach and the results show the same tendencies as under isothermal crystallization conditions.

1.5.2 Immiscible PEO-based blend

Miscibility and crystallization of PEO and PCL was studied by Qiu *et al*., (2003). By adopting compositional-dependent single T_g technique to evaluate the miscibility of PEO/PCL blends is difficult since the T_gs of PEO and PCL are very close to each other. Therefore, the miscibility of the blend cannot be determined from the appearance of single T_g. An alternative way is to use the phase contrast microscopy (PCM) to determine the miscibility of the blends. DSC and PCM instruments were used to study the crystallization of blends. A defined biphasic separation is observed for all compositions of PCL/PEO blend under PCM which indicates that PEO/PCL blends are immiscible.

1.5.3 Compatible ENR-based blend

Mechanical properties and fracture of different compositions of poly(vinyl chloride) (PVC) and ENR50 were studied by Varughese *et al*., (1988). Examination of fracture surfaces of blends does not show any features of phase separation of ENR or PVC by Scanning Electron Microscope (SEM). Tensile fracture surface of rigid PVC exhibits partially fused particle structures of PVC and that of blends exhibits features of shearing and horizontal discontinuous striations. The torn surface of rigid PVC shows evidence of intrinsic crazing and that of blends shows features of shear fibrils, vertically changed discontinuous striations, steps, unstable and stable tear fronts.

A study of thermal properties of ENR/poly(methyl methacrylate) (PMMA) was carried out by Nakason *et al*., (2004). A two phase morphology was observed with SEM. The small domains of the minor components were dispersed in the major phase. For the determination of blend compatibility, two distinct T_g peaks from the tan δ/temperature curves were found. Shifts in T_g to a higher temperature for the elastomeric phase and to a lower temperature for the PMMA phase were observed. ENR/PMMA blends could be

described as partly miscible blends. For thermogravimetry results, the decomposition temperatures of the blends increased as the epoxide level in ENR and epoxide molar percentage increased which might be caused by the chemical interactions between the different phases of the blends.

1.5.4 Immiscible ENR-based blend

Chan *et al*., (2004) carried out the study on melt reaction in blends of PHBV and ENR. PHBV with hydroxyvalerate content of 12 mol% thermally decomposed to shorter chains with carboxyl end groups when the temperature is rise above its melting point. These carboxyl chain ends may trigger reactions between the constituents since the ENR provide the epoxy reactive sites. T_g studies reveal immiscibility of the polymers over the entire composition range. Therefore, any reaction between the constituents is restricted to the interfacial region between the components. Two T_gs corresponding to the neat constituents were found before the melt reaction. After melt reaction took place, only one broad T_g could be detected. Rates of melt reaction increase with descending PHBV content in the composition range where PHBV forms the disperse phase. Rate of crystallization at 50 ℃ is dramatically reduced in blends after melt reaction whereas the crystallinity of PHBV remains approximately constant.

Immiscible blend of poly(3-hydroxybutyrate) (PHB) and ENR50 was revealed by Lee *et al*., (2005). Two T_gs observed at -18.4 ℃ and 1.2 ℃ for PHB/ENR blends which indicates the immiscibility of ENR50 and PHB phases. After annealing the blend sample at 190 ℃, an inward shift was observed. The inward shift observation gradually closing in with increasing annealing time and eventually merging into a single transition. This is an indication of progressive change in miscibility of the blends as an effect of melt reaction. FTIR spectra provide further evidence that supports the ring opening reaction of the epoxide group by the carboxyl group.

A study was done by Sulaiman *et al.*, (2009) to investigate the thermal properties and morphologies of poly(ethylene terephthalate) (PET) with ENR using DSC and POM. Immiscibility of the two polymers is revealed by observation of two distinct T_gs that correspond to the neat constituents. Equilibrium melting temperature (T°_m) of PET in blends was estimated by Hoffmann-Weeks method. There is no significant change of T°_m for PET in blends of ENR25 and ENR50. The degree of crystallinity of PET in PET/ENR25 blends remains constant whereas the degree of crystallinity in PET/ENR50 blends increase. The rate of crystallization of PET in blends is characterized by reciprocal half time. It displays an Arrhenius-like behaviour with respect to temperature and it stays constant at isothermal crystallization as long as PET in excess. Rate of crystallization of PET in blends decreases exponentially as the isothermal crystallization temperature increases. Dispersed phases of ENR25 and ENR50 in the matrix of PET can be observed when the content of PET is in excess.

1.6 ENR and PEO blends studies

Morphology, chemical interaction and conductivity of PEO-ENR50-lithium triflate ($LiCF_3SO_3$) based solid polymer electrolyte was studied by Noor *et al.*, (2010). Pure PEO shows a rough surface morphology with a lot of rumples which shows the presence of crystalline phase under Field Emission Scanning Electron Microscopy (FESEM) observation. For ENR50, a smooth surface morphology was observed due to its fully amorphous nature of natural rubber. Surface morphology of PEO changes from rough to almost smooth after addition of salt indicates reduction of PEO crystallinity. Degree of crystallinity in the blend decreases causes more amorphous phase in the system generated. Interaction of polymer host and lithium salt was observed by using Fourier-transform infrared (FTIR) analysis where triple peak of C-O-C stretching was combined to form a broad peak centered at 1096 cm^{-1} when 20 wt % of salt was added

to the electrolyte system. Ionic conductivity of the system also increases with weight percent (wt %) of salt under impedance spectroscopy analysis. The maximum conductivity value was observed at 1.4×10^{-4} S cm^{-1} at 20 wt % of $LiCF_3SO_3$.

In the study of preparation and characterization of a solid polymer electrolyte PEO/ENR50 (80/20)/$LiCF_3SO_3$ done by Noor *et al*., (2009), greatest room temperature ionic conductivity of 7.5×10^{-5} S cm^{-1} was obtained at 25 wt % of $LiCF_3SO_3$ salt. This result was supported by DSC and X-ray diffraction (XRD) analysis. DSC analysis showed the relative percentage of crystallinity and T_m of PEO decreased with the increasing wt % of $LiCF_3SO_3$ in PEO/ENR50/$LiCF_3SO_3$. XRD analysis suggested that the semicrystalline nature of PEO turned to amorphous due to the presence of $LiCF_3SO_3$. Decrease in PEO matrix crystallinity is an advantageous way in improving the ionic conductivity of PEO/ENR50/$LiCF_3SO_3$.

Modified natural rubber has desirable properties making it suitable for the use in polymer electrolytes. These include low T_g, soft elastomeric characteristics at room temperature and good elasticity. Study done by Glasse *et al*., (2002) on ENR25 and ENR50 with PEO, investigated the ionic conductivity and thermal properties for both unplasticized and plasticized polymer electrolyte systems with $LiCF_3SO_3$. Samples were in the form of free standing films with mixtures of ethylene carbonate (EC) and propylene carbonate (PC) which were used as plasticizers. From this study, it was found that unplasticized modified natural rubber-based systems exhibit ionic conductivities in the range of 10^{-6} to 10^{-5} S cm^{-1} at ambient temperatures. Incorporating 100 % of EC/PC by weight fraction of ENR/PEO polymer to the systems yielded mechanically stable films and ionic conductivities in the range of 10^{-4} S cm^{-1} at ambient temperature. The DSC traces of the salt-doped polymer electrolytes displayed a single T_g when increasing amount of PEO concentration was introduced into the matrix.

Idris *et al*., (2001) investigated on polymer electrolytes based on modified natural rubber for use in rechargeable lithium batteries. Three types of modified natural rubber, namely ENR25, ENR50 and PMMA grafted NR were employed to incorporated with $LiCF_3SO_3$. Results are reported for ionic conductivity and thermal properties for both unplasticized and plasticized polymer electrolyte system. For unplasticized system at a fixed polymer concentration, the conductivity of the gel increases as the salt concentration is increased. Ionic conductivities in $10^{-6} – 10^{-4}$ S cm^{-1} range are possible. The ionic conductivity is 6.2×10^{-5} S cm^{-1} at room temperature when the salt content is 20 wt % and is 1.8×10^{-4} S cm^{-1} at 60 wt % salt content. For plasticized system with mixtures of EC and PC enhance their ionic conductivities at room temperature. The conductivity value of the plasticized ENR25 system is 5.1×10^{-5} S cm^{-1} at ambient temperature when the liquid electrolyte content is 50 wt % and reaches 1.8×10^{-4} S cm^{-1} at 100 wt % liquid electrolyte. Addition of 100 wt % of EC/PC (1:1) into the salt-doped polymer system has considerably increased an average ionic conductivity by almost twofold magnitude to $10^{-4} – 10^{-3}$ S cm^{-1} range at room temperature. DSC traces of salt-doped polymer electrolyte displayed a single and increasing trend of T_g when increasing amount of salt concentration was introduced into the polymer matrix. However, incorporation of EC/PC into the system has resulted in a marked reduction in their T_g values.

Properties of solid solutions of PEO/ENR/12 wt % lithium perchlorate ($LiClO_4$) blends were studied by Chan and Kammer, (2008). Over the entire composition range, two T_gs corresponding to the T_g of the constituents were observed implying the immiscibility of the polymers. T_gs of both polymers slightly increase after addition of salt to the blends and this is approximately constant over the whole range of blend composition. T_g measurements reveal that $LiClO_4$ salt dissolves to approximately equal relative amounts in the two phases. The degree of crystallinity of PEO in blends with

ENR descends only to a minor extent with ENR content. But, addition of $LiClO_4$ salt leads first to decreasing crystallinity and second this decrease becomes more pronounced with addition of ENR. Isothermal crystallization rate decreases in a certain range of crystallization temperatures when ENR is added and this shows that $LiClO_4$ salt is favourably dissolved in PEO.

A study had done by Sim *et al*., (2010) comprising a system of ENR, PEO and $LiClO_4$. FTIR was used to investigate the ion-dipole interactions between the Li^+ ions and the polymer components of the PEO/ENR/$LiClO_4$ as to verify the selective localization of the salt in different phases of the blends. FTIR results show that Li^+ ion coordinate selectively with PEO which correlates with the higher ion mobility in PEO when 12 wt % of $LiClO_4$ is added to selected compositions of the PEO/ENR blend. Selective solubility of Li^+ in PEO serves as a percolating pathway for the ion transport in the PEO/ENR blend which enhances the ionic conductivity of PEO in the blend as compared to neat PEO.

1.7 Scope of study

Chapter 1 describes about the materials used and background of polymer blending and its applications. Literature reviews, problem statement and objectives are also stated in this chapter. Chapter 2 describes about methodology of the project and type of instruments used. Chapter 3 summarizes the results and discussion from the instruments analysis. Chapter 4 shows the conclusion from this study as well as suggestions for future work in this field.

1.8 Problem statement

Until now, thermal properties and morphologies of acetic acid-modified ENR50/PEO blends have not been explored. This research study is important to

investigate the compatibility of acetic acid-modified ENR50/PEO blends and comparison of physical and thermal properties between acetic acid-modified ENR50/PEO blends with ENR50/PEO blends in order to determine its suitability for various application purposes. One of the potential applications of the blends is as solid polymer electrolyte which serves as membrane separator in lithium-ion battery for hybrid vehicles.

1.9 Research objectives

Modification of ENR to modified-ENR which posses the acetate group, CH_3COO- and hydroxyl group, -OH is a new system that has not been explored. ENR50/PEO blend had been reported earlier, but not for the blend of acetic acid-modified ENR50/PEO. This semicrystalline and amorphous blend system may show better compatibility compare to ENR50/PEO due to the presence of polar groups on acetic acid-modified ENR50 backbone.

The objectives of the research are:

i) Synthesis of acetic acid-modified ENR50 and characterization of this modified rubber.

ii) Comparison between physical and chemical properties of ENR50 and acetic acid-modified ENR50.

iii) To investigate on the miscibility of acetic acid-modified ENR50/PEO blends using DSC.

iv) To investigate the morphologies of acetic acid-modified ENR50/PEO blends by using POM.

v) Conductivity measurements on ENR50/PEO/$LiClO_4$, acetic acid-modified ENR50/PEO and acetic acid-modified ENR50/PEO/$LiClO_4$ blends.

CHAPTER 2

METHODOLOGY

2.1 Materials

2.1.1 ENR50

ENR50 was supplied by Malaysia Rubber Board (Sungai Buloh, Malaysia) and its chemical structure is shown in Figure 2.1 below.

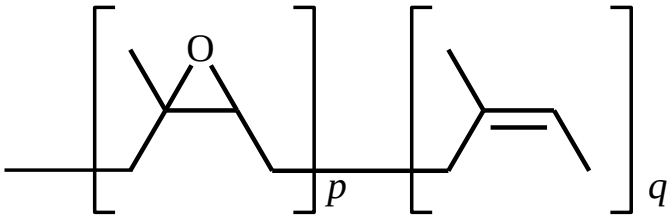

Figure 2.1: Chemical structure of ENR50 where $p = q$.

2.1.2 PEO

PEO was purchased from Sigma-Aldrich Corporation (St. Louis, Missouri, USA). The chemical structure of PEO is shown in Figure 2.2.

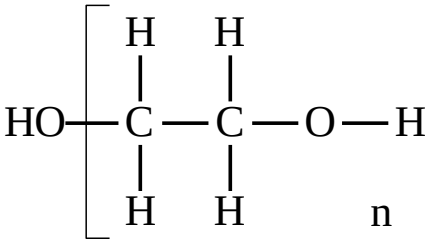

Figure 2.2: Chemical structure of PEO.

2.1.3 $LiClO_4$

$LiClO_4$ with 99% purity was purchased from Acros Organic Company (Geel, Belgium). The chemical structure of $LiClO_4$ is shown in Figure 2.3.

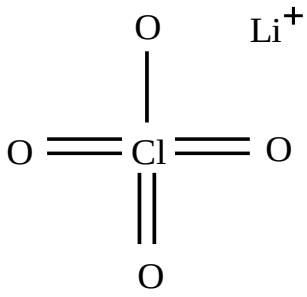

Figure 2.3: Chemical structure of $LiClO_4$.

Toluene, glacial acetic acid, methanol, chloroform, THF and deuterated chloroform ($CDCl_3$) were reagent grade chemicals, purchased from Merck, and they were used as supplied.

2.2 Synthesis of acetic acid-modified ENR50

20 g of ENR50 was mechanically masticated on a laboratory two rolls milling machine (Sk-W, Osaka, Japan) for forty cycles with the aim of breaking down the molecular weight of ENR50 which lead to the increase of the solubility of ENR50 in toluene. Gap width of the milling machine was adjusted to 4 mm width by using the nip gap controllers.

The masticated rubber was cut into smaller pieces with dimension of 5 mm × 5 mm and placed in a one-litre round bottom reaction flask, equipped with a mechanical stirrer (IKA RW20 digital, Staufen, Germany), two-blade impeller (half-moon type, Illinos, USA), water condenser and closed with glass lid as depicted in Figure 2.4.

100 mL of toluene was added and stirred at 150 rpm at room temperature. This stirring process was carried out overnight until the ENR50 dissolved completely.

2 mL of initial sample (ENR50 in toluene) was precipitated in 10 mL of methanol. The precipitated sample was placed on a flat glass surface and pressed into sheet form. This action is to remove the excess methanol trapped in the sample. The

sample was placed on Teflon dish and dried in vacuum oven under reduced pressure at 50 ℃ for 24 h. ENR50 in toluene is served as reference for subsequent comparison study.

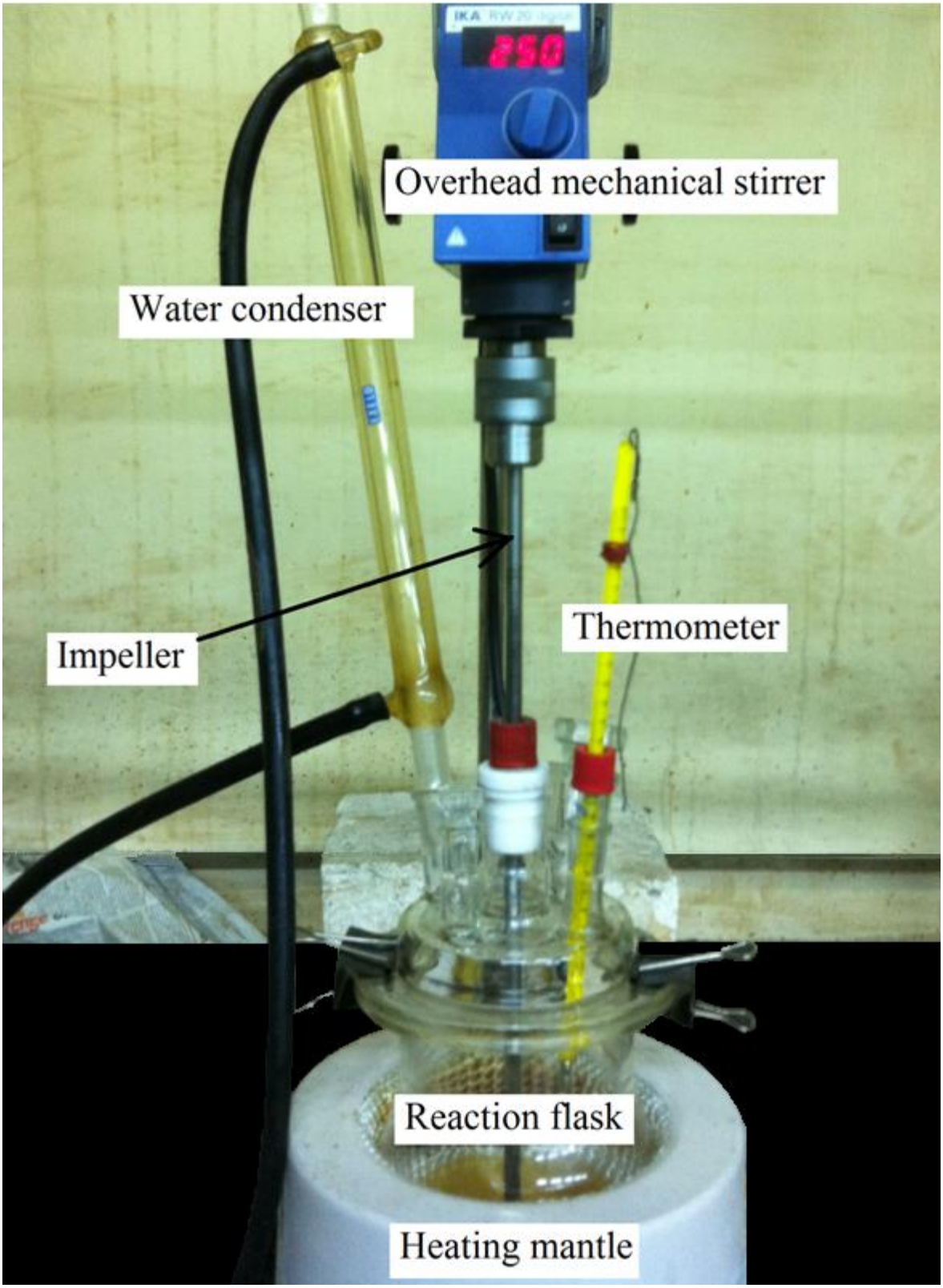

Figure 2.4: Reaction setup for synthesis of acetic acid-modified ENR50.

The ENR50 solution was heated up slowly to 100 ℃ and the stirrer speed increased to 250 rpm. 16 mL of glacial acetic acid was added drop-wise into the reaction flask through a dropping funnel within 15 min.

Samples were drawn from the reaction flask at different time intervals of 30 min, 2 h, 7 h, 16 h and 18 h after the addition of acetic acid. 2 mL of the reaction mixture was treated with 10 mL of methanol, and the precipitated modified rubber was isolated and dried in vacuum oven at 50 ℃ for 24 h before analysis. Heating and stirring were stopped at 18 h and the reactor was allowed to cool down to room temperature. All of the modified ENR was precipitated into excess methanol with the ratio of toluene solution to methanol at 1:5. The isolated modified ENR was placed on Teflon dish and dried in vacuum oven at 50 ℃ for 24 h. Samples were stored in desiccators after drying for further analyses.

2.3 Purification of 18-h acetic acid-modified ENR50

20 g of 18-h acetic acid-modified ENR50 was cut into smaller pieces and dissolved in 500 g of chloroform in a conical flask. Teflon coated magnetic stirrer was added to the conical flask and the polymer solution was placed on stirring hotplate (IKA yellow line 9008100, Staufen, Germany) with stirrer speed of 300 rpm at 50 ℃ for 24 h.

Then, the solution was filtered using nylon cloth to remove gel content. The filtered polymer solution was placed on stirring hotplate at 50 ℃ with stirring speed of 200 rpm to concentrate the solution by removing the solvent. The final solution was quite viscous. The final viscous solution was poured slowly into a big beaker containing methanol and the solution was kept stirring until gel-like precipitate formed. The ratio of polymer solution to methanol was 1:5.

The purified acetic acid-modified ENR50 was placed on Teflon dish and left overnight in fume hood to evaporate off excess solvent. Sample was dried in oven at

50 ℃ for 24 h and further dried in vacuum oven for another 24 h at 50 ℃. Samples were stored in desiccators after drying for further analyses.

2.4 Preparation of blends

ENR50/PEO/$LiClO_4$, 18-h acetic acid-modified ENR50/PEO and 18-h acetic acid-modified ENR50/PEO/$LiClO_4$ polymer blends were prepared by solution casting method. ENR50, acetic acid-modified ENR50 and PEO were dissolved respectively in THF to form individual 5% (*w*/*w*) polymer solutions according to the blend composition shown in Tables 2.1, 2.2 and 2.3. The polymer solutions were stirred with Teflon coated magnetic stirring bars for 24 h at 50 ℃ on stirring hotplate. The polymer solutions were mixed according to the mass content of ENR50 or acetic acid-modified ENR50 in the blends ranged from 25%, 50% and 75%. Blends of ENR50/PEO and acetic acid-modified ENR50/PEO doped with 12 wt. % of $LiClO_4$ were prepared as shown in Tables 2.1 and 2.3. The mixtures were continuously stirred for another 24 h after addition of $LiClO_4$ to obtain homogeneous solution.

Thin films of the blends were prepared by casting the solution mixtures in Teflon dish. THF was allowed to evaporate at room temperature overnight in fume hood. Thin films of blends were first dried in oven at 50 ℃ for 24 h and further dried in vacuum oven at 50 ℃ for another 24 h to ensure the films were completely dried. The dried films were stored in desiccators for further analyses. The concentration of $LiClO_4$ salt in the solid polymer film is given by equation (1).

$$\text{Concentration of } LiClO_4 = \frac{\text{Mass of } LiClO_4}{\text{Total mass of polymer}} \quad (1)$$

Table 2.1: Blend composition for ENR50/PEO/$LiClO_4$.

ENR50/PEO/$LiClO_4$ (*w/w/w*)	Solution 1		Solution 2		Weight of $LiClO_4$ (g)
	Weight of ENR50 (g)	Weight of THF (g)	Weight of PEO (g)	Weight of THF (g)	
75/25/12	0.375	7.5	0.125	2.5	0.06
50/50/12	0.250	5.0	0.250	5.0	0.06
25/75/12	0.125	2.5	0.375	7.5	0.06

Table 2.2: Compositions of acetic acid-modified ENR50/PEO blends ranged from 75/25 to 25/75 in steps of 25 wt %.

Acetic acid-modified ENR50/PEO (*w/w*)	Solution 1		Solution 2	
	Weight of acetic acid-modified ENR50 (g)	Weight of THF (g)	Weight of PEO (g)	Weight of THF (g)
75/25	0.375	7.5	0.125	2.5
50/50	0.250	5.0	0.250	5.0
25/75	0.125	2.5	0.375	7.5

Table 2.3: Blend composition for acetic acid-modified ENR50/PEO/$LiClO_4$.

Acetic acid-modified ENR50/PEO/$LiClO_4$ (*w/w/w*)	Solution 1		Solution 2		Weight of $LiClO_4$ (g)
	Weight of acetic acid-modified ENR50 (g)	Weight of THF (g)	Weight of PEO (g)	Weight of THF (g)	
75/25/12	0.375	7.5	0.125	2.5	0.06
50/50/12	0.250	5.0	0.250	5.0	0.06
25/75/12	0.125	2.5	0.375	7.5	0.06

2.5 Characterization of acetic acid-modified ENR50, PEO and acetic acid-modified ENR50/PEO blends

2.5.1 Molecular mass of ENR50 and acetic acid-modified ENR50

Gel permeation chromatography (GPC) (Waters, Milford, Massachusetts, USA) was employed to determine molecular weight distribution of ENR50 and acetic acid-modified ENR50. The GPC was fitted with Styragel Columns HR1, HR2 and HR5 connected in series (Milford, Massachusetts, USA). THF was used as eluent at a flow rate of 0.1 mL min^{-1} and sample solution was prepared with concentration of 1.0 mg mL^{-1}. Monodispersed polystyrene standards (Easical, Darmstadt, Germany) (Weight average molecular mass (M_w) = 370 to 6,770,000 g mol^{-1}) were used to calibrate the column.

2.5.2 Thermal gravimetric analysis (TGA)

Perkin Elmer TGA 6 (Norwalk, Connecticut, USA) was used for the analysis of thermal stability of the sample. Sample (6 - 10 mg) was heated from 50 - 900 ℃ at a heating rate of 10 K min^{-1} under nitrogen atmosphere. The maximum rate of decomposition temperature was taken as $T_{d,\ inflection}$ by referring to its derivative weight loss curve, onset temperature ($T_{d,\ onset}$) and decomposition temperature for 5 % weight loss ($T_{d,\ 5\%\ wt\ loss}$) on the weight loss curves were recorded.

TGA was carried out to determine decomposition temperature for sample. Therefore for DSC analysis, sample cannot be heated above its decomposition temperature and it is recommended to heat 50 ℃ below its decomposition temperature. The reaction between the constituents has to be far below decomposition temperature to ensure minimal decomposition of sample during the reaction at relatively high temperature.

2.5.3 FTIR spectroscopy

FTIR spectra were recorded on Perkin Elmer Spectrum 400 Spectrometer (Waltham, Massachusetts, USA) in the transmittance mode over the range of 450 - 4000 cm^{-1} by an averaging 16 scans at a maximum resolution of 4 cm^{-1}. 5 % (*w*/*v*) of sample solution is prepared by dissolving 0.2 g of sample in 4 mL of toluene. Thin film of sample was cast on potassium bromide (KBr) cell and was dried thoroughly before the analysis was carried out. Absorbance spectra were normalized using Abex function of Spectrum One v5.0.1 software (Perkin Elmer, Beaconsfield, UK) for absorbance ratio determination.

2.5.4 ^{1}H NMR spectroscopy

^{1}H NMR spectra were recorded on JEOL JNM-GSX 270 MHz Fourier-transform NMR spectrometer (Peabody, Massachusetts, USA). 0.2 g of sample was dissolved in 5 mL of $CDCl_3$ with tetramethylsilane (TMS) as internal standard.

2.5.5 DSC analysis

TA DSC Q200 (New Castle, Delaware, USA) coupled with refrigerator cooling system (RCS 90, New Castle, Delaware, USA) were used to study the T_g, T_m, melting enthalpy (ΔH_m), crystallization temperature (T_c) and crystallization enthalpy (ΔH_c). DSC was calibrated with indium standard and nitrogen atmosphere was maintained throughout the analysis. 6 – 10 mg sample was encapsulated in aluminium sample pan. For isothermal crystallization determination, blends of acetic acid-modified ENR50 were held at 80 ℃ for 5 min followed by cooling to 49 ℃ at a cooling rate of 20 ^oC min^{-1} and allow to crystallize for five half times of crystallization. Afterwards, samples were heated to 80 ℃ at a heating rate of 10 ^oC min^{-1}. For T_g analysis, the same procedure as above was used, except cooling the samples to -70 ℃ and held for 1 min.

2.5.6 POM analysis

Morphologies of growing spherulites in PEO of the blends were studied using Q Win Software (Leica, Cambridge, UK) installed on the attached Nikon microscope (Eclipse ME 600, Yokohama, Japan). The microscope was equipped with a heating/cooling unit (Linkam THM 600/s, Surrey, UK). 1 % (*w*/*v*) of polymer solution was prepared by dissolving 0.04 g of sample in 4 mL of chloroform and kept overnight in oven at 50 ℃ which capped in a 5 mL vial. Polymer solution was cast on cover slip to form a thin film and it was dried before second layer of thin film was applied. The cover slip was first dried in oven at 50 ℃ for 24 h and further dried in vacuum oven for

another 24 h at 50 ℃. For radial growth rate determination, samples were heated from 30 to 80 ^{o}C at a heating rate of 10 ^{o}C min^{-1} and held at 80 ^{o}C for 5 min followed by cooling to 49 ^{o}C at a cooling rate of 20 ^{o}C min^{-1}. During isothermal crystallization at 49 ℃, micrographs were captured at suitable time intervals ranged from 1-15 sec. Measurement of diameter of the growing spherulites was carried out by using Leica Q Win software. For morphology of sample after isothermal crystallization determination, heating and cooling cycles were applied as before and micrograph was taken after 60 min of crystallization at 49 ℃.

2.6 Conductivity measurements for ENR50/PEO/$LiClO_4$, acetic acid-modified ENR50/PEO and acetic acid-modified ENR50/PEO/$LiClO_4$ blends

Ionic conductivity (σ) at 30 ^{o}C was determined from ac-impedance measurements using a Hioki 3532-50 LCR Hi-Tester (Nagano, Japan) together with a computer for data acquisition over the frequency range between 100 Hz and 1 MHz. Films of polymer electrolyte were sandwiched between two stainless steel disk electrodes, which serve as blocking electrodes for ions. σ was calculated from the bulk electrolyte resistance (R_b) value by adopting equation $\sigma = L/(R_b S_a)$. Quantities L and S_a denote thickness of the polymer electrolyte film and its surface area in contact with the stainless steel disk electrodes respectively. Diameter of the electrode is 20 mm. Film thickness was measured by Mitutoyo Digimatic Caliper (Model: ID-C1012XBS, Kawasaki, Japan). The average of thickness L was calculated from four measurements of thickness on the polymer film at different positions that were in contact with the stainless steel disk electrodes.

CHAPTER 3

RESULTS AND DISCUSSION

3.1 Characterization of ENR50 and acetic acid-modified ENR50

Acetic acid-modified ENR50 comprising of ester and hydroxyl groups was synthesized from ENR50. Sample characterization was carried out to compare starting material, ENR50, and acetic acid-modified ENR50. GPC was used to determine the molecular distribution of polymers. FTIR spectroscopy was used to identify the chemical structure of the newly synthesized acetic acid-modified ENR50. Chemical structure of acetic acid-modified ENR50 and its composition were further confirmed by using ^{1}H NMR spectroscopy. Decomposition temperature of ENR50 and acetic acid-modified ENR50 were determined by TGA to investigate on the thermal stability of the samples. DSC was used to determine the T_g of ENR50 and acetic acid-modified ENR50.

3.1.1 GPC determination

M_w, number average molecular mass (M_n), polydispersity index and viscosity average molecular mass (M_η) of various polymers were summarize in Table 3.1.

Chemical modification of ENR50 by acetic acid causes M_w and M_n of 18-h acetic acid-modified ENR50 decreases. This might be due to high temperature was employed throughout the synthesis process and chain scission occurred along the ENR50 backbone. Thus, increase in polydispersity index was observed for 18-h acetic acid-modified ENR50.

Table 3.1: Molecular mass and polydispersity index of ENR50, 18-h acetic acid-modified ENR50 and PEO.

Polymer	ENR50	18-h acetic acid-modified ENR50	PEO
M_w (g mol^{-1})	346 000	302 000	-
M_n (g mol^{-1})	110 000	50 000	-
Polydispersity	3.1	6.0	-
M_η [a)] (g mol^{-1})	-	-	100 000

[a)] Viscosity average molecular mass of PEO provided by supplier.

3.1.2 FTIR spectroscopy

FTIR was used to investigate the formation of acetic acid-modified ENR50 as a function of reaction time. The band characteristics for the starting material, ENR50 was shown in Table 3.2.

Table 3.2: Band characteristics for ENR50.

Wavenumber (cm^{-1})	Assignment	Functional group	References
2963	CH_2 asymmetrical stretching	Methylene	Van Zyl *et al*., (2003)
2933	CH_2 asymmetrical stretching	Methylene	Van Zyl *et al*., (2003)
2859	CH_2 symmetrical stretching	Methylene	Van Zyl *et al*., (2003)
1664	C=C stretching	Olefin	Smith, (1999)
1449	C-CH_2 scissors	Alkene	Smith, (1999)
1374	C-CH_3 symmetric bend	Alkene	Smith, (1999)
1250	Epoxy, whole ring stretching	Epoxy ring	Nakanishi *et al*., (1977)
873	Epoxy, half ring stretching	Epoxy ring	Simons, (1978)

Within 18 h reaction time, reaction solution became more brownish in colour. Changes on the characteristic bands of FTIR spectrum of acetic acid-modified ENR50 were noticed and recorded. Table 3.3 shows the band characteristics for acetic acid-modified ENR50 after 18 h sample.

Table 3.3: Band characteristics for acetic acid-modified ENR50 after 18 h sample.

Wavenumber (cm^{-1})	Assignment	Functional group	References
3469	-OH stretching	Hydroxyl	Gelling, (1988)
2963	CH_2 asymmetrical stretching	Methylene	Van Zyl *et al*., (2003)
2933	CH_2 asymmetrical stretching	Methylene	Van Zyl *et al*., (2003)
2859	CH_2 symmetrical stretching	Methylene	Van Zyl *et al*., (2003)
1735	C=O stretching for ester	Ester	Gan & Hamid, (1997)
1664	C=C stretching	Olefin	Smith, (1999)
1449	CH_2 scissoring	Alkene	Smith, (1999)
1374	C-CH_3 symmetric bend	Alkene	Smith, (1999)
1241	C-O stretching for ester	Ester	Loo, (1988)
1026	C-O stretching for ester	Ester	Loo, (1988)
839	=C-H out plane deformation cis C=C	Alkene	Hallensleben *et al*., (1995)

The overlapping FTIR spectra for ENR50 and 18-h acetic acid-modified ENR50 are shown in Figure 3.1, there are five absorbance (A) bands from the FTIR spectra can be compared.

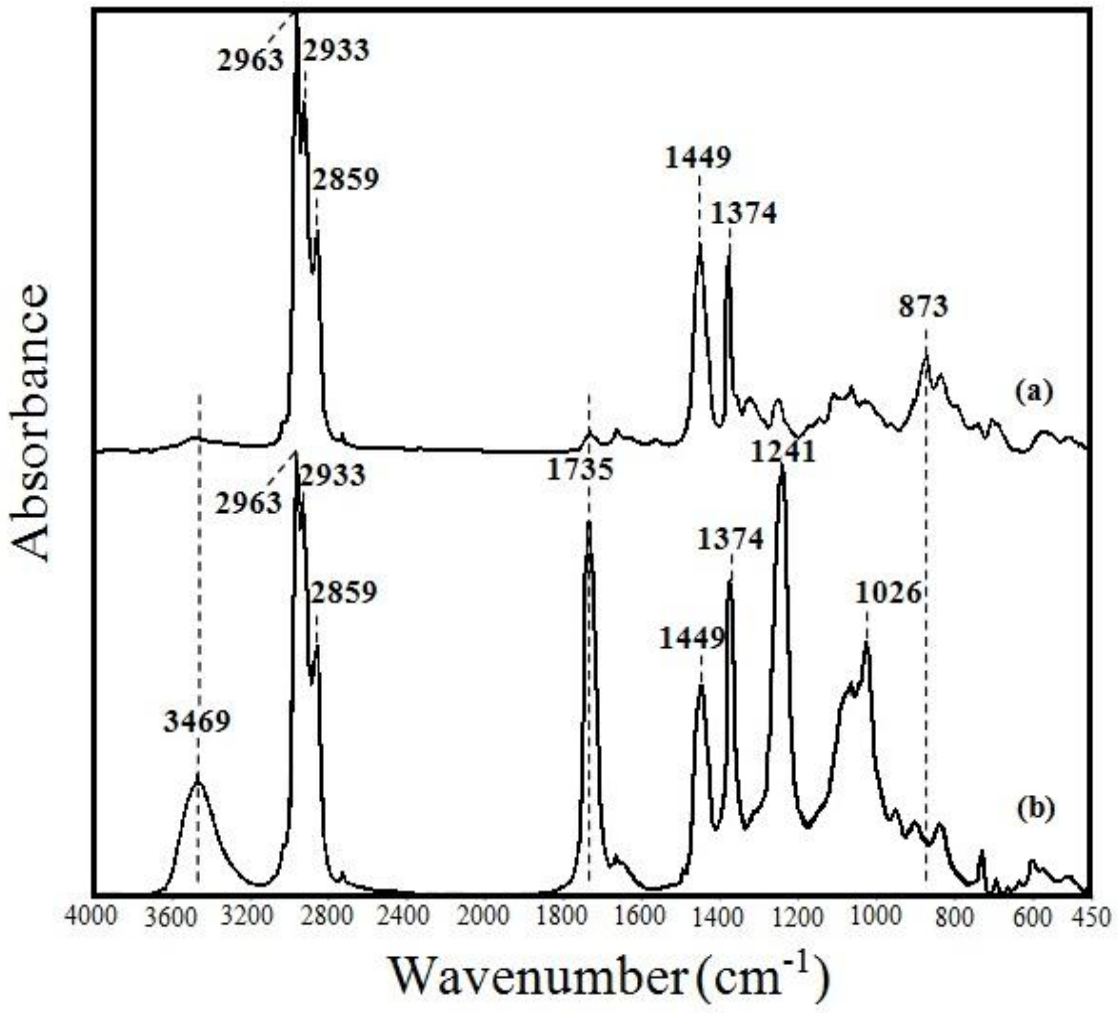

Figure 3.1: FTIR spectra of (a) ENR50 and (b) 18-h acetic acid-modified ENR50.

Firstly, ring-opening of epoxide group by carboxylic acid produces hydroxyl group that gives rise to a broad band at wavenumber 3469 cm^{-1}. This absorbance band becomes more intensified as a function of reaction time, which implies the formation of -OH group becomes more significant as shown in Figure 3.2.

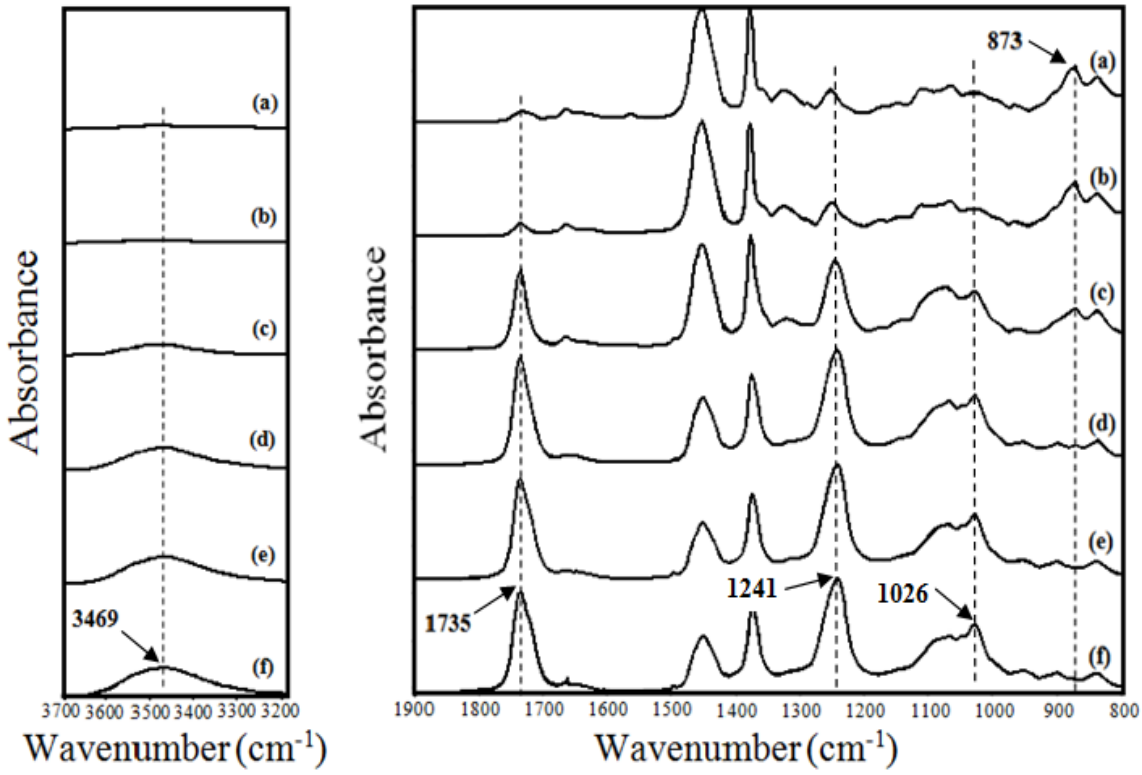

Figure 3.2: FTIR spectra in the region of 800-1900 cm^{-1} and 3200-3700 cm^{-1} of (a) ENR50, acetic acid-modified ENR50 at various reaction time (b) 30 min, (c) 2 h, (d) 7 h, (e) 16 h and (f) 18 h.

Secondly, formation of C=O and C-O bond in ester group is reflected in the absorbance bands at wavenumber of 1026, 1241 and 1735 cm^{-1} and these absorbance bands are clearly observed in FTIR spectrum of acetic acid-modified ENR50 samples (refer Figure 3.2). Thirdly, absorbance band of epoxy ring at wavenumber of 873 cm^{-1} on ENR50 was gradually decreased as reaction time increase (shown in Figure 3.2). Change of this band in the course of time gives conversion of the epoxy group.

Relative absorbances, given as ratio of area heights, with reference to internal standard at 1449 cm^{-1} are listed in Table 3.4. The internal standard band corresponds to $–CH_2–$ bond stretching which does not participate in chemical modification during the reaction and is assumed to remain constant. The results in Table 3.4 showed clearly the consumption of epoxy group and growing of hydroxyl and ester with reaction time.

Table 3.4: Changes in absorbance peaks for epoxy, ester and hydroxyl groups with reaction time.

Reaction time (h)	A_{873}/A_{1449} (Epoxy ring)	A_{1735}/A_{1449} (Ester)	A_{3469}/A_{1449} (Hydroxyl)
0	0.33	0.055	0.048
0.5	0.31	0.095	0.052
2	0.25	0.81	0.23
7	0.11	1.9	0.51
16	0.063	2.3	0.63
18	0.057	2.3	0.67

As the reaction time persists from 0 - 18 h, the absorbance ratio of epoxy groups decreases, which is consistent to the increase of the absorbance ratio of -OH stretching and C=O stretching. This serves as a strong indication of the consumption of epoxy level in ENR50.

For the absorbance ratio of A_{1735}/A_{1449}, the value increases from 0.055 for 0-h sample to 2.3 at 18 h reaction time indicates the formation of C=O bond for ester. Absorbance ratio of A_{3469}/A_{1449} corresponding to hydroxyl group formation increases from 0.048 for 0-h sample to 0.67 for 18-h sample. These results give further evidence that esterification process and formation of hydroxyl group had occurred with decrease of epoxy groups.

3.1.3 ^{1}H NMR spectroscopy

^{1}H NMR spectroscopy was carried out to verify chemical structure of ENR50 and investigate the possible chemical structure of acetic acid-modified ENR50. The areas of the chemical shift were used to calculate the epoxide content of rubber by using the following equation:

$$\% \text{ Epoxide} = \left(\frac{a\ 2.7\ ppm}{a\ 5.1\ ppm + a\ 2.7\ ppm}\right) \times 100\% \qquad (2)$$

where *a* is the area of the chemical shift concerned,

2.7 ppm is the chemical shift for oxirane hydrogen,

5.1 ppm is corresponds to chemical shift of olefinic proton.

^{1}H NMR spectrum for ENR50 and its chemical structure were shown in Figure 3.3. Amount of epoxide content was calculated using equation (2). Areas of chemical shift at 2.7 ppm and 5.1 ppm for ENR50 spectrum in Figure 3.3 were used for epoxide level determination. The epoxide level estimated for ENR50 is 50 mol%.

By using FTIR and NMR spectroscopies, the chemical structure of 18-h acetic acid-modified ENR50 with its composition was derived. 18-h acetic acid-modified ENR50 together with its chemical structure was shown in Figure 3.4. Chemical shift assignments for ENR50 and 18-h acetic acid-modified ENR50 were shown in Table 3.5 and 3.6 respectively.

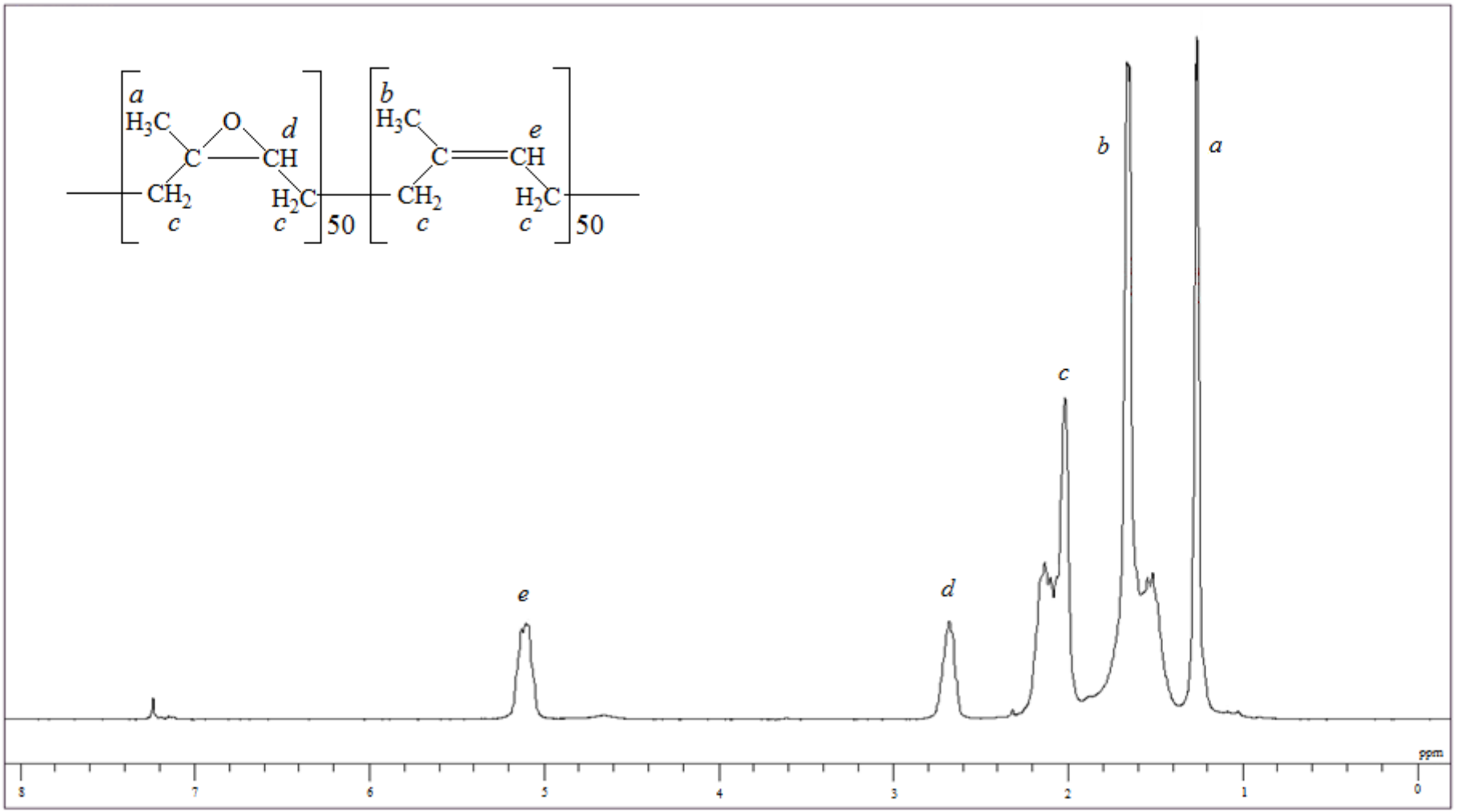

Figure 3.3: ^{1}H NMR spectrum of ENR50.

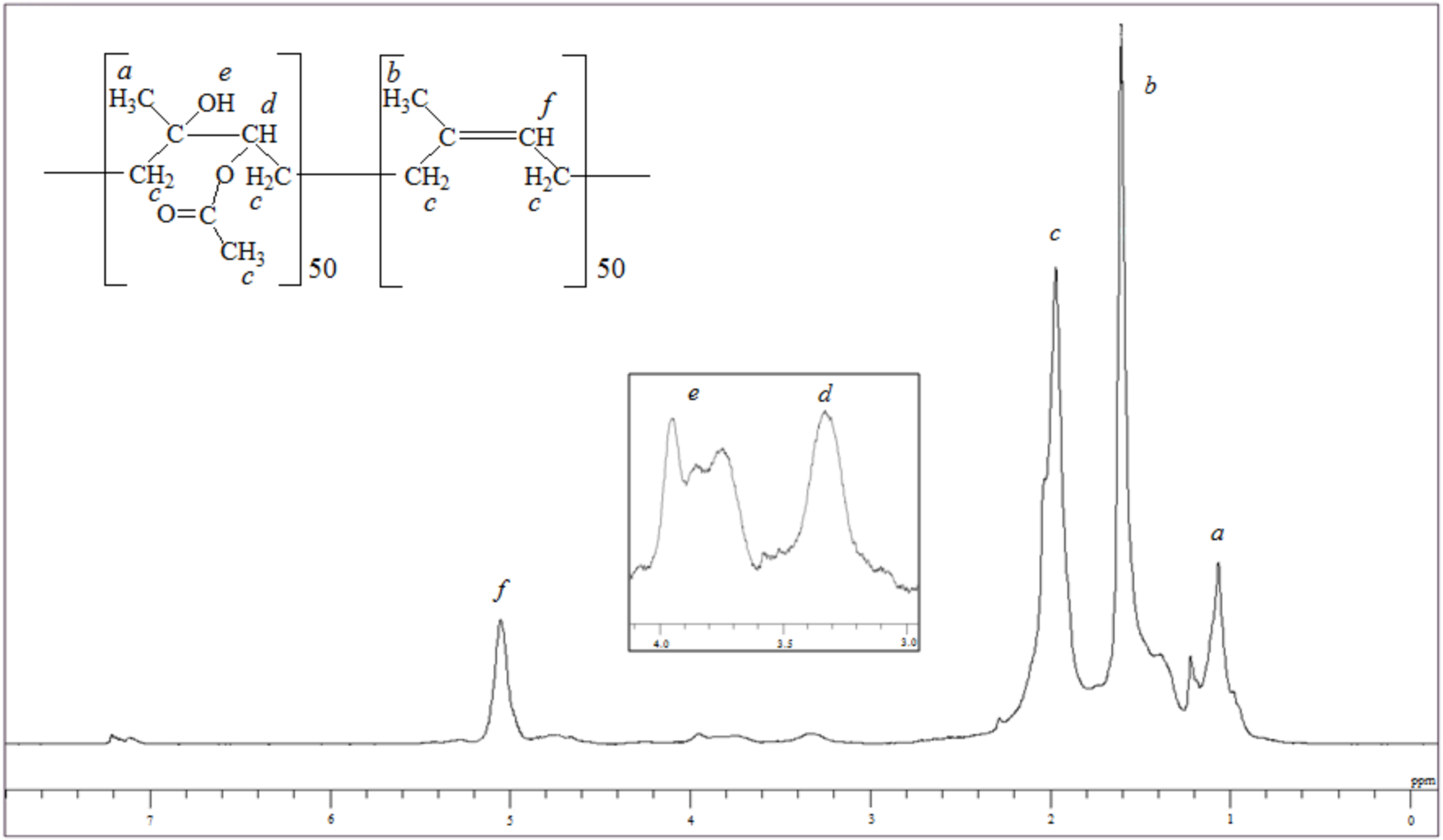

Figure 3.4: ^{1}H NMR spectrum of 18-h acetic acid-modified ENR50.

Table 3.5: Chemical shift assignments for ENR50.

Chemical shift (ppm)	Assignment	References
1.3	-CH_3 group (epoxide)	Hallensleben *et al*., (1995)
1.6	-CH_3 group (isoprene)	Hallensleben *et al*., (1995)
2.1	-CH_2- (epoxide and isoprene)	Hallensleben *et al*., (1995)
2.7	Oxirane hydrogen, C-H	Bradbury & Perera, (1985)
5.1	Olefinic proton, C=C-H	Hayashi *et al*., (1981)

Table 3.6: Chemical shift assignments for 18-h acetic acid-modified ENR50.

Chemical shift (ppm)	Assignment	References
1.1	-CH_3 group (hydroxyl and ester)	Hallensleben *et al*., (1995)
1.6	-CH_3 group (isoprene)	Hallensleben *et al*., (1995)
2.1	-CH_2- (epoxide and isoprene)	Hallensleben *et al*., (1995)
3.3	Hydroxyl group, -OH	Gan & Hamid, (1997)
3.7	Oxirane hydrogen, C-H	Gan & Hamid, (1997)
5.1	Olefinic proton, C=C-H	Hayashi *et al*., (1981)

Chemical demonstration of random distribution of ENR had been proved by Davey and Loadman, 1984. Hence, all the functional groups discussed further are assumed to be randomly distributed as well. By taking the integration of area values the mol% of protons for respective functional groups may be determined. Figure 3.3 and 3.4 present the spectra; data are listed in Table 3.7. By varying the reaction time, the composition of the monomer units of acetic acid-modified ENR50 can be finally adjusted. NMR spectra were used for estimating conversion of epoxy group in the

course of reaction. Conversion is simply given in terms of number of moles of epoxy, n_{ep}, by

$$\alpha(t) = \frac{n_{ep}(0) - n_{ep}(t)}{n_{ep}(0)} \quad (3)$$

where n_{ep} (0) is initial number of moles of epoxy

n_{ep} (t) is number of moles of epoxy at time t

Table 3.7: Variation of n_{ep} (t) and degree of conversion, α with reaction time.

Reaction time, t /h	n_{ep} (t) / mol%	α
0	50.0	0
0.5	47.1	0.06
2	40.6	0.19
7	21.5	0.57
16	3.2	0.94
18	0	1.00

n_{ep} (t) values gradually decrease as reaction time increase. 50 mol% of epoxy level was utilized throughout the 18 h reaction period. Degree of conversion, α increases as reaction time increases. Hence, acetic acid-modified ENR50 synthesis had attained its maximum conversion by 18 h.

3.1.4 TGA

Different time intervals of acetic acid-modified ENR50 samples were analyze by TGA. Thermogram for weight percentage of acetic acid-modified ENR50 samples against temperature was shown in Figure 3.5.

$T_{d,\ onset}$ is defined as onset of weight loss curve for TGA thermogram. $T_{d,\ inflection}$ is defined as the temperature of maximum decomposition rate curve for TGA thermogram. $T_{d,\ 5\%\ wt\ loss}$ is the decomposition temperature for 5% of sample out of the

total weight from weight loss curve of TGA thermogram. $T_{d,\ 5\%\ wt\ loss}$ was taken from decomposition temperature table generated by Pyris software (v10.1, Connecticut, USA). $T_{d,\ onset}$, $T_{d,\ inflection}$ and $T_{d,\ 5\%\ wt\ loss}$ obtained were tabulated in Table 3.8.

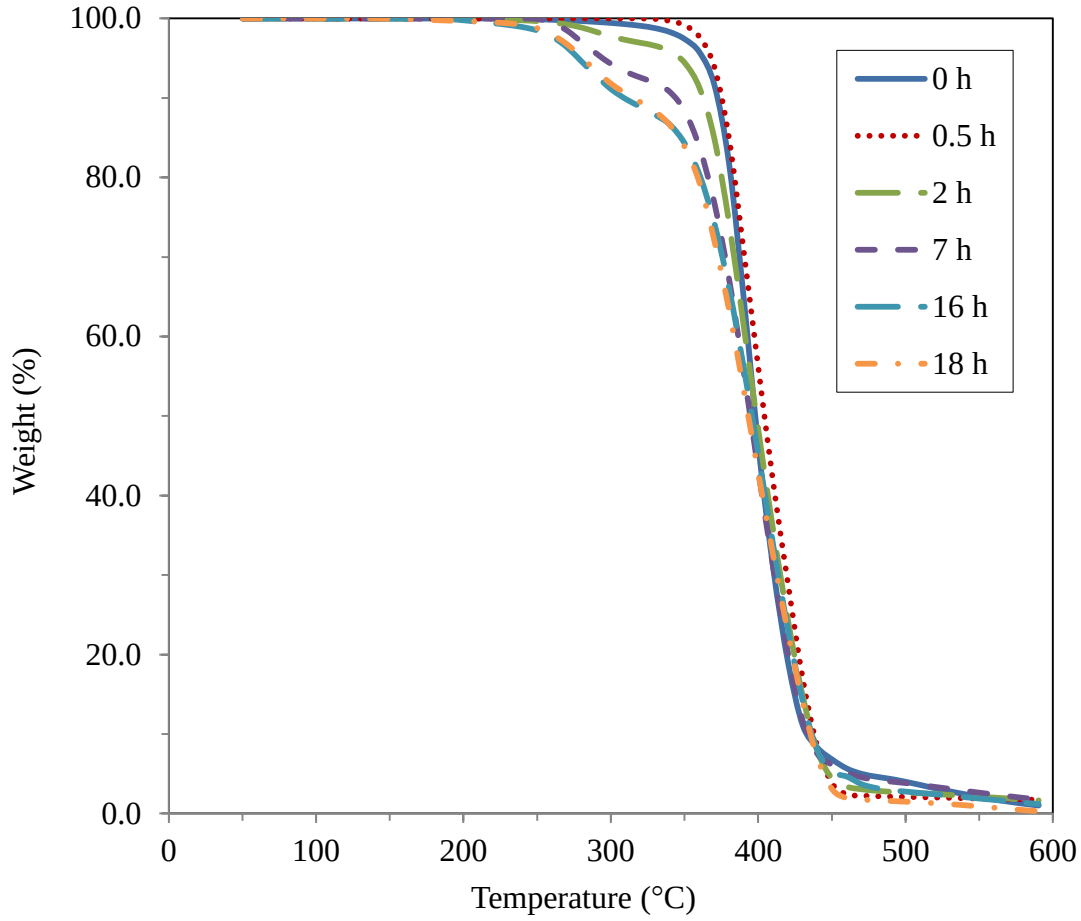

Figure 3.5: Weight percentage against temperature of different reaction time for acetic acid-modified ENR50 samples.

Table 3.8: $T_{d,\ onset}$, $T_{d,\ inflection}$ and $T_{d,\ 5\%\ wt\ loss}$ of different reaction time for acetic acid-modified ENR50 samples.

Time (h)	1^{st} $T_{d,\ onset}$ (℃)	2^{nd} $T_{d,\ onset}$ (℃)	1^{st} $T_{d,\ inflection}$ (℃)	2^{nd} $T_{d,\ inflection}$ (℃)	$T_{d,\ 5\%\ wt\ loss}$ (℃)
0	-	372	-	391	366
0.5	-	372	-	390	365
2	269	364	290	388	347
7	266	361	288	392	294
16	261	360	278	403	283
18	260	358	283	392	280

There is no noticeable weight loss for different reaction times of acetic acid-modified ENR50 samples before the first $T_{d,\ onset}$ at around 260 ℃. ENR50 and 30-min acetic acid-modified ENR50 samples preceded in single thermal decomposition step from 320 to 550 ℃ whereas 2-h, 7-h, 16-h and 18-h acetic acid-modified ENR50 samples exhibit two thermal decomposition steps.

Figure 3.6 shows the TGA thermogram of the two-steps thermally decomposed 18-h acetic acid-modified ENR50 sample. For two-steps thermally decomposed samples, the lower $T_{d,\ onset}$ (1^{st} $T_{d,\ onset}$) corresponds to the loss of less thermally stable segments in the acetic acid-modified ENR50 whereas higher $T_{d,\ onset}$ (2^{nd} $T_{d,\ onset}$) corresponds to the loss of thermally more stable segments.

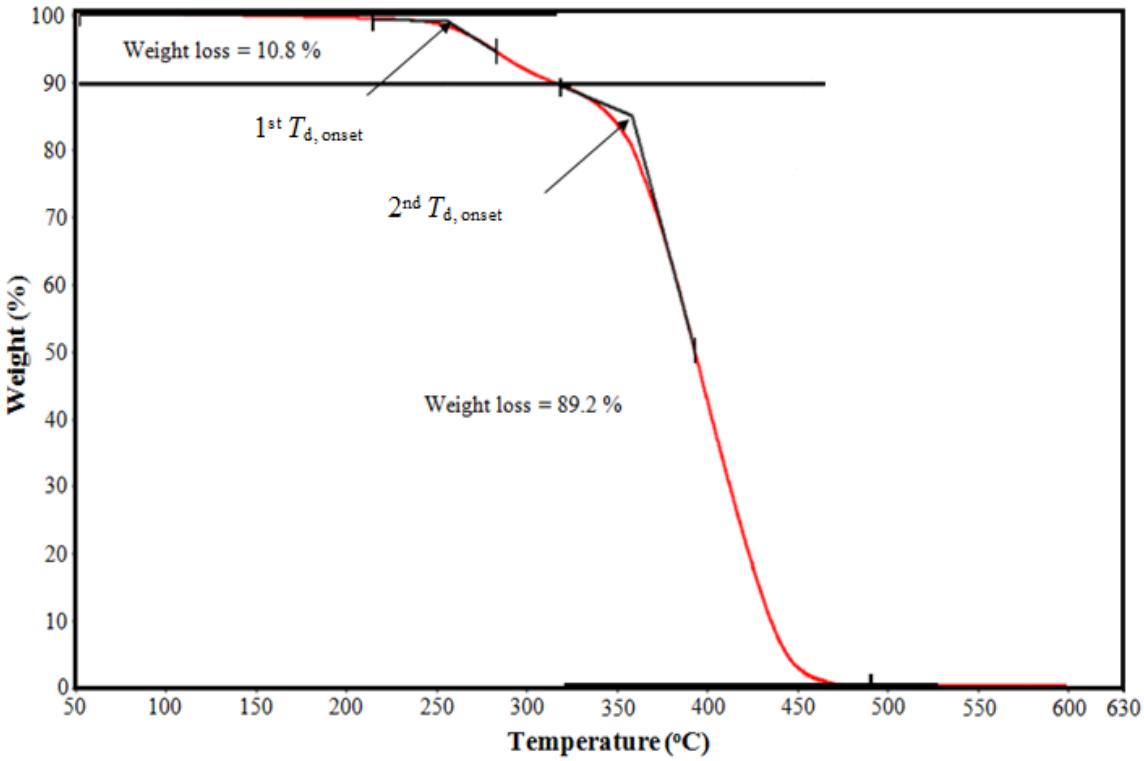

Figure 3.6: TGA thermogram for 18-h acetic acid-modified ENR50.

The isoprene units and epoxide units which made up of ENR50 were thermally more stable compounds in this investigated system. After the modification of ENR50 with acetic acid, thermally less stable segments were formed in 30-min, 2-h, 7-h, 16-h and 18-h acetic acid-modified ENR50 samples. NMR spectroscopy results showed that functional groups of ester and hydroxyl group compounds were formed in 30-min, 2-h, 7-h, 16-h and 18-h acetic acid-modified ENR50 samples. Less thermally stable segments in acetic acid-modified ENR50 are most probably contributed by these ester and hydroxyl functional groups.

For the initial 0-h sample which made up of epoxide unit and isoprene unit only contribute to a higher value of $T_{d, onset}$ and $T_{d, inflection}$. For 30-min sample, conversion of epoxide group to ester and hydroxyl functional group is not significant yet ($\alpha = 0.06$, Table 3.7). Hence, only one higher value of $T_{d, onset}$ and $T_{d, inflection}$ were observed for 30-min sample TGA thermogram. By using NMR spectroscopy inspection, only 2.9 mol%

of epoxy groups were consumed in 30-min sample for formation of ester and hydroxyl groups as shown in Table 3.7.

1st $T_{d,\ onset}$ showed a decreasing trend from 269 ℃ for 2-h sample to 260 ℃ for 18-h sample. 2nd $T_{d,\ onset}$ showed the similar trend from 372 ℃ for 0-h sample to 358 ℃ for 18-h sample (shown in Figure 3.7 (a)). Hence, formation of acetic acid-modified ENR50 causes $T_{d,\ onset}$ values decrease as reaction time increase.

For 1st and 2nd $T_{d,\ inflection}$ as observed in Table 3.8, the values neither exhibit any increasing or decreasing trend for acetic acid-modified ENR50 samples as shown in Figure 3.7 (b).

For $T_{d,\ 5\%\ wt\ loss}$ recorded for acetic acid-modified ENR50 samples, a decreasing trend observed as reaction time increases. 366 ℃ of $T_{d,\ 5\%\ wt\ loss}$ was observed for 0-h sample and decreases to 280 ℃ for 18-h sample as shown in Figure 3.7 (c). Formation of acetic acid-modified ENR50 causes $T_{d,\ 5\%\ wt\ loss}$ decreases when reaction time increases.

Percentage weight loss of the 1st $T_{d,\ onset}$ and 2nd $T_{d,\ onset}$ for the two-steps thermal decomposition by TGA of acetic acid-modified ENR50 were shown in Table 3.9. 0-h and 30-min acetic acid-modified ENR50 samples do not exhibit two-steps thermal decomposition. These two samples only possess of single decomposition step. On the other hand, 2-h, 7-h, 16-h and 18-h samples possess of two-steps thermal decomposition.

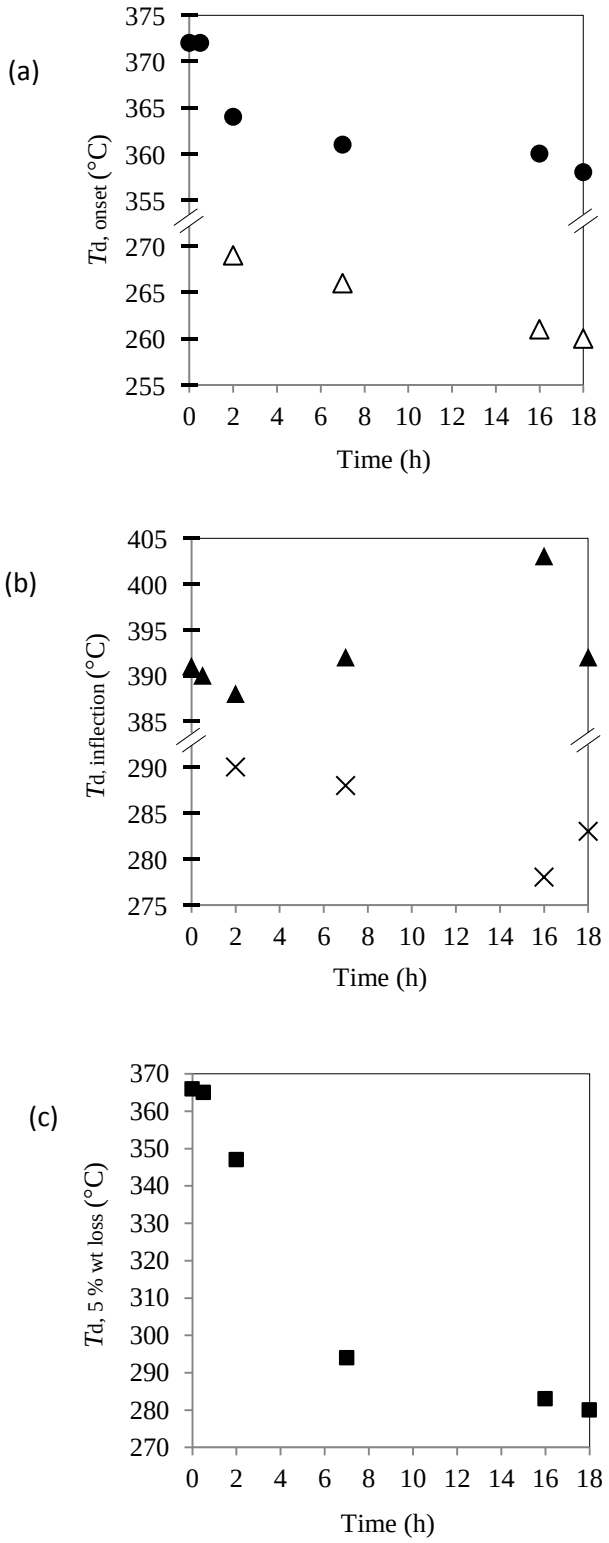

Figure 3.7: Decomposition temperatures of (a) 1st $T_{d,\ onset}$ [Δ], 2nd $T_{d,\ onset}$ [●], (b) 1st $T_{d,\ inflection}$ [×], 2nd $T_{d,\ inflection}$ [▲] and (c) $T_{d,\ 5\%\ wt\ loss}$ [■] for various reaction time of acetic acid-modified ENR50.

Table 3.9: Percentage weight loss of the 1st $T_{d,\ onset}$ and 2nd $T_{d,\ onset}$ for the two-steps decomposition by TGA of various reaction time acetic acid-modified ENR50.

Reaction time (h)	% weight loss for 1st $T_{d,\ onset}$	% weight loss for 2nd $T_{d,\ onset}$
0	-	100
0.5	-	100
2	5	95
7	10	90
16	11	89
18	11	89

For 0-h acetic acid-modified ENR50 sample, this sample is made up of isoprene unit and epoxide unit which is thermally more stable and do not decomposed at a lower temperature. Therefore, during 2nd decomposition step only observed for its 100% decomposition between temperatures of 320-550 ^{o}C. For 30-min sample, there is no 1st decomposition step observed under TGA. This might be due to a small amount of hydroxyl and ester functional groups formed (α = 0.06, Table 3.7) in 30-min sample which could not be detected for its decomposition under TGA analysis.

For 2-h, 7-h and 16-h acetic acid-modified ENR50 samples, the data obtained from 1st decomposition step show ascending values of 5 %, 10 % and 11% respectively. For 18-h acetic acid-modified ENR50 sample shows the similar 1st decomposition step percentage weight loss as with 16-h acetic acid-modified ENR50 sample which is 11%.

As a conclusion, formation of acetic acid-modified ENR50 samples caused the occurrence of less thermally stable compound which was decomposed at a much lower $T_{d,\ onset}$, $T_{d,\ inflection}$ and $T_{d,\ 5\ \%\ wt\ loss}$ compared to ENR50 sample.

3.1.5 DSC analysis

T_gs and delta heat capacity (δC_p) for ENR50 and 18-h acetic acid-modified ENR50 were recorded in Table 3.10. T_g is derived from half of the δC_p value of DSC heat flow curve. T_g for ENR50 sample was observed at -29 ^oC. After chemical modification by acetic acid, 18-h acetic acid-modified ENR50 sample possess a higher T_g, that is 10 ^oC. There are no differences for 1st and 2nd T_g readings for the samples tested.

Table 3.10: T_gs and δC_p for ENR50 and 18-h acetic acid-modified ENR50 samples.

Sample	1st Reading		2nd Reading	
	T_g (℃)	δC_p (J/(g.^{o}C))	T_g (℃)	δC_p (J/(g.^{o}C))
ENR50	-29	0.50	-29	0.49
18-h acetic acid-modified ENR50	10	0.56	10	0.55

ENR50 undergoes chemical modification to form acetic acid-modified ENR50. Epoxide group of ENR50 had been converted to form ester and hydroxyl functional groups. T_g of ENR50 changes from -29 ^oC to 10 ^oC for 18-h acetic acid-modified ENR50. The increase in T_g value is related to the chemical structure of the 18-h acetic acid-modified ENR50.

Formation of intermolecular interactions between neighbouring groups which attached to the acetic acid-modified ENR50 backbone restrict the internal rotational about the backbone. The mobility of polymer chains is affected by the barrier for rotation around the chain backbone to take place (Sanguansap *et al.*, 2005).

Formation of intermolecular hydrogen bondings are possible between –OH groups in acetic acid-modified ENR50 with electronegative atom present in another chain of acetic acid-modified ENR50. Figure 3.1 (b) shows the FTIR spectrum for 18-h acetic acid-modified ENR50 possess a broad band for –OH group in the region of 3200 - 3700 cm^{-1} and it might be due to the intermolecular hydrogen bonding occur between the molecules. The possible intermolecular hydrogen bonding is shown in Figure 3.8. These intermolecular bondings explained the increase of T_g for 18-h acetic acid-modified ENR50. Figure 3.9 (a) shows the picture of ENR50 sample and Figure 3.9 (b) shows the picture of 18-h acetic acid-modified ENR50 sample. ENR50 is flexible and elastic but 18-h acetic acid-modified ENR50 sample was broken into two pieces when bending it. This further confirms that 18-h acetic acid-modified ENR50 sample is brittle and has lot of crosslinkings.

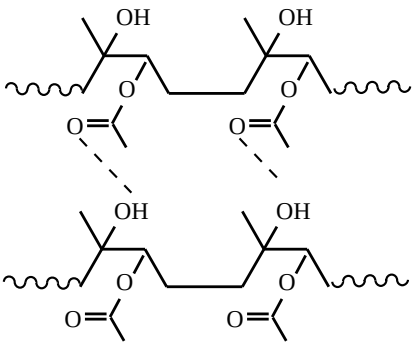

Figure 3.8: Possible intermolecular hydrogen bondings in 18-h acetic acid-modified ENR50 sample.

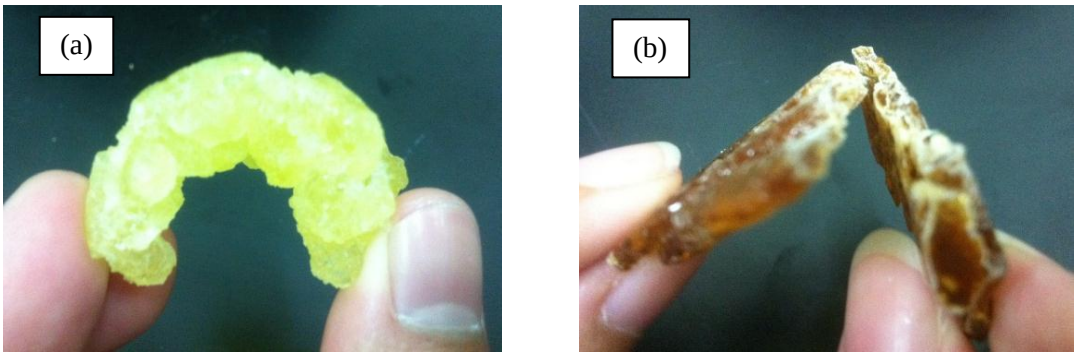

Figure 3.9: Pictures of (a) ENR50 sample and (b) 18-h acetic acid-modified ENR50 sample.

Interpretation and comparison between the results of NMR spectroscopy and DSC instrument are useful in determining the acetic acid modification reaction extent. T_g was enhanced by 39 ^oC in the acetic acid-modified ENR50 as compared to ENR50. The difference of T_g for 0-h and 18-h samples was 39 ^oC. The mol% of epoxide level utilized was 50 mol% from 0-h to 18-h samples. Reaction of 1 mol% of epoxy group leads to an increase in T_g by approximately 0.8 ^oC. This method is used to estimate the extent of acetic acid modification reaction.

3.2 Characterization of PEO

3.2.1 FTIR spectroscopy

FTIR analysis was carried out on neat PEO. The FTIR spectrum for neat PEO is shown in Figure 3.10. Table 3.11 shows the band characteristics for PEO by referring to Bailey & Koleske, 1976. C-H stretching mode can be observed at 2879 cm^{-1}, CH_2 scissoring mode at 1466 cm^{-1}, CH_2 wagging mode at 1341 cm^{-1}, CH_2 twisting mode at 1279 cm^{-1} and 1241 cm^{-1} while CH_2 rocking mode at 959 cm^{-1} and 841 cm^{-1} for PEO. Characteristic peaks of PEO are identified by the present of triplet peak of C-O-C stretching at 1144 cm^{-1}, 1094 cm^{-1} and 1060 cm^{-1} vibrations with maximum peak at 1095 cm^{-1}.

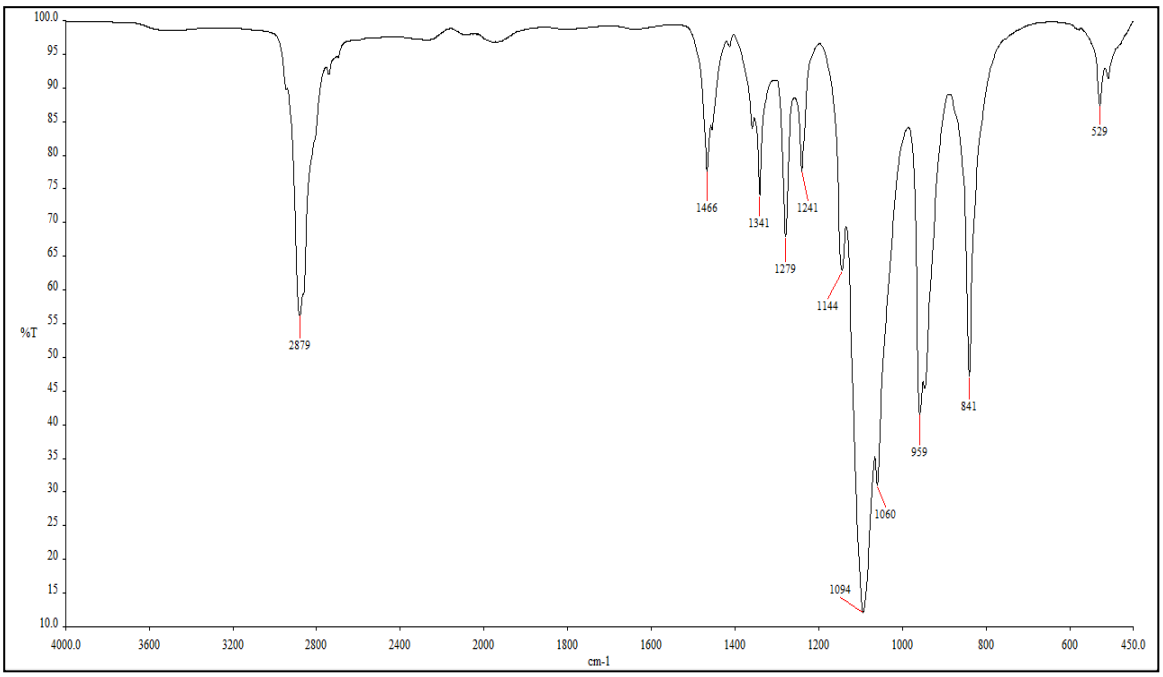

Figure 3.10: FTIR spectrum for neat PEO.

Table 3.11: Band characteristics of PEO for FTIR spectrum.

Wavenumber (cm^{-1})	Assignment	Functional group
2879	C-H stretching	Alkyl
1466	CH_2 scissoring mode	Alkyl
1341	CH_2 wagging mode	Alkyl
1279	CH_2 twisting mode	Alkyl
1241	CH_2 twisting mode	Alkyl
1144	C-O-C stretching	Ether
1094	C-O-C stretching	Ether
1060	C-O-C stretching	Ether
959	CH_2 rocking mode	Alkyl
841	CH_2 rocking mode	Alkyl

3.2.2 ^{1}H NMR spectroscopy

^{1}H NMR spectroscopy was carried out on neat PEO sample before the blending work was carried out. PEO has the chemical shifts of 2.0 ppm and 2.7 ppm as observed in ^{1}H NMR spectrum (refer Figure 3.11). Chemical structure and chemical shift assignments of neat PEO are shown in Figure 3.12.

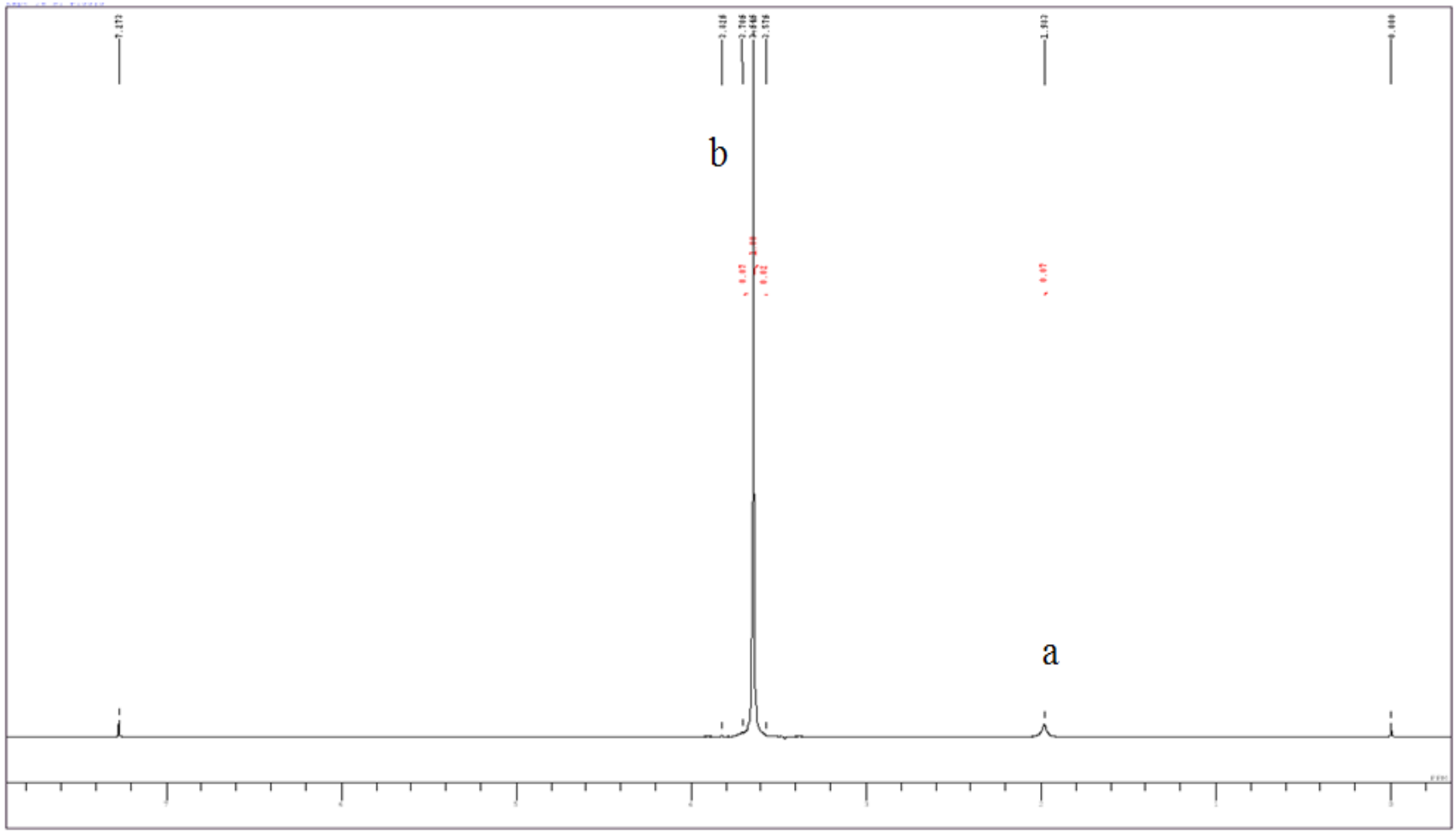

Figure 3.11: ^{1}H NMR spectrum for neat PEO sample.

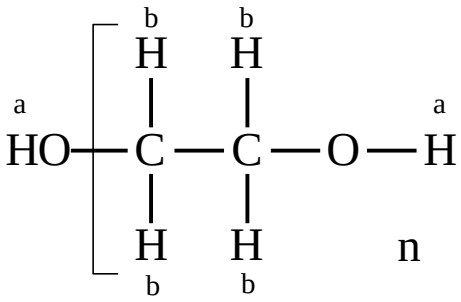

Figure 3.12: Chemical structure and chemical shift assignments for neat PEO.

3.2.3 TGA

TGA analysis was carried out on neat PEO sample. TGA thermogram of neat PEO is shown in Figure 3.13. $T_{d,\ onset}$, $T_{d,\ inflection}$ and $T_{d,\ 5\%\ wt\ loss}$ together with one-step thermal decomposition composition may be derived from thermogram of PEO as shown in Table 3.12.

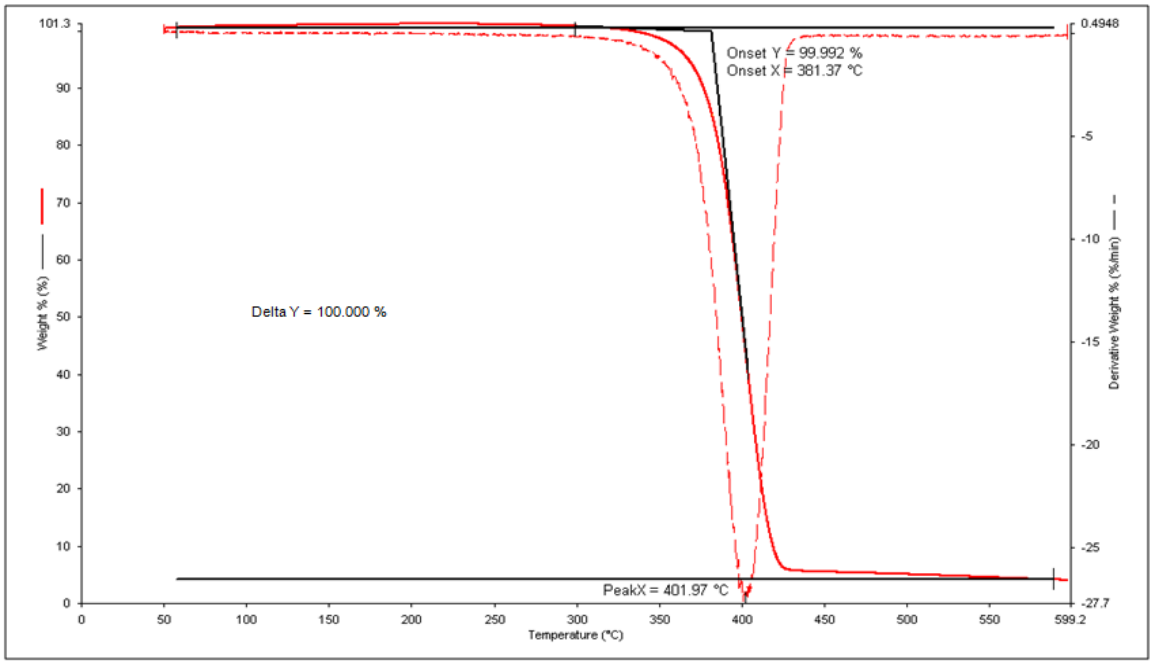

Figure 3.13: TGA thermogram of neat PEO.

Table 3.12: $T_{d,\ onset}$, $T_{d,\ inflection}$, $T_{d,\ 5\%\ wt\ loss}$ and weight percentage decomposition of neat PEO.

Sample	PEO
$T_{d,\ onset}$ (^{o}C)	381
$T_{d,\ inflection}$ (^{o}C)	402
$T_{d,\ 5\%\ wt\ loss}$ (^{o}C)	368
Weight percentage decomposition (wt %)	100

3.2.4 DSC analysis

PEO is a semicrystalline polymer. T_g, T_c, ΔH_c, T_m and ΔH_m are observed for PEO and data are tabulated in Table 3.13. T_g for PEO was observed at -58 ^{o}C and T_m for PEO was 67 ^{o}C with ΔH_m of 135 J g^{-1}. Degree of crystallinity for PEO, X_{PEO} could be calculated from the equation below:

$$\text{Degree of crystallinity for PEO, } X_{PEO} = \frac{\Delta H_m}{W_{PEO} \cdot \Delta H_{m\,ref}} \quad (4)$$

ΔH_m= Melting enthalpy for PEO (J g^{-1})

W_{PEO} = Weight fraction of PEO in the blend

$\Delta H_{m\ ref}$ = Melting enthalpy of 100% crystalline PEO, 188.3 J g^{-1} is adopted from Cimmino *et al*., 1990.

Table 3.13: T_g, T_c, ΔH_c, T_m, ΔH_m and X_{PEO} for neat PEO sample.

PEO	Value
T_g (℃)	-58
T_c (^oC)	45
ΔH_c (J g^{-1})	135
T_m (℃)	67
ΔH_m (J g^{-1})	139
X_{PEO}	0.74

3.3 18-h acetic acid-modified ENR50 and PEO blends

3.3.1 FTIR spectroscopy

FTIR is used to identify the chemical interactions of 18-h acetic acid-modified ENR50 and PEO blends. Identification of functional groups present is carried out by using FTIR spectroscopy on acetic acid-modified ENR50/PEO blends. Comparison of FTIR spectra for neat acetic acid-modified ENR50, neat PEO, acetic acid-modified ENR50/PEO blend 25/75, 50/50 and 75/25 were carried out as shown in Figure 3.14.

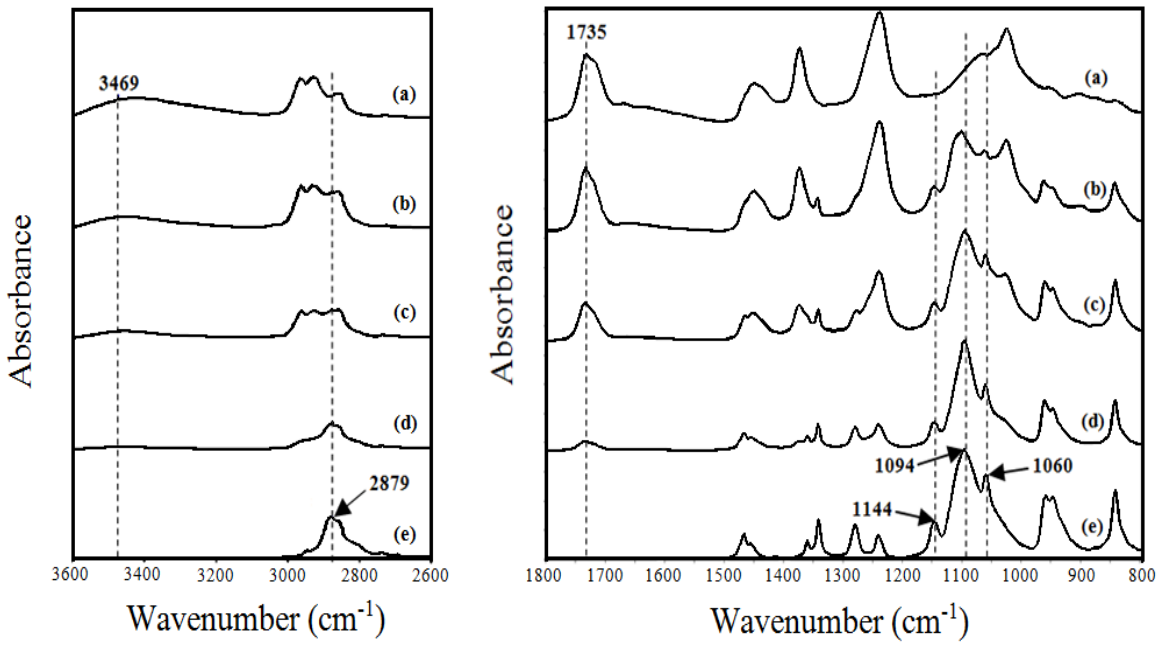

Figure 3.14: FTIR spectra in the region of 800-1800 cm^{-1} and 2600-3600 cm^{-1} for (a) neat acetic acid-modified ENR50; acetic acid-modified ENR50/PEO blend samples: (b) 75/25, (c) 50/50, (d) 25/75; and (e) neat PEO.

There are four basic absorbance band regions could be compared from infra-red absorbance spectra of Figure 3.14. Firstly, the wavenumber at 3469 cm^{-1} corresponds to the hydroxyl functional group (-OH) from acetic acid-modified ENR50 (Gelling, 1988) which becomes more intensified in the blend system when the amount of acetic acid-modified ENR50 increases to 100% as shown in Figure 3.14. There is no change in the band position of –OH group implying that the two blend polymers do not interact with each other.

Secondly, the wavenumber at 2879 cm^{-1} corresponds to the C-H stretching of PEO (Bailey & Koleske, 1976). This absorbance band is clearly observed for neat PEO and acetic acid-modified ENR50/PEO 25/75 blend. The absorbance band for acetic acid-modified ENR50/PEO 50/50 and 75/25 blends overlaps with the methylene group, $–CH_2–$ from acetic acid-modified ENR50. Figure 3.14 shows the absorbance band at

2879 cm^{-1} becomes intensified from acetic acid-modified ENR50/PEO 75/25 sample to acetic acid-modified ENR50/PEO of 0/100 sample.

Thirdly, the absorbance band at wavenumber of 1735 cm^{-1} corresponds to the ester group in acetic acid-modified ENR50 (Gan & Hamid, 1997). This absorbance band is present in acetic acid-modified ENR50/PEO 25/75 blend sample and it becomes more significant as observed in Figure 3.14 when the amount of acetic acid-modified ENR50 increases. The band position and its shape do not change when the amount of PEO increases in the acetic acid-modified ENR50/PEO blend which implies that the two components do not undergoes interaction.

Lastly, the characteristic triplet bands of C-O-C stretching for PEO at wavenumbers of 1060 cm^{-1}, 1094 cm^{-1} and 1144 cm^{-1} with the strong intensity and sharp centre band present in all PEO contained samples (Bailey & Koleske, 1976). Figure 3.14 shows obviously the presence of triplet peaks in PEO for acetic acid-modified ENR50/PEO 75/25 to 25/75 blend samples. The triplet maintains its intensity and shape while the position of the maximum peak slightly shifts from 1094 cm^{-1} to 1099 cm^{-1} for acetic acid-modified ENR50/PEO 75/25 blend. In view of the resolution of the instrument being 4 cm^{-1}, the peak shift is not an indication of any significant interaction between the two constituents of the blend. DSC was used to verify the interactions and miscibility of PEO and acetic acid-modified ENR50 as discussed in section 3.3.3. There is no reduction in intensity of the two shoulders at 1060 and 1144 cm^{-1} implying that crystallinity of PEO remains unchanged with increasing amount of acetic acid-modified ENR50.

From the FTIR spectra observed, there is no significant shifting of absorbance bands as observed in Figure 3.14. Blending of these two polymers is only involves physical interactions and there is no chemical interaction on both the acetic acid-modified ENR50 and PEO constituents.

Further comparison between acetic acid-modified ENR50/PEO blends FTIR spectra with neat polymers is carried out in order to determine the physical mixing of all constituents in the systems. If there is any chemical interactions between acetic acid-modified ENR50 and PEO, shifting of infra-red bands and changes on shape could be easily detected by comparing the FTIR spectra of the neat polymers with the blends by using Spectrum One v5.0.1 software (Perkin Elmer, Beaconsfield, UK). The software is used to compare the generated spectrum with the experimental spectrum in order to obtain matching ratio (*Q*) value of acetic acid-modified ENR50/PEO blends by using calculator function of Spectrum One software.

If $Q = 1$, this points toward no interaction between the constituents in the blend. It is a perfect match between the generated and the experimental spectra. Emerging of new absorption band or shifting of absorption bands or both in FTIR spectrum could be observed provided there is any interaction between the constituents.

If $Q = 0$, it means the generated and experimental spectra are wholly unrelated. This is unlikely to be observed because there are always some small similarities between spectra. We note here, when $Q \geq 0.8$, only physical mixing of all the constituents in the blend (or immiscibility) is assumed.

Mass ratio (*r*) of different constituents in the samples is defined as equation (5) below:

$$\text{Mass ratio}, r = \frac{\text{Mass of the constituent}}{\text{Total mass of the constituents in the sample}} \quad (5)$$

Quantities r values of acetic acid-modified ENR50 and PEO in the blends system are shown below. For acetic acid-modified ENR50/PEO 25/75 blends, 0.125 g of acetic acid-modified ENR50 was blend with 0.375 g of PEO and the total mass of the sample is 0.500 g.

$r_{\text{acetic acid-modified ENR50}} = \frac{0.125\ g}{0.500\ g}$ $r_{\text{PEO}} = \frac{0.375\ g}{0.500\ g}$

$= 0.25$ $= 0.75$

The same calculations are carried out for acetic acid-modified ENR50/PEO blends of 50/50 and 75/25 compositions. The *r* values for the acetic acid-modified ENR50/PEO are summarize in Table 3.14.

Table 3.14: *r* values for acetic acid-modified ENR50/PEO blends system of mass ratio 25/75, 50/50 and 75/25.

Acetic acid-modified ENR50/PEO blend ratio	*r* value for acetic acid-modified ENR50	*r* value for PEO
25/75	0.25	0.75
50/50	0.50	0.50
75/25	0.75	0.25

The mass ratio obtained is used to determine the generated FTIR spectrum in a blend system using the following calculations:

Generated FTIR spectrum for a blend = ($r_{\text{acetic acid-modified ENR50}}$ × experimental FTIR spectrum of acetic acid-modified ENR50) + (r_{PEO} × experimental FTIR spectrum of PEO) (6)

Generated FTIR spectrum was compared with the experimental spectrum in order to obtain *Q* value of acetic acid-modified ENR50/PEO blends by using the calculator function of Spectrum One software. *Q* values of acetic acid-modified ENR50/PEO blends are summarize in Table 3.15. For all blends ratio, quantity $Q \geq 0.8$,

this may suggest that there is only physical interaction between the constituents in the systems.

Table 3.15: Matching ratio (*Q*) for acetic acid-modified ENR50/PEO blends.

Acetic acid-modified ENR50/PEO blends	*Q*
25/75	0.9
50/50	0.8
75/25	0.8

3.3.2 TGA

TGA analysis was carried out on acetic acid-modified ENR50/PEO blend system. Table 3.16 summarizes the $T_{d,\ onset}$, $T_{d,\ inflection}$ and $T_{d,\ 5\%\ wt\ loss}$ for acetic acid-modified ENR50/PEO samples.

Table 3.16: $T_{d,\ onset}$, $T_{d,\ inflection}$ and $T_{d,\ 5\%\ wt\ loss}$ for different ratio of acetic acid-modified ENR50/PEO samples.

Acetic acid-modified ENR50/PEO ratio	$1^{st}\ T_{d,\ onset}$ (℃)	$2^{nd}\ T_{d,\ onset}$ (℃)	$1^{st}\ T_{d,\ inflection}$ (℃)	$2^{nd}\ T_{d,\ inflection}$ (℃)	$T_{d,\ 5\%\ wt\ loss}$ (℃)
0/100	-	381	-	402	368
25/75	260	381	284	410	346
50/50	260	380	282	412	309
75/25	260	375	283	414	272
100/0	260	358	283	389	271

For acetic acid-modified ENR50/PEO 0/100 sample, there is only one $T_{d,\ onset}$ observed at 381 ^{o}C for this sample. While for other samples, there are two $T_{d,\ onset}$s observed. 1st $T_{d,\ onset}$ is observed at a constant value of 260 ^{o}C for all samples containing acetic acid-modified ENR50. Hence, 1st $T_{d,\ onset}$ is solely contributed by acetic acid-modified ENR50 but not PEO. 2nd $T_{d,\ onset}$ shows a decreasing trend as the amount of PEO decreases in the blend. This is due to 2nd $T_{d,\ onset}$ is contributed by both PEO and also acetic acid-modified ENR50. The 2nd $T_{d,\ onset}$ reported by acetic acid-modified ENR50 itself is 358 ^{o}C. As the amount of acetic acid-modified ENR50 increases in the blend samples, it causes 2nd $T_{d,\ onset}$ to decrease. The presence of less thermally stable acetic acid-modified ENR50 causes the blend samples show lower $T_{d,\ onset}$. 1st and 2nd $T_{d,\ onset}$ of the blend samples are shown in Figure 3.15 (a).

Only one higher $T_{d,\ inflection}$ is being observed for acetic acid-modified ENR50/PEO 0/100. For other blend ratio samples, there are two $T_{d,\ inflection}$s recorded. The 1st $T_{d,\ inflection}$ observed is quite stable which is in the range of 282 - 284 ^{o}C for all range of samples. For 2nd $T_{d,\ inflection}$, these values are contributed by acetic acid-modified ENR50 and PEO. The 2nd $T_{d,\ inflection}$ is in the range of 389 to 414 ^{o}C. 1st and 2nd $T_{d,\ inflection}$ do not exhibit any significant variation for the acetic acid-modified ENR50/PEO blend samples as shown in Figure 3.15 (b).

$T_{d,\ 5\%\ wt\ loss}$ shows a decreasing trend as the amount of PEO in blend samples decreases which is shown in Figure 3.15 (c). $T_{d,\ 5\%\ wt\ loss}$ of 368 ^{o}C was recorded for acetic acid-modified ENR50/PEO 0/100 sample and the value decreases to 271 ^{o}C for acetic acid-modified ENR50/PEO 100/0 sample. Acetic acid-modified ENR50/PEO 0/100 sample is thermally more stable than acetic acid-modified ENR50/PEO 100/0 sample.

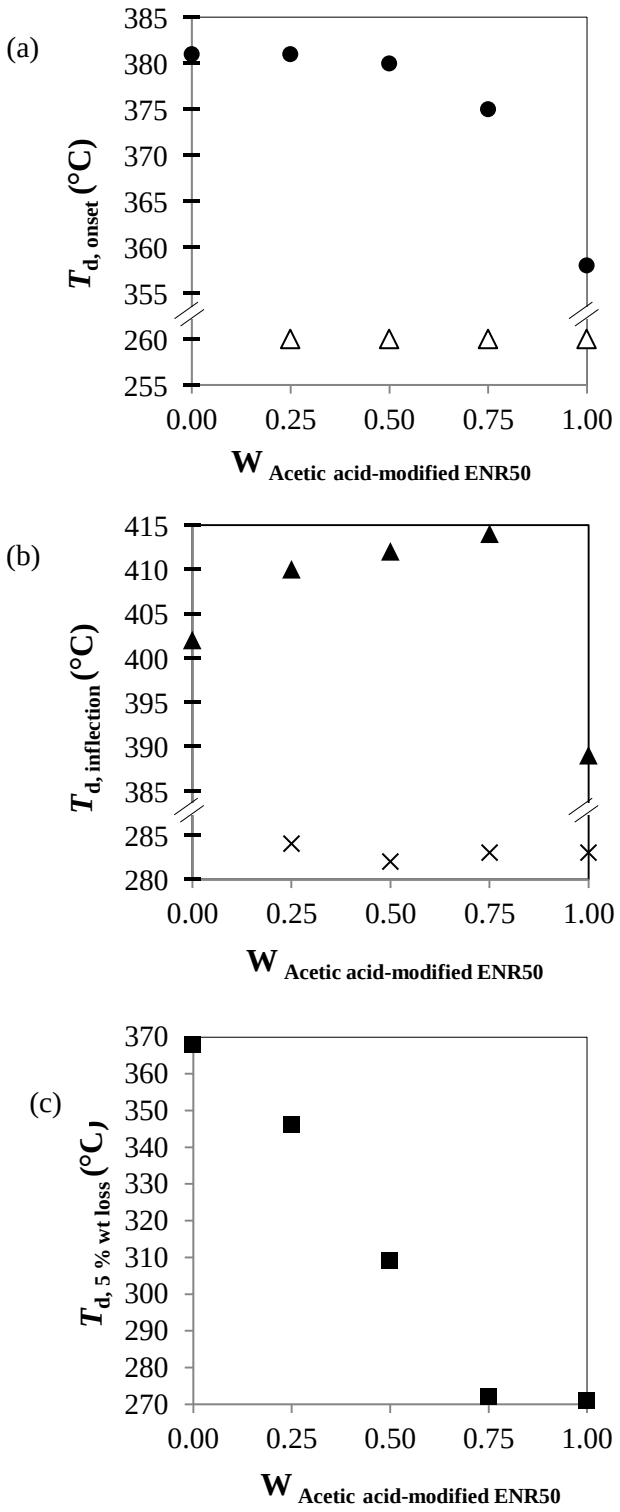

Figure 3.15: Decomposition temperatures of (a) 1st $T_{d,\ onset}$ [Δ], 2nd $T_{d,\ onset}$ [●], (b) 1st $T_{d,\ inflection}$ [×], 2nd $T_{d,\ inflection}$ [▲] and (c) $T_{d,\ 5\%\ wt\ loss}$ [■] for various reaction times of acetic acid-modified ENR50.

From TGA analysis, percentage weight of different decomposition steps is recorded. For acetic acid-modified ENR50/PEO 0/100 sample, it proceeds with one-step thermal decomposition whereas two-steps thermal decomposition is observed for other blend samples. Weight percentages for the 1st and 2nd decomposition steps of acetic acid-modified ENR50 are tabulated in Table 3.17.

Table 3.17: Weight percentages for the 1st and 2nd decomposition steps of acetic acid-modified ENR50.

Acetic acid-modified ENR50/PEO mass ratio	$W_{\text{Acetic acid-modified ENR50}}$	Weight percentage of 1st decomposition step (%)	Weight percentage of 2nd decomposition step (%)
0/100	0.00	-	100
25/75	0.25	2	98
50/50	0.50	5	95
75/25	0.75	8	92
100/0	1.00	11	89

From Table 3.17, as the amount of acetic acid-modified ENR50 increases in the blends, the weight percentage of 1st decomposition step increases as well. Acetic acid-modified ENR50 contained blends are less thermally stable and exhibit two decomposition steps.

3.3.3 DSC analysis

T_gs for neat polymers and 18-h acetic acid-modified ENR50/PEO blends were obtained from DSC analysis using Universal Analysis 2000 software (version 4.5A, TA Instruments, USA).

T_g of acetic acid-modified ENR50/PEO 0/100 is -58 ^oC whereas the T_g of acetic acid-modified ENR50/PEO 100/0 is 10 ^oC. For samples of acetic acid-modified ENR50/PEO 25/75, 50/50 and 75/25, there are two T_gs observed and the values are recorded in Table 3.18. There are two T_gs observed for the blend which correspond to the neat constituents of acetic acid-modified ENR50 and PEO. This may indicate the immiscibility of the blends.

Table 3.18: 1st and 2nd T_gs for acetic acid-modified ENR50/PEO blend samples.

Acetic acid-modified ENR50/PEO mass ratio	1st T_g (^oC)	2nd T_g (^oC)
0/100	-58	-
25/75	-58	9
50/50	-58	10
75/25	-59	9
100/0	-	10

PEO is a semicrystalline polymer, therefore T_m and ΔH_m could be observed as recorded in Table 3.19. T_m of PEO for acetic acid-modified ENR50/PEO 0/100 sample is 67 ^oC whereas for acetic acid-modified ENR50/PEO 25/75 sample is 66 ℃. T_m of acetic acid-modified ENR50/PEO 50/50 and 75/25 are 62 ^oC and 58 ^oC, respectively. These two acetic acid-modified ENR50/PEO systems have slightly lower T_m value. This may be due to the disturbance of acetic acid-modified ENR50 on the growing PEO

spherulites as shown in Figure 3.19 (c) for 50/50 blend (Chan *et al.*, 2011), even though PEO is immiscible with acetic acid-modified ENR50. If acetic acid-modified ENR50 causes disturbance to the PEO spherulites, then lower radial growth rate of PEO spherulites is expected and this is in agreement to results shown in Figure 3.18. ΔH_m of PEO is used to calculate X_{PEO} which tabulated in Table 3.19. X_{PEO} could be calculated from equation (3).

Table 3.19: T_m, ΔH_m and X_{PEO} for acetic acid-modified ENR50/PEO blend samples.

Acetic acid-modified ENR50/PEO ratio sample	T_m (^oC)	ΔH_m (J g^{-1})	X_{PEO}
0/100	67	139	0.74
25/75	66	94	0.67
50/50	62	49	0.52
75/25	58	8	0.17
100/0	-	-	-

There is no 100 % crystalline structure of PEO can be observed. That is only applied to ideal case where all the PEO chains are aligned in a parallel form. The X_{PEO} values decrease from acetic acid-modified ENR50/PEO 0/100 to 75/25 blend samples. Acetic acid-modified ENR50/PEO 50/50 and 75/25 blend samples have a much lower X_{PEO} values. The PEO spherulites in blend samples are disturbed by the second component in the blends.

3.3.4 POM analysis

Phase behavior and morphology of a semicrystalline/amorphous blend depend strictly on its composition, chemical nature of components and interaction between components (Smith & Andries, 1974).

The radial growth rate (G) of PEO spherulites in acetic acid-modified ENR50/PEO system was determined by POM. Morphology of growing spherulites for acetic acid-modified ENR50/PEO blend was observed at T_c = 49 ^oC with appropriate intervals of time for all compositions. The spherulite diameter for each micrograph was estimated by using Q Win software as shown in Figure 3.16. No crystallization of PEO can be observed for acetic acid-modified ENR50/PEO 75/25 blend at 49 ℃ after 1 h.

Table 3.20 exhibits the estimation of radius of growing spherulites, R, from the PEO growing spherulites diameter measurements with time interval, 15 s, for acetic acid-modified ENR50/PEO 50/50 at T_c = 49 ^oC. It is found that R values increase linearly with time as shown in Figure 3.17. G of PEO spherulites are extracted from the gradient of radius versus time plot.

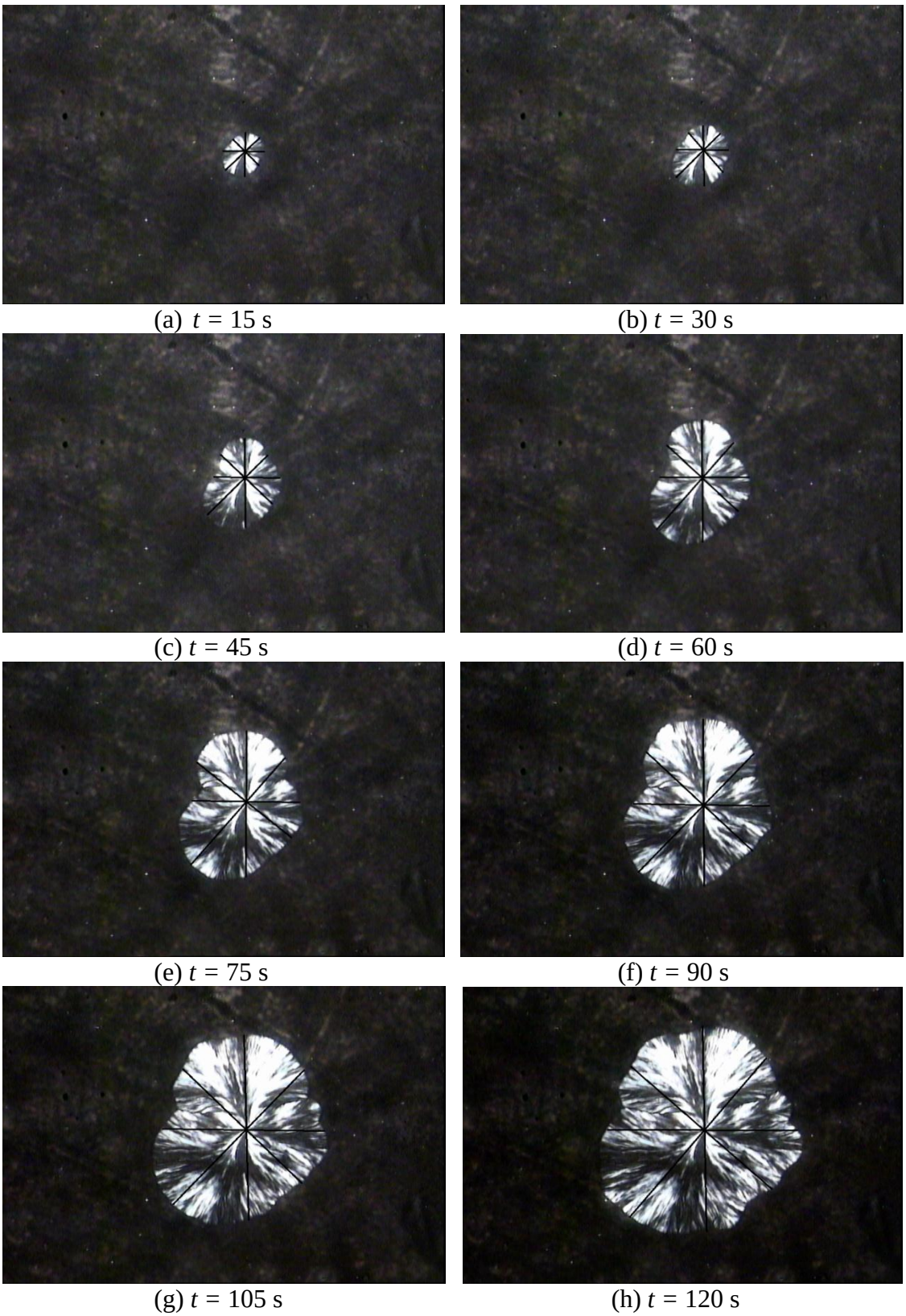

(a) t = 15 s (b) t = 30 s

(c) t = 45 s (d) t = 60 s

(e) t = 75 s (f) t = 90 s

(g) t = 105 s (h) t = 120 s

Figure 3.16: Micrographs of PEO growing spherulites for the blend of acetic acid-modified ENR50/PEO 50/50 at T_c = 49 ^{o}C for different time interval (t). (Magnification: 5 ×).

Table 3.20: Measurement of diameter and radius for the growing spherulites with time interval of 15 s for acetic acid-modified ENR50/PEO 50/50 blend at T_c = 49 ^{o}C.

		TIME INTERVAL, *t* (s)									
		15	30	45	60	75	90	105	120	135	150
d (μm)	1	133.23	184.56	229.27	278.26	297.78	351.06	383.91	426.53	467.21	516.58
	2	117.68	162.83	183.41	236.94	261.54	319.73	347.59	398.41	428.95	478.02
	3	128.79	184.27	216.30	270.33	295.62	346.44	372.04	425.96	461.84	502.41
	4	119.45	164.96	192.26	246.83	265.89	347.89	378.16	427.62	469.72	512.63
$\bar{d}$ (μm)		124.79	174.16	205.31	258.09	280.21	341.28	370.43	419.63	456.93	502.41
s (μm)		7.45	11.88	21.17	19.41	19.15	14.50	15.98	14.16	18.94	17.32
R (μm)		62.39	87.08	102.66	129.05	140.10	170.64	185.21	209.82	228.47	251.21

Abbreviations used in following discussion:

d = diameter for growing PEO spherulite (μm)

$\bar{d}$ = mean of diameter for growing PEO spherulite (μm)

s = standard deviation (μm)

R = radius for growing PEO spherulite (μm)

n = number of micrograph captured

c= correlation coefficient

s_x = standard deviation for *x* value [time (s)]

s_y = standard deviation for *y* value [radius (μm)]

G = radial growth rate (μm/s)

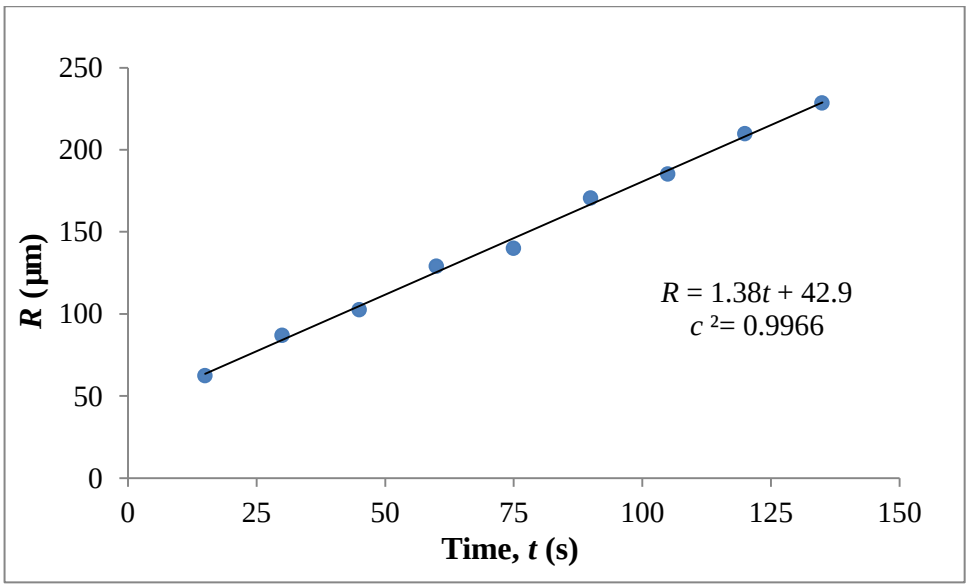

Figure 3.17: Radius of PEO growing spherulites as the function of time for acetic acid-modified ENR50/PEO 50/50 blend at T_c = 49 ^{o}C.

G for acetic acid-modified ENR50/PEO 50/50 at T_c = 49 ^{o}C was extracted from gradient of the linear curve in Figure 3.17. Quantity *G* in this case is 1.38 µm /s.

For a linear regression, the statistical errors for the slope can be calculated as follows

Let the equation be $y = a + bx$ (7)

Then the error for the slope is given by:

$$|\bar{b} - b| < (t_{0.95,\, n-2}) \bullet \left[\frac{S_y\sqrt{1-c^2}}{S_x\sqrt{n-2}}\right] \quad (8)$$

$|\bar{b} - b|$ = The errors for b

$t_{0.95, n-2}$ = The measure of 2-tailed student's t-test distribution that the experimental values are situated in a confidence interval of 95%.

n = The number of data

s_y = Standard deviation of y value

s_x = Standard deviation of x value

c = Correlation coefficient

Estimation of statistical errors for quantity G for acetic acid-modified ENR50/PEO 50/50 at T_c = 49 ^oC is demonstrated as follow:

n = 9

c = 0.9983

c^2 = 0.9966

$\sqrt{1-c^2}$ = 0.058

s_x = 41.08 s

s_y = 56.66 μm

$\sqrt{n-2}$ = 2.65

$\sqrt{\sum_{i=1}^{n} x_i^2}$ = 253.23 s

G = 1.38 μm/s (From the gradient of linear curve R versus t)

$$|\bar{G} - G| < (2.36) \bullet \left[\frac{(56.66)(0.058)}{(41.08)(2.65)}\right]$$

$$< 0.071$$

ΔG = 0.07 μm/s

Therefore, $G = 1.38 \pm 0.07$ μm/s

In all blends, G show increasing values at T_c = 49 ^oC when ascending content of PEO in polymer blends as shown in Figure 3.18. The rate of crystallization and

equivalently the spherulite growth rate of PEO decrease with ascending acetic acid-modified ENR50 content.

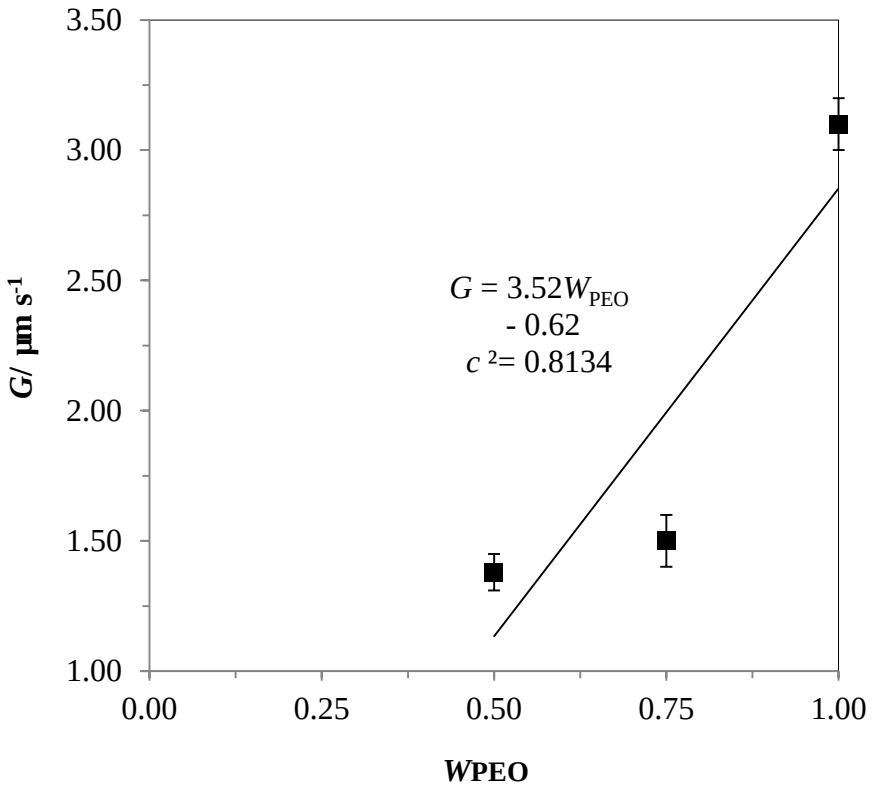

Figure 3.18: The radial growth rate of PEO spherulites, as a function of weight fraction of PEO for acetic acid-modified ENR50/PEO blends at T_c = 49 ^{o}C.

For the blends of acetic acid-modified ENR50/PEO, morphology of PEO spherulites are observed at T_c = 49 ^{o}C (as shown in Figure 3.19).

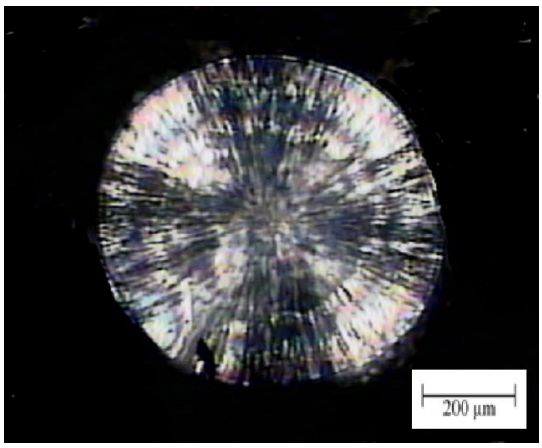

(a) Acetic acid-modified ENR50/PEO 0/100

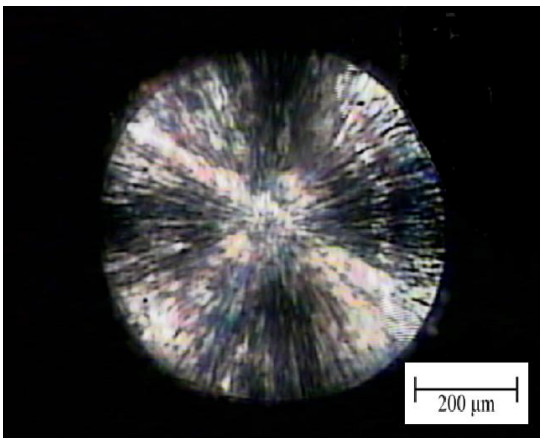

(b) Acetic acid-modified ENR50/PEO 25/75

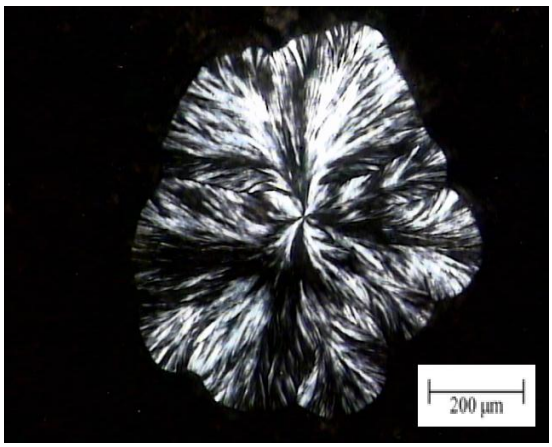

(c) Acetic acid-modified ENR50/PEO 50/50

Figure 3.19: Micrographs of PEO growing spherulites for the blends of acetic acid-modified ENR50/PEO (a) 0/100, (b) 25/75 and (c) 50/50 samples at T_c = 49 ^{o}C. (Magnification: 5 ×).

Fibrillar texture of spherulites could be observed for samples of acetic acid-modified ENR50/PEO 0/100 and 25/75. When the content of acetic acid-modified ENR50 increases, the fibrous texture becomes slightly less obvious for PEO spherulites of acetic acid-modified ENR50/PEO 50/50 blend system. PEO spherulites of acetic acid-modified ENR50/PEO 50/50 sample are slightly disturbed under POM observation. This is supported by *G* of PEO spherulites value in acetic acid-modified ENR50/PEO 50/50 which is much lower than the other two blend samples.

Spherulites of acetic acid-modified ENR50/PEO 50/50 were shown less regular structure which caused by coarseness of crystalline fibrillar compare to neat PEO. Addition of acetic acid-modified ENR50 reduces the crystallinity of PEO, therefore increases the amorphous region as observed from the appearance of dark regions in the blend.

3.4 Thermal behaviour and morphology of ENR50/PEO and acetic acid-modified ENR50/PEO blends

3.4.1 T_gs of ENR50/PEO and acetic acid-modified ENR50/PEO blends

T_gs of the PEO blends, measured in heating cycle are depicted in Figure 3.20. Two T_gs which corresponding to the neat constituents was found for all blends and this shows the immiscibility of the constituents. T_gs of ENR50/PEO blends were taken from Chan *et al*., (2011) as a comparison value.

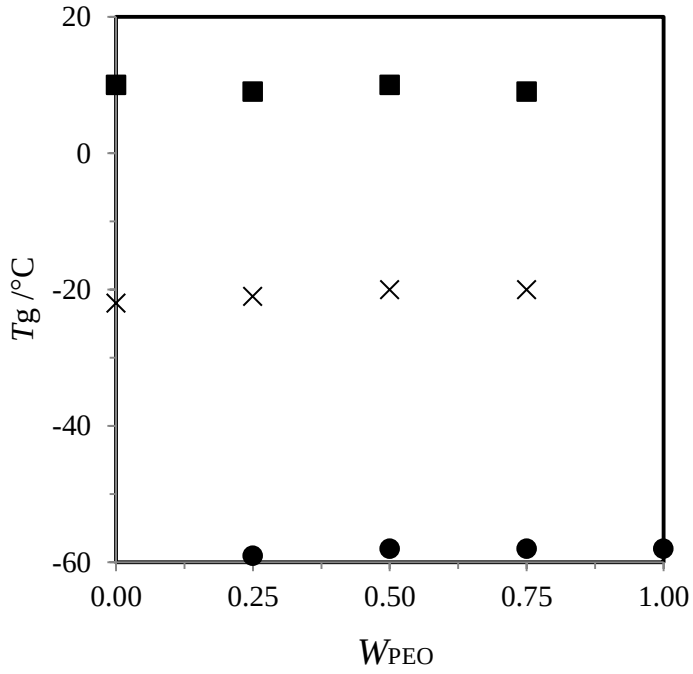

Figure 3.20: T_g of (●) PEO and its blends with (■) acetic acid-modified ENR50 and (×) ENR50.

3.4.2 Radial growth rate (*G*) of PEO and blend morphologies

The *G* value of PEO spherulites in acetic acid-modified ENR50/PEO system was determined by POM whereas the *G* value of PEO spherulites in ENR50/PEO was extracted from Chan *et al*., (2011). *G* value of PEO spherulites in both systems are shown in Figure 3.21. The spherulite diameter for each micrograph was estimated by using the software. For all ENR50/PEO blends show a higher *G* value for PEO spherulites whereas the acetic acid-modified ENR50/PEO blends exhibit a lower spherulites growth rate. Lower crystallization rates were observed for the acetic acid-modified ENR50/PEO blends.

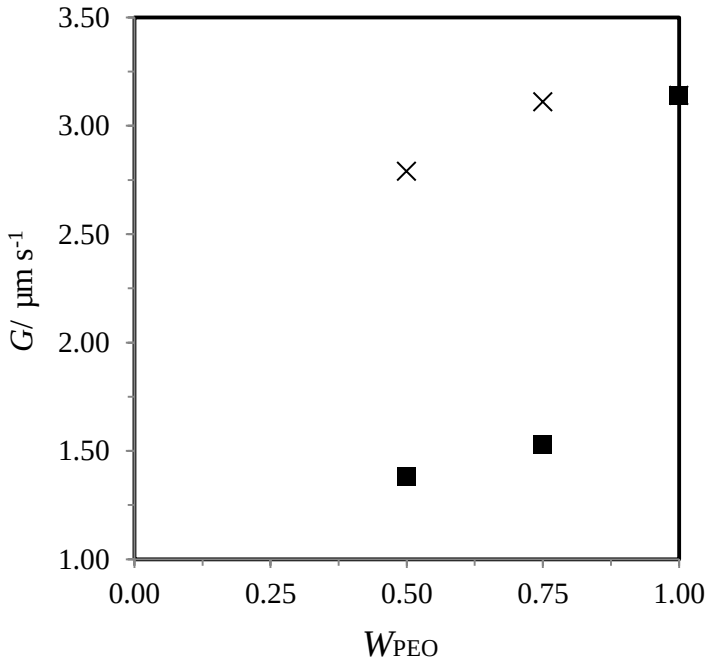

Figure 3.21: Radial growth rates of spherulites for the blend of PEO with (■) acetic acid-modified ENR50 and (×) ENR50.

For the blend of ENR50/PEO, morphology of PEO spherulites at 49 ^{o}C was obtained from Chan *et al.*, (2011) and shown in Figure 3.22. Fibrillar texture of spherulite can be observed for blend of ENR50/PEO 50/50. The fibrous texture becomes slightly less obvious and disturbed for PEO spherulites of acetic acid-modified ENR50/PEO 50/50 as shown in Figure 3.23. Spherulite of acetic acid-modified ENR50/PEO 50/50 blend was shown less regular structure which caused by coarseness of crystalline fibrillar.

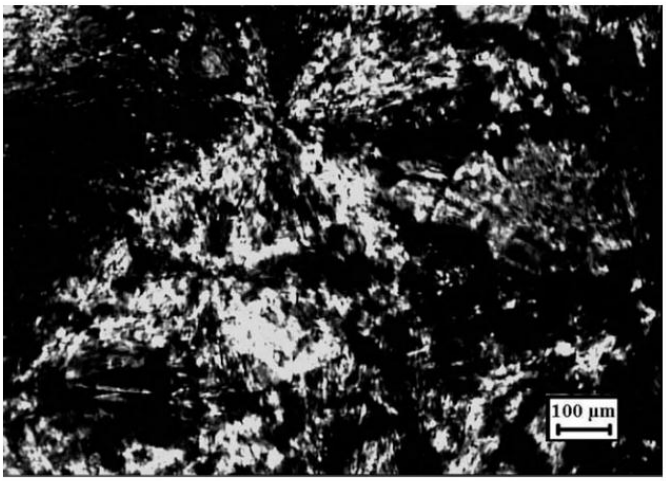

Figure 3.22: Morphology in ENR50/PEO 50/50 blend; the micrograph was taken at 49 ℃ after crystallizing the sample for 60 min. (Magnification: 5 ×).

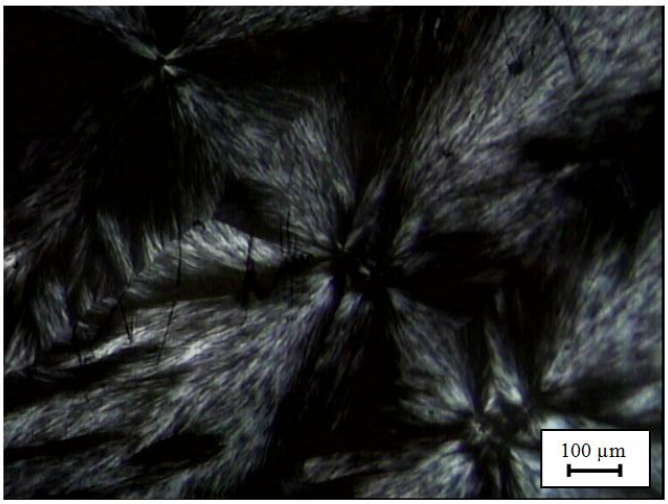

Figure 3.23: Morphology in acetic acid-modified ENR50/PEO 50/50 blend; the micrograph was taken at 49 ℃ after crystallizing the sample for 60 min. (Magnification: 5 ×).

3.5 Conductivity

Impedance analysis was carried out on ENR50/PEO/$LiClO_4$, acetic acid-modified ENR50/PEO and acetic acid-modified ENR50/PEO/$LiClO_4$ blend films at 30 ^oC. The ionic conductivity values were calculated using $\sigma = L/(R_bS_a)$ as described in section 2.6. An example of impedance plot with calculation is demonstrated in Figure 3.24. The R_b value for each sample was obtained from the real axis of an impedance plot. The thickness (L) is an average of four measurements taken at four different positions that were in contact with the stainless steel disk electrodes while S_a = 3.142 cm^2 denotes the surface area of the block electrode. Four impedance measurements were measured for each sample and the average σ value was applied for the following discussion.

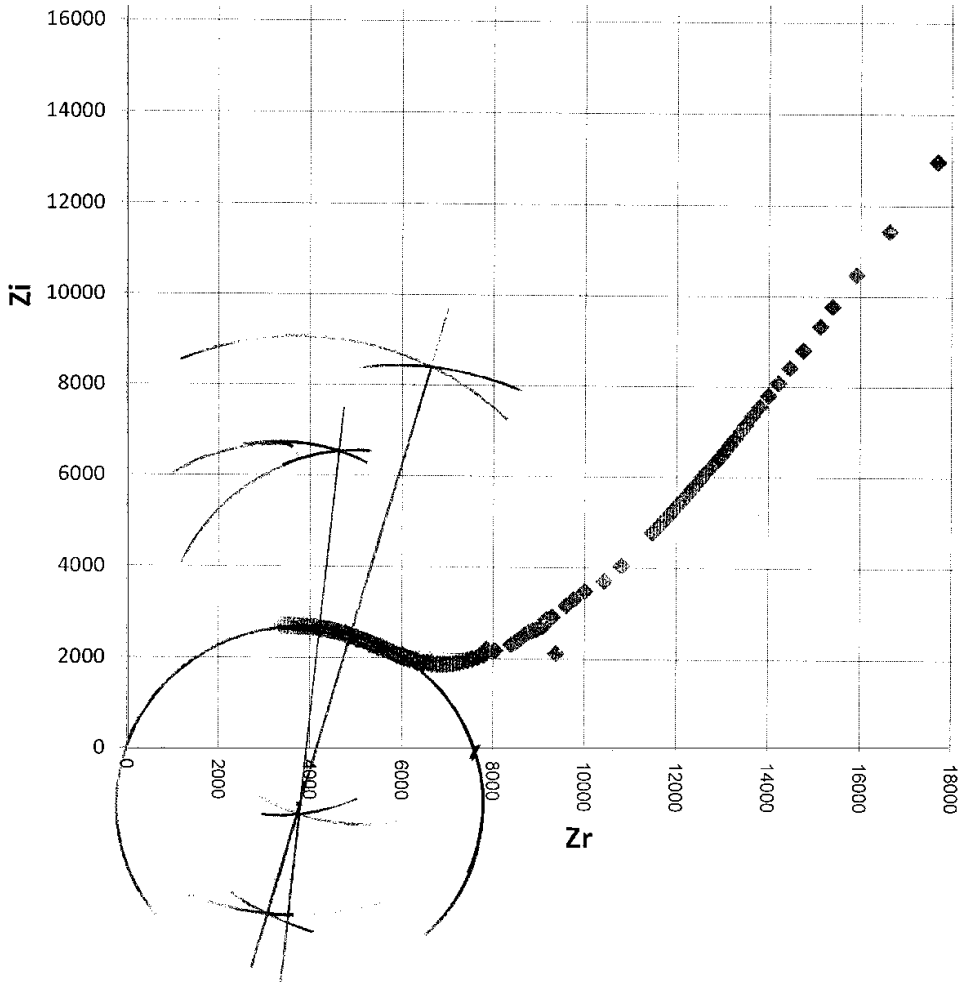

Figure 3.24: Impedance plot for acetic acid-modified ENR50/PEO/$LiClO_4$ 75/25/12 blend.

Example of ionic conductivity (σ) calculation for acetic acid-modified ENR50/PEO/$LiClO_4$ 75/25/12 blend:

Frequency: 100 Hz to 1 MHz

Thickness of film, L: 0.051 cm

Diameter of electrode: 2.0 cm

Surface area of film or electrode, S_a $= \pi r^2$

$= (3.142)(1.0\ cm)^2$

$= 3.142\ cm^2$

Bulk electrolyte resistance, R_b = x-intercept of impedance plot (as shown in Figure 3.24)

$= 6000\ \Omega + [(1.15\ cm/1.45\ cm) \times 2000\ \Omega]$

$= 7586\ \Omega$

Conductivity, σ $= L/(R_b S_a)$

$= 0.051\ cm / (7586\ \Omega \times 3.142\ cm^2)$

$= 2.14 \times 10^{-6}\ S\ cm^{-1}$

The conductivity results for ENR50/PEO/$LiClO_4$, acetic acid-modified ENR50/PEO and acetic acid-modified ENR50/PEO/$LiClO_4$ blends are depicted in Figure 3.25. Conductivity of ENR50/PEO/$LiClO_4$, acetic acid-modified ENR50/PEO and acetic acid-modified ENR50/PEO/$LiClO_4$ blends increase with increasing weight fraction of PEO in the blend as observed from this study. The ether group in the PEO polymer structure plays a major role to solvate the Li cation significantly as the weight fraction of PEO in the blend increases.

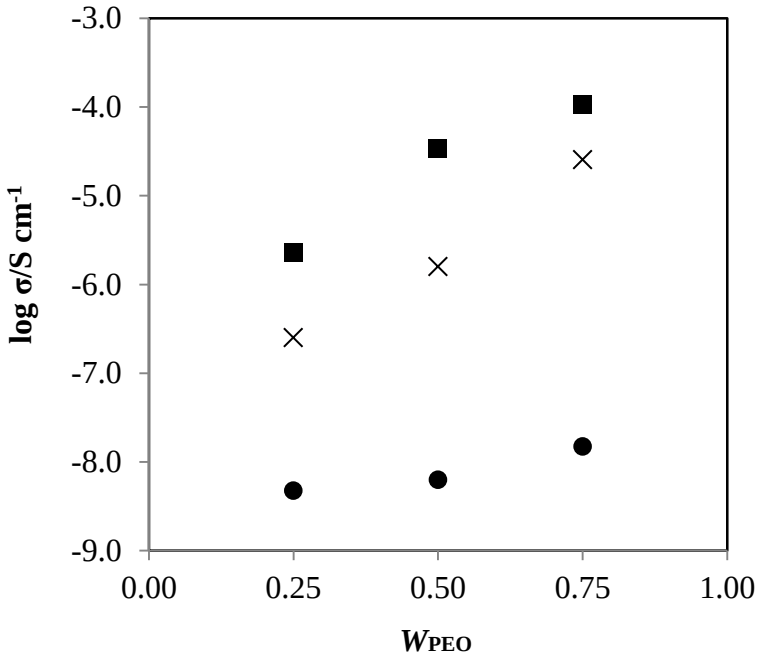

Figure 3.25: Conductivity as a function of weight fraction of PEO for (●) acetic acid-modified ENR50/PEO, (■) acetic acid-modified ENR50/PEO/$LiClO_4$ and (×) ENR50/PEO/$LiClO_4$.

Acetic acid-modified ENR50/PEO blend samples exhibit the conductivity in the range of 10^{-9} to 10^{-8} S cm^{-1}. These blend samples do not contain $LiClO_4$ salt and exhibit a lower conductivity values compare to the same blend composition with lithium salt.

For acetic acid-modified ENR50/PEO/$LiClO_4$ blend, this system shows better conductivity property compare to the ENR50/PEO/$LiClO_4$ blends at 30 ^oC. It was observed that as the weight fraction of PEO increases, the conductivity values for acetic acid-modified ENR50/PEO/$LiClO_4$ blend increase in the same manner. Acetic acid-modified ENR50/PEO/$LiClO_4$ 25/75/12 exhibits the highest conductivity value of 1.07 $\times 10^{-4}$ S cm^{-1} followed by 3.45 $\times 10^{-5}$ S cm^{-1} for 50/50/12 sample and 2.32 $\times 10^{-6}$ S cm^{-1} for 75/25/12 sample. Molecular structure of acetic acid-modified ENR50 has higher polarity compared to ENR50 which probably have more coordination sites for Li cation

salvation (Glasse *et al.*, 2002). Thus, it resulted in improved conductivity for acetic acid-modified ENR50/PEO/$LiClO_4$ blend.

At 30 ^{o}C, the ionic conductivity is 2.56 $\times 10^{-5}$ S cm^{-1} for ENR50/PEO/$LiClO_4$ 25/75/12 blend. For ENR50/PEO/$LiClO_4$ 50/50/12 blend, the conductivity is 1.60 $\times 10^{-6}$ S cm^{-1} followed by 75/25/12 sample with conductivity value of 2.53 $\times 10^{-7}$ S cm^{-1}.

Polarity of the materials used for solid polymer electrolyte is one of the key factors for attaining high ionic conductivity and only polymers possessing high dipole moments are suitable candidates. By considering these factors, acetic acid-modified ENR50 has fulfilled the above criteria to serve the function of polymer electrolyte for potential use in lithium batteries (Chan & Kammer, 2008; Idris *et al.*, 2001, Noor *et al.*, 2010).

CHAPTER 4

CONCLUSION

4.1 Summary

ENR50 was used as a starting material for chemical reaction with acetic acid. Acetic acid-modified ENR50 was successfully synthesized from ENR50. Different characterization methods were employed to identify the structure and thermal behaviour of acetic acid-modified ENR50 formed such as FTIR, NMR, TGA, DSC and GPC.

Acetic acid-modified ENR50/PEO blend with different sample ratio were prepared using solution casting method. DSC was used to determine the T_gs of the blends to verify the miscibility of the blend samples. POM was used to estimate the spherulite growth rates and to study the morphologies of the blends.

4.1.1 Formation of acetic acid-modified ENR50

Chemical modification of ENR50 was carried out with present of acetic acid. Acetic acid-modified ENR50 was successfully synthesized from ENR50. Epoxide level of ENR50 reduces and it was substituted by ester and hydroxyl groups. ^{1}H NMR results were with good agreements with FTIR. Formation of hydroxyl group could be observed in chemical shifts of ^{1}H NMR spectrum as well. Formation of acetic acid-modified ENR50 causes $T_{d,\ onset}$ and $T_{d,\ 5\%\ wt\ loss}$ decrease to lower temperature compared to ENR50. T_g of ENR50 is -29 ^{o}C and T_g of 18-h acetic acid-modified ENR50 is 10 ^{o}C. Reaction of 1 mol% of epoxy group leads to an increase in T_g by 0.8 ^{o}C.

4.1.2 Polymer blends of acetic acid-modified ENR50/PEO

Physical mixing of all constituents in system with comparison of acetic acid-modified ENR50/PEO blends and neat polymers were analyzed using FTIR. From the matching ratio obtained, it showed that there is only physical mixing of all constituents. TGA analysis reveals that as the amount of PEO decreases in the blends, 1st $T_{d,\ onset}$ remained the same value but 2nd $T_{d,\ onset}$ decreases down the trend. $T_{d,\ 5\%\ wt\ loss}$ also decreases as in ascending content of acetic acid-modified ENR50 in the blend system. For DSC analysis, two T_gs which correspond to neat polymers in the blend system were observed. These two T_gs serve as a strong indication for the immiscibility between PEO and acetic acid-modified ENR50. Melting enthalpies of PEO for acetic acid-modified ENR50/PEO blend also decrease as in descending content of PEO. The spherulite growth rate of PEO decreases with descending PEO content. The fibrillar texture of PEO becomes irregular and coarse when the amount of acetic acid-modified ENR50 in the blend increases. The morphologies studies of blend system by POM further confirm the immiscibility of the two neat polymers. As the weight fraction of PEO increases, the conductivity values for acetic acid-modified ENR50/PEO/$LiClO_4$ blend increase in the same manner. The ionic conductivity was found to increase with the weight fraction of PEO in the acetic acid-modified ENR50/PEO/$LiClO_4$ blend and it shows the maximum value of 1.07×10^{-4} S cm^{-1} for 25/75/12 blend at 30 ^oC. Acetic acid-modified ENR50/PEO/$LiClO_4$ blend shows better conductivity property compare to the conventional ENR50/PEO/$LiClO_4$ blends at 30 ^oC. Molecular structure of acetic acid-modified ENR50 has higher polarity compared to ENR50 which probably have more coordination sites for Li cation salvation and resulted in improved conductivity for acetic acid-modified ENR50/PEO/$LiClO_4$ blend.

4.2 Suggestions for future works

Mechanical properties of acetic acid-modified ENR50/PEO blends could be determined as well to determine tensile strength, tear properties, modulus, elongation at break and etc.

REFERENCES

Acosta, J. L., & Morales, E. (1996). Structural, morphological and electrical characterization of polymer electrolytes based on poly(ethylene oxide)/poly(propylene oxide) blends. *Solid State Ionics, 85*, 85-90.

Bailey, F. E., & Koleske, J. V. (1976). *Poly(ethylene oxide).* New York: Academic Press.

Baker, C. S. L., Gelling, I. R., & Newell, R. (1985). Epoxidised natural rubber. *Rubber Chemistry and Technology, 58*, 67-85.

Baker, C. S. L., Gelling, I. R., & Samsuri, A. (1986). Epoxidised natural rubber. *Journal of Natural Rubber Research, 1*, 135-144.

Billmeyer, F. W. (1971). *Textbook of Polymer Science* (2nd ed.). New York: Wiley Interscience.

Blanton, T. N., Majumdar, D., Kress, R. J., & Schwark, D. W. (2003). Reduced crystallinity polyethylene oxide with intercalated clay. US Patent 6555610.

Boon, J. & Aczue, J. M. (1968). *Journal of Polymer Science, 6*, 885.

Bradbury, J. H., & Perera, M. C. (1985). Epoxidation of natural rubber studied by NMR spectroscopy. *Journal of Applied Polymer Science, 30*, 3347-3364.

Chan, C. H., & Kammer, H. W. (2008). Properties of solid solutions of poly(ethylene oxide)/epoxidized natural rubber blends and $LiClO_4$. *Journal of Applied Polymer Science, 110*(1), 424-432.

Chan, C. H., Ismail, J., & Kammer, H. W. (2004). Melt reaction in blends of poly(3-hydroxybutyrate-*co*-3-hydroxyvalerate) and epoxidized natural rubber. *Polymer Degradation and Stability, 85*(3), 947-955.

Chan, C. H., Sulaiman, S. F., Kammer, H. W., Sim, L. H., & Harun, M. K. (2011). Thermal properties of epoxidized natural rubber-based polymer blends. *Journal of Applied Polymer Science, 120,* 1774-1781.

Cimmino, S., Di Pace, E., Martuscelli, E., & Silvestre, C. (1990). Evaluation of the equilibrium melting temperature and structure analysis of poly(ethylene oxide)/poly(methyl methacrylate) blends. *Macromolecule Chemistry and Physics, 191*(10), 2447-2454.

Cowie, J. M. G. (1973). *Polymers: Chemistry and Physics of Modern Materials*. London: Blackie Academic & Professional.

Davey, J. E., & Loadman, M. J. (1984). A chemical demonstration of the randomness of epoxidation of natural rubber. *British Polymer Journal, 16,* 134-138.

Fink, J. K. (2011). *Handbook of Engineering and Specialty Thermoplastics, Water Soluble Polymers*. Salem, Massachusetts: Scrivener.

Gan, S. N., & Burfield, D. R. (1989). D.S.C. studies of the reaction between epoxidized natural rubber and benzoic acid. *Polymer, 30*(10), 1903-1908.

Gan, S. N., & Hamid, Z. A. (1997). Partial conversion of epoxide groups to diols in epoxidized natural rubber. *Polymer, 38*(8), 1953-1956.

Gelling, I. R. (1988). Chemistry, structure and properties of epoxidized natural rubber. In L. L. Amin, & K. T. Lau (Eds.). Proceedings from *International Rubber Technology Conference, Penang*.

Gelling, I. R., & Smith, J. R. (1979). Controlled viscoelasticity by natural rubber modification. Proceedings from *International Rubber Conference, Venice.*

Glasse, M. D., Idris, R., Latham, R. J., Linford, R. G., & Schlindwein, W. S. (2002). Polymer electrolytes based on modified natural rubber. *Solid State Ionics, 147,* 289-294.

Haldar, B., Singru, R. M., & Chandra, S. (1997). Positron annihilation lifetime studies of free volume on a polymer electrolyte poly(ethylene oxide) complexed with NH_4I. *Journal of Polymer Science and Polymer Physics, 36*, 969-976.

Hallensleben, M. L., Schmidt, H. R., & Schuster, R. H. (1995). Epoxidation of poly(cis-1,4-isoprene) microgels. *Macromolecular Materials and Engineering, 227*, 87-99.

Hayashi, O., Takahashi, T., Kurihara, H., & Ueno, H. (1981). Monomer unit sequence distribution in partly-epoxidized trans-1,4-polyisoprene. *Polymer Journal, 13*, 215-223.

Hoogenboom, R. (2009). Polyethers and Polyoxazolines. In P. Dubois, O. Coulembier & J. M. Raquez (Eds.), *Handbook of Ring-Opening Polymerization*. Weinheim: Wiley-VCH.

Hossel, P., Sperling, K., & Schehlmann, V. (2001). Aqueous compositions and their use. US Patent 6191188.

Idris, R., Glasse, M. D., Latham, R. J., Linford, R. G., & Schlindwein, W. S. (2001). Polymer electrolytes based on modified natural rubber for use in rechargeable lithium batteries. *Journal of Power Sources, 94*, 206-211.

Kammer, H. W., Kressler, J., & Kummerlöwe, C. (1993). Phase behavior of polymer blends-effects of thermodynamics and rheology. *Advances in Polymer Science, 106*, 31-85.

Kienzle, S. Y. (1988). *Advanced in Polymer Blends and Alloys Technology* (M. A. Kohudic, Ed.). Lancaster, PA: Technomic Publishing.

Lee, H. K., Ismail, J., Kammer, H. W., & Bakar, M. A. (2005). Melt reaction in blends of poly(3-hydroxybutyrate) (PHB) and epoxidized natural rubber (ENR50). *Journal of Applied Polymer Science, 95*(1), 113–129.

Linford, R. G., Radhakrishna, S., & Daud, A. (1991). *Solid State Material*s. India: Narosa Publishing House.

Loo, C. T. (1985). Vulcanisation of epoxidised natural rubber with dibasic acids. Proceedings from *International Rubber Conference*. Kuala Lumpur: Rubber Research Institute of Malaysia.

Loo, C. T. (1988). Enhancing oil resistance of epoxidised natural rubber by carboxylic acid modification. Proceedings from *International Rubber Technology Conference*. Penang: Rubber Research Institute of Malaysia.

Mazzarella, E. D., Wood, L. J., & Maliczyszyn, W. (1977). Method of sizing paper. US Patent 4040900.

Moyse, J. A. (1969). Improvements in the laundering of synthetic polymeric textile materials. GB Patent 1154730.

Murata, K., Izuchi, S., & Yoshihisa, Y. (2000). An overview of the research and development of solid polymer electrolyte batteries. *Electrochemica Acta, 45*, 1501-1508.

Nakanishi, K., & Solomon, P. H. (1977). *Infrared Absorption Spectroscopy* (2^{nd} ed.). San Francisco: Holdenday.

Nakason, C., Panklieng, Y., & Kaesaman, A. (2004). Rheological and thermal properties of thermoplastic natural rubbers based on poly(methyl methacrylate)/epoxidized-natural-rubber blends. *Journal of Applied Polymer Science, 92*(6), 3561–3572.

Niu, B. J., Schuttel, S., & Schaer, M. (2006). Print media products for generating high quality images and methods for making the same. US Patent 7112629.

Noor, S. A. M., Ahmad, A., Rahman, M. Y. A., & Talib, I. A. (2009). Preparation and characterization of a solid polymer electrolyte PEO-ENR50 (80/20)-$LiCF_3SO_3$. *Journal of Applied Polymer Science, 113*, 855-859.

Noor, S. A. M., Ahmad, A., Talib, I. A., & Rahman, M. Y. A. (2010). Morphology, chemical interaction and conductivity of a PEO-ENR50 based on solid polymer electrolyte. *Ionics*, *16*, 161-170.

Okwu, U. N., & Okieimen, F. E. (2001). Preparation and properties of thioglycollic acid modified epoxidised natural rubber and its blends with natural rubber. *European Polymer Journal*, *37*, 2253-2258.

Olabisi, O., Robensen, L. M., & Shaw, M. T. (1979). *Polymer Miscibility*. New York: Academic Press.

Pereira, A. G. B., Paulino, A. T., Nakamura, C. V., Britta, E. A., Rubira, A. F., & Muniz, E. C. (2011). Effect of starch type on miscibility in poly(ethylene oxide) (PEO)/starch blends and cytotoxicity assays. *Materials Science and Engineering C, 31*(2), 443-451.

Pire, M., Norvez, S., Iliopoulos, I., Le Rossignol, B., & Leibler, L. (2010). Epoxidized natural rubber/dicarboxylic acid self-vulcanized blends. *Polymer, 51*(25), 5903-5909.

Prabhakaran, N. K. P. (2010). The Agronomy and Economy of Important Tree Crops of the Developing World. London: Elsevier.

Qiu, Z., Ikehara, T., & Nishi, T. (2003). Miscibility and crystallization of poly(ethylene oxide) and poly(ε-caprolactone) blends. *Polymer, 44*, 3101-3106.

Rocco, A. M., Fonseca, C. P., Loureiro, F. A. M., & Pereira, R. P. (2003). A polymeric solid electrolyte based on a poly(ethylene oxide)/poly(bisphenol A-co-epichlorohydrin) blend with $LiClO_4$. *Solid State Ionics, 166*, 115-126.

Rocco, A. M., Fonseca, C. P., & Pereira, R. P. (2002). A polymeric solid electrolyte based on a binary blend of poly(ethylene oxide), poly(methyl vinyl ether-maleic acid) and $LiClO_4$. *Polymer, 43*, 3601-3609.

Sanguansap, K., Suteewong, T., Saendee, P., Buranabunya, U., & Tangboriboonrat, P. (2005). Composite natural rubber based latex particles: a novel approach. *Polymer, 46,* 1373-1378.

Shafee, E. E., & Ueda, W. (2002). Crystallization and melting behavior of poly(ethylene oxide)/poly(n-butyl methacrylate) blends. *European Polymer Journal, 38,* 1327-1335.

Silvestre, C., Cimmino, S., & Di Pace, E. (1991). Crystallizable Polymer Blends. In *Polymeric materials encyclopedia* (Vol. 2, pp. 1606-1607) New York: CRC Press, Boca Raton.

Sim, L. H., Chan, C. H., & Kammer, H. W. (2010). Selective localization of lithium perchlorate in immiscible blends of poly(ethylene oxide) and epoxidized natural rubber. Proceedings from CSSR 2010: *International Conference on Science and Social Research*. Kuala Lumpur: IEEE Xplore Digital Library.

Simons, W. W. (1978). *The Sadler Handbook of Infrared Spectra*. Philadelphia: Sadler.

Smith, B. (1999). *Infrared Spectral Interaction, A Schematic Approach*. New York: Boca Raton.

Smith, R. W., & Andries, J. C. (1974). New methods for electron microscopy of polymer blends. *Rubber Chemistry and Technology, 47(1),* 64-78.

Sommer, J. G. (2009). *Engineered Rubber Products: Introduction to Design, Manufacture and Testing*. Ohio: Hanser.

Sotele, J. J., Soldi, V., & Pires, A. T. N. (1997). Characterization and morphology of novolak or poly(vinyl phenol)/poly(ethylene oxide) blends. *Polymer, 38*(5), 1179-1185.

Stevens, M. P. (1990). *Polymer Chemistry: An Introduction*. New York: Oxford University Press.

Subramaniam, A. (1987). Natural Rubber. In M. Morton (Ed.), *Rubber Technology* (3rd ed.). New York: Van Nostrand Reinhold Co.

Sulaiman, S. F., Chan, C. H., & Harun, M. K. (2009). Thermal properties and morphologies of poly(ethylene terephthalate) in blends with epoxidised natural rubber of 25 and 50 mol.-% of epoxy content. *Materials Research Innovations, 13*(3), 225-228.

Tan, S. M., Ismail, J., Kummerlöwe, C., & Kammer, H. W. (2006). Crystallization and melting behavior of blends comprising poly(3-hydroxy butyrate-*co*-3-hydroxy valerate) and poly(ethylene oxide). *Journal of Applied Polymer Science, 101*(5), 2776-2783.

Tanrattanakul, V., Wattanathai, B., Tiangjunya, A., & Muhamud, P. (2003). In situ epoxidized natural rubber: improved oil resistance of natural rubber. *Journal of Applied Polymer Science, 90*, 261-269.

Van Zyl, A. J., Graef, S. M., Sanderson, R. D., Klumperman, B., & Pasch, H. (2003). Monitoring the grafting of epoxidized natural rubber by size-exclusion chromatography coupled to FTIR spectroscopy. *Journal of Applied Polymer Science, 88*, 2539-2549.

Varughese, K. T., Nando, G. B., De, P. P., & De, S. K. (1988). Miscible blends from rigid poly(vinyl chloride) and epoxidized natural rubber: part 1 phase morphology. *Journal of Materials Science, 23*, 3894-3902.

Zhong, Z., & Guo, Q. (2000). Crystallization kinetics of miscible thermosetting polymer blends of novolac resin and poly(ethylene oxide). *Polymer, 41*(5), 1711-1718.

APPENDIX 1

Chemical modification of ENR50

Gel permeation chromatography

ENR50

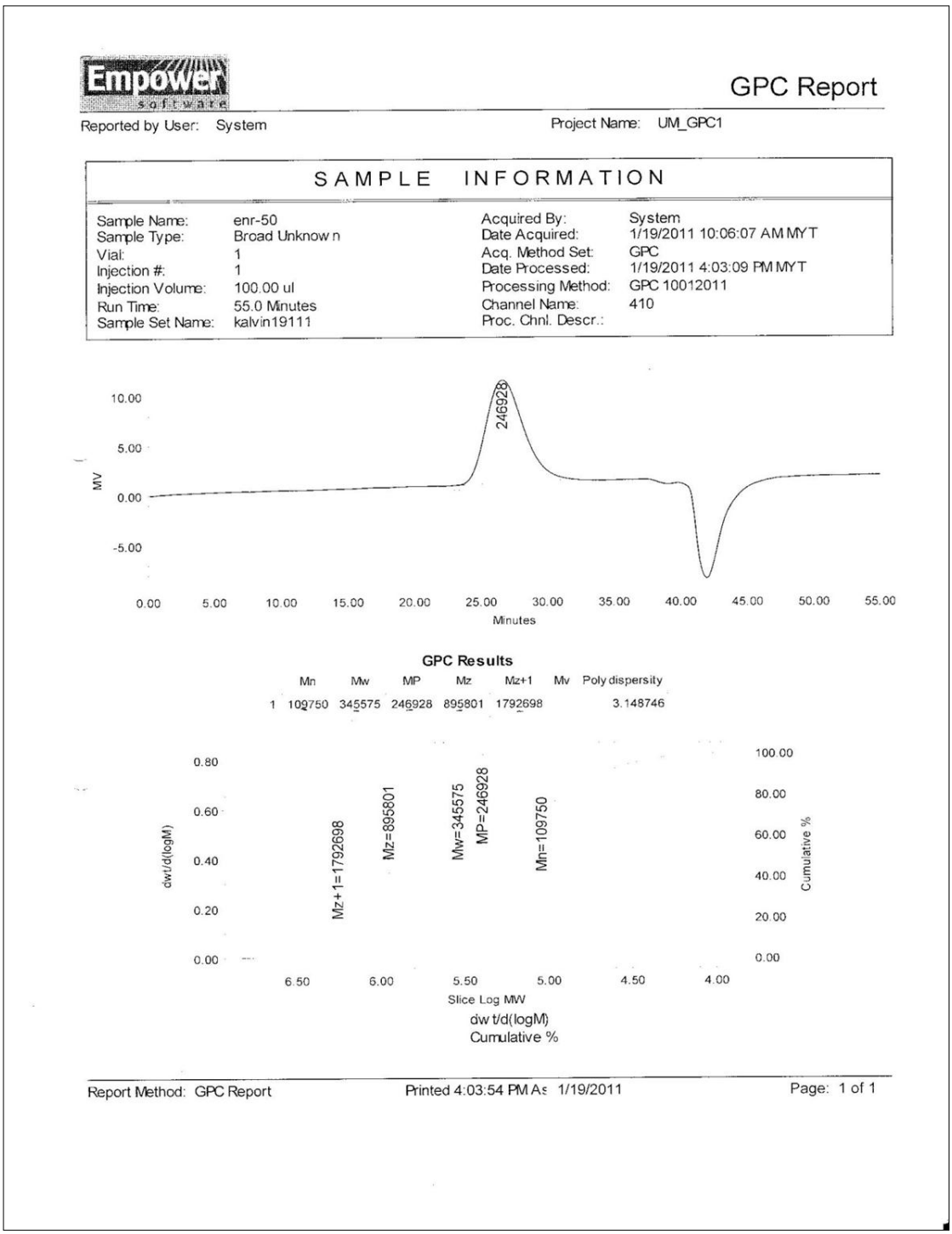

18-h acetic acid-modified ENR50

Empower software

GPC Report

Reported by User: System Project Name: UM_GPC1

SAMPLE INFORMATION

Sample Name:	enr-50 ester purified	Acquired By:	System
Sample Type:	Broad Unknown	Date Acquired:	1/19/2011 11:02:55 AM MYT
Vial:	2	Acq. Method Set:	GPC
Injection #:	1	Date Processed:	1/19/2011 3:52:50 PM MYT
Injection Volume:	100.00 ul	Processing Method:	GPC 10012011
Run Time:	55.0 Minutes	Channel Name:	410
Sample Set Name:	kalvin19111	Proc. Chnl. Descr.:	

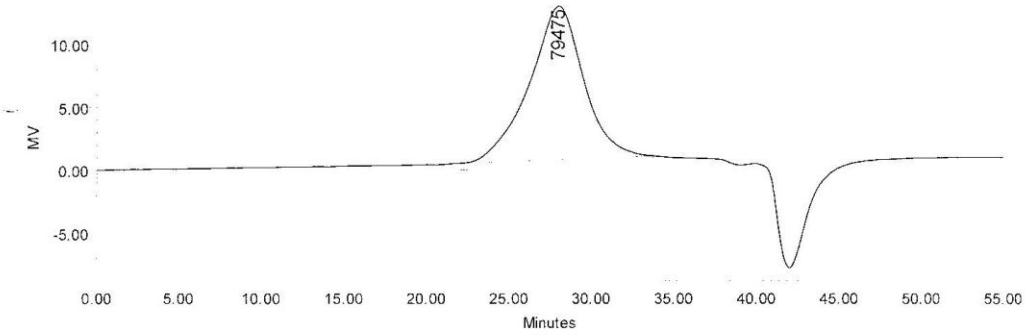

GPC Results

	Mn	Mw	MP	Mz	Mz+1	Mv	Polydispersity
1	50297	302430	79475	2654112	7653407		6.012913

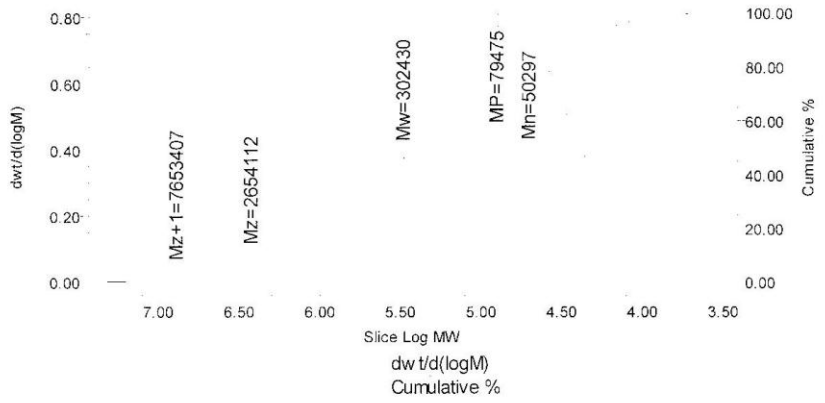

Report Method: GPC Report Printed 3:53:38 PM As 1/19/2011 Page: 1 of 1

FTIR Spectroscopy

ENR-50 (initial sample) at 0 hour

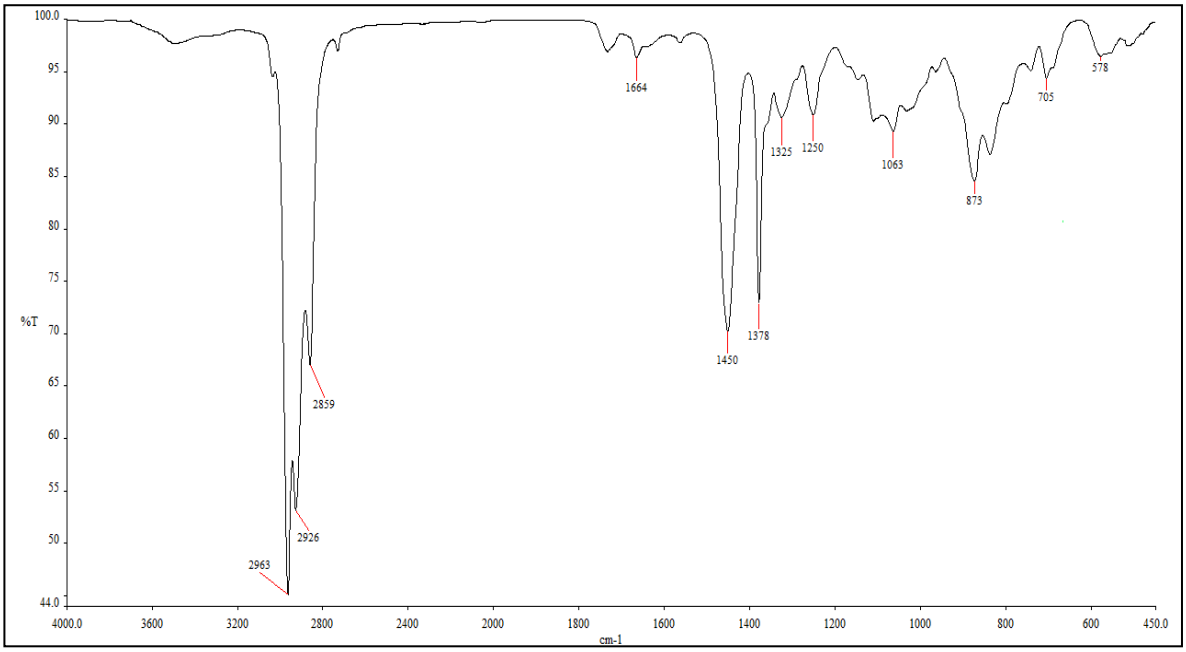

Acid-Modified ENR for 30 minutes sample

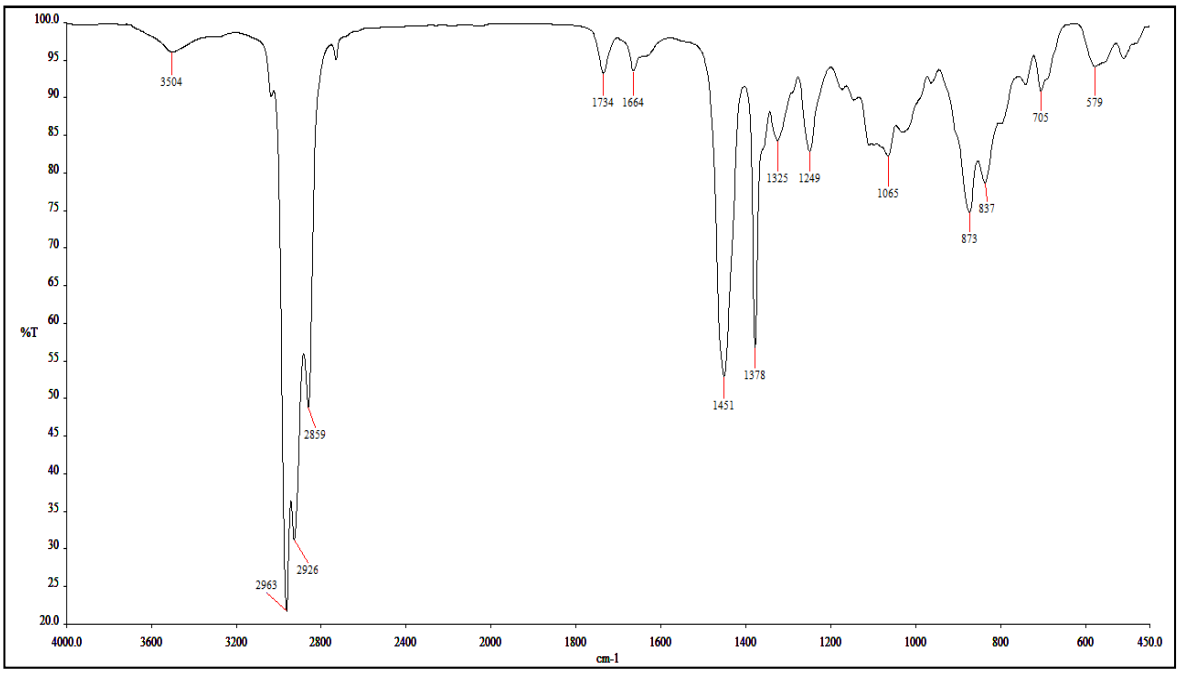

Acid-Modified ENR for 2 hours sample

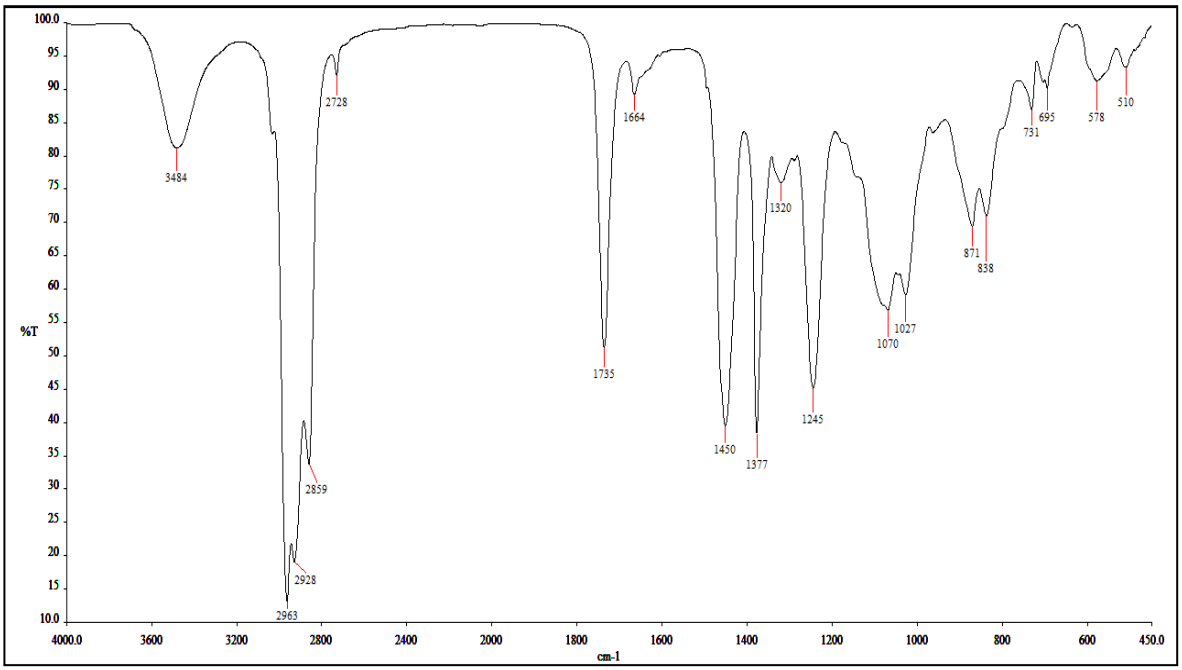

Acid-Modified ENR for 7 hours sample

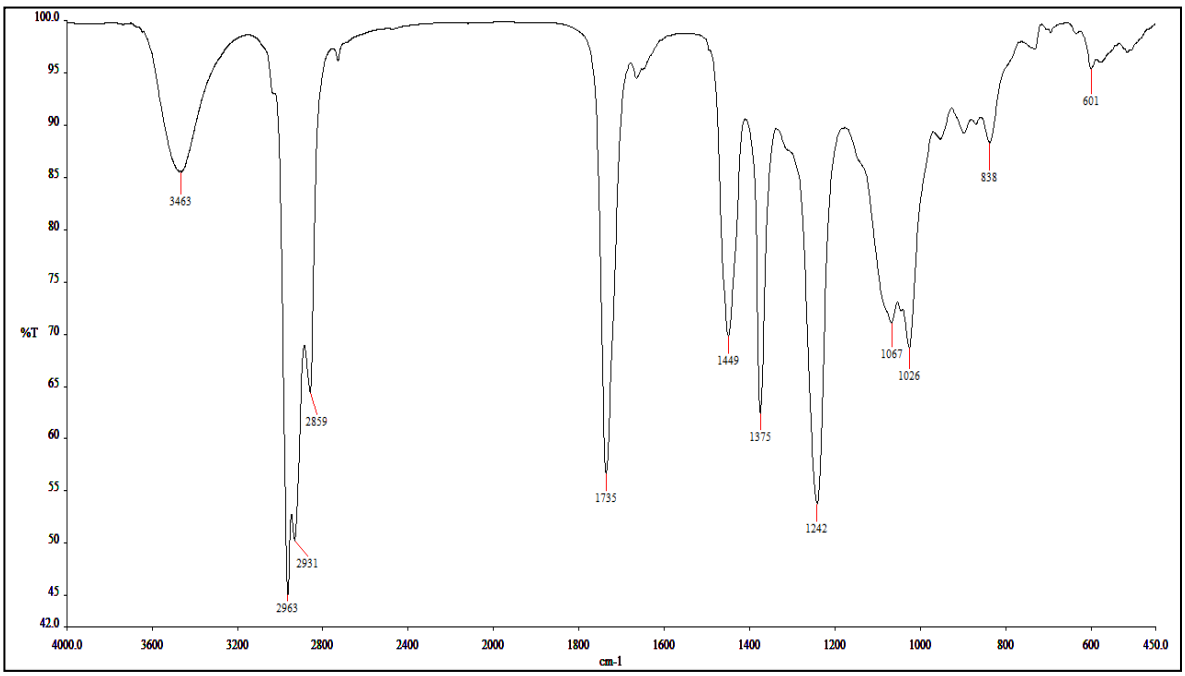

Acid-Modified ENR for 16 hours sample

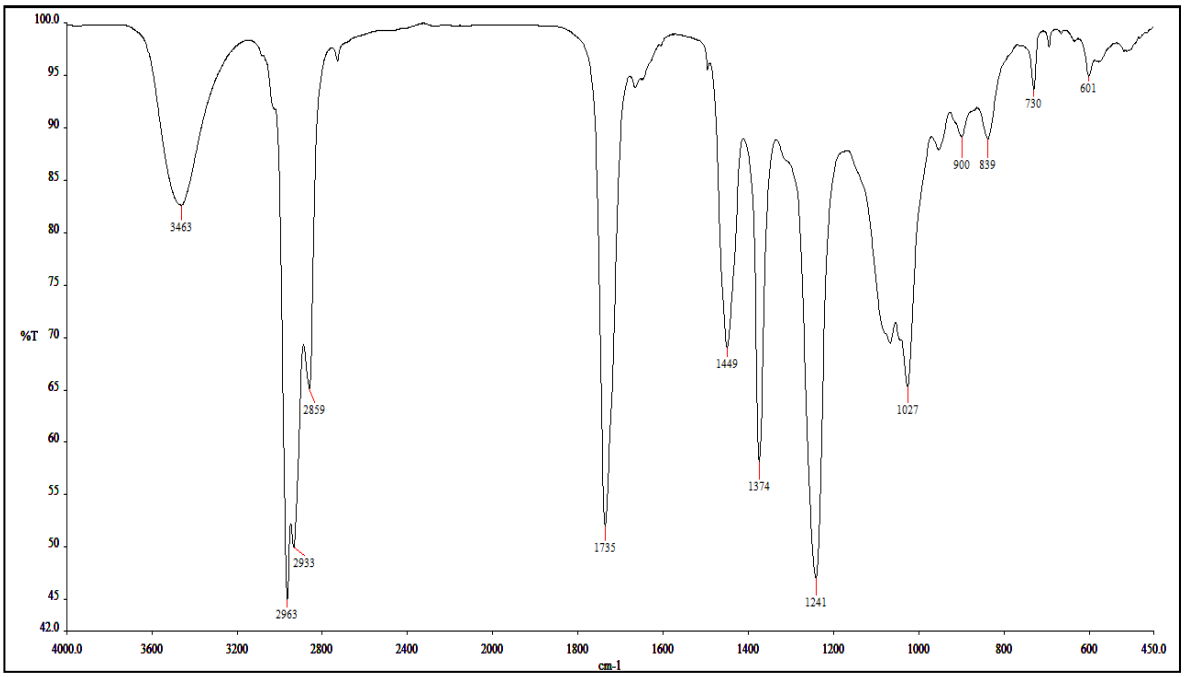

Acid-Modified ENR for 18 hours sample

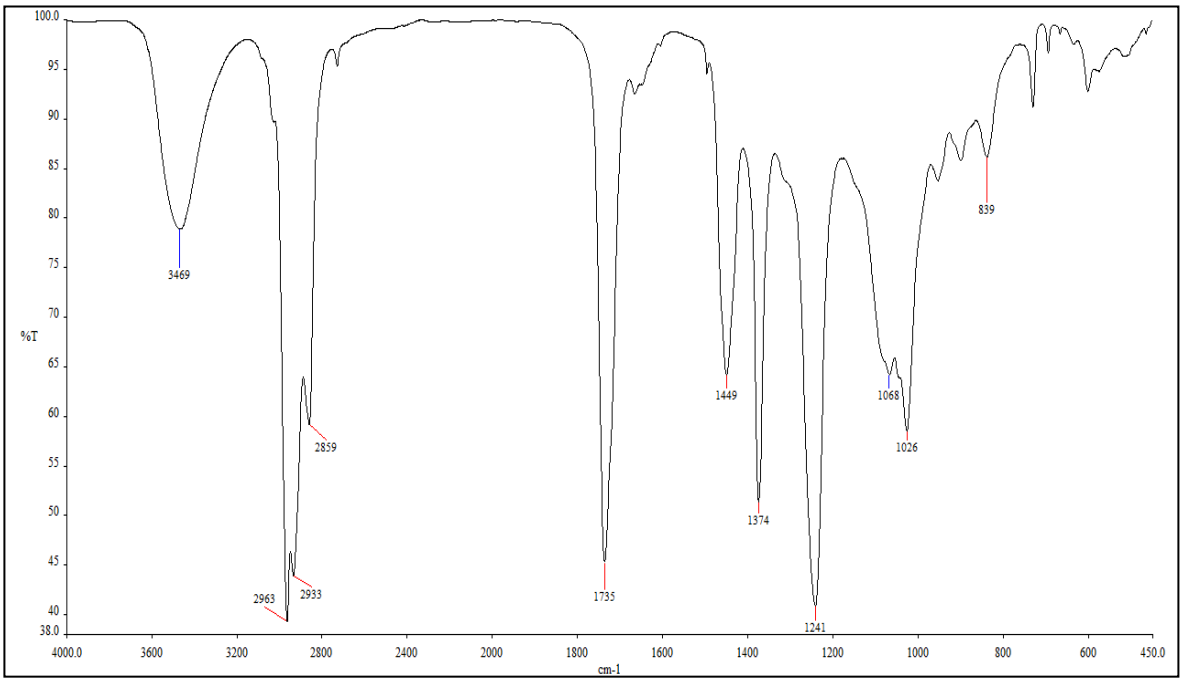

NMR Spectroscopy

ENR-50 (initial sample) at 0 hour

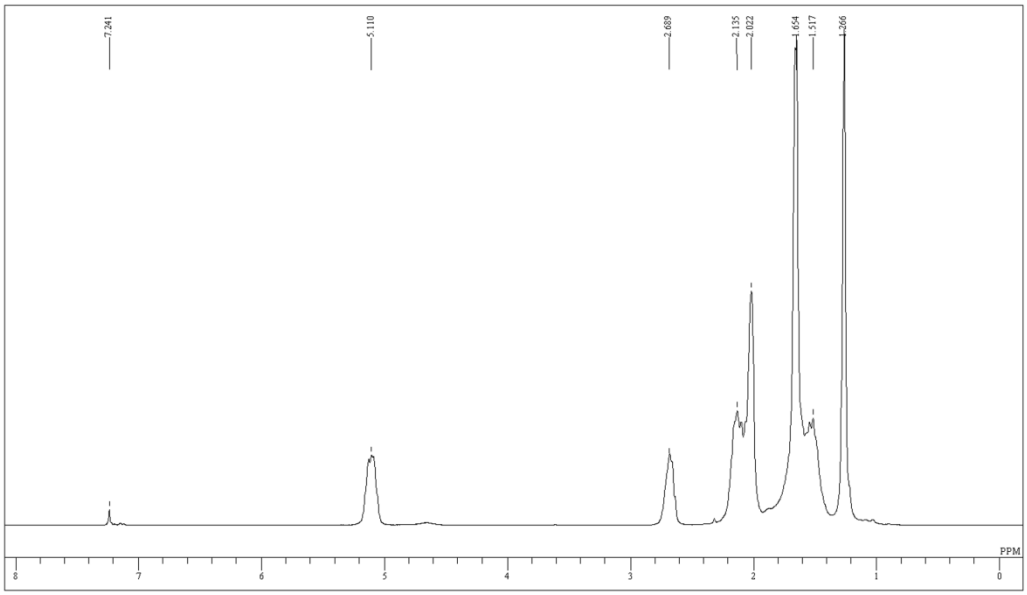

Acid-Modified ENR for 30 minutes sample

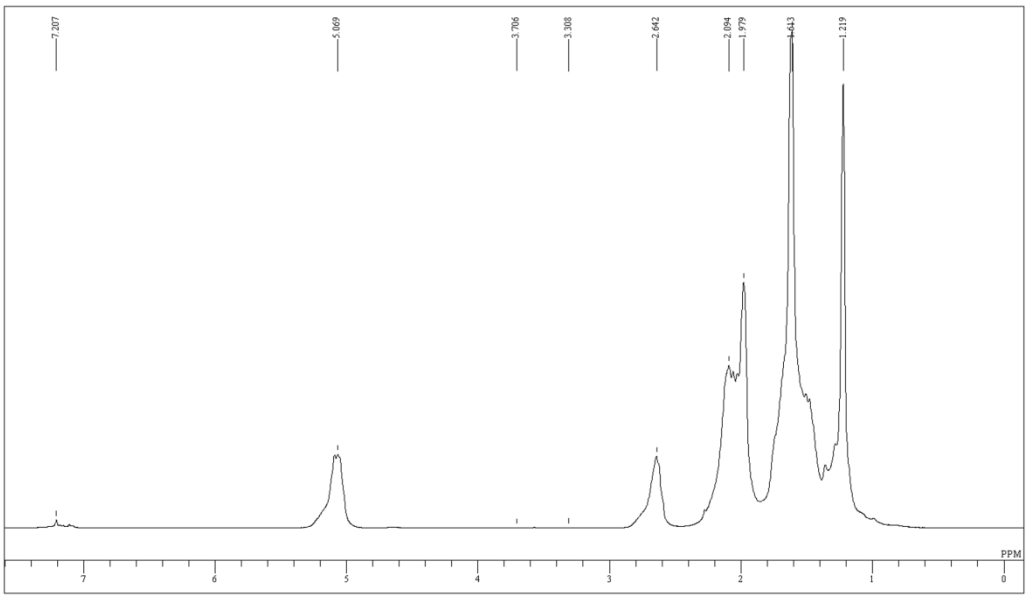

Acid-Modified ENR for 2 hours sample

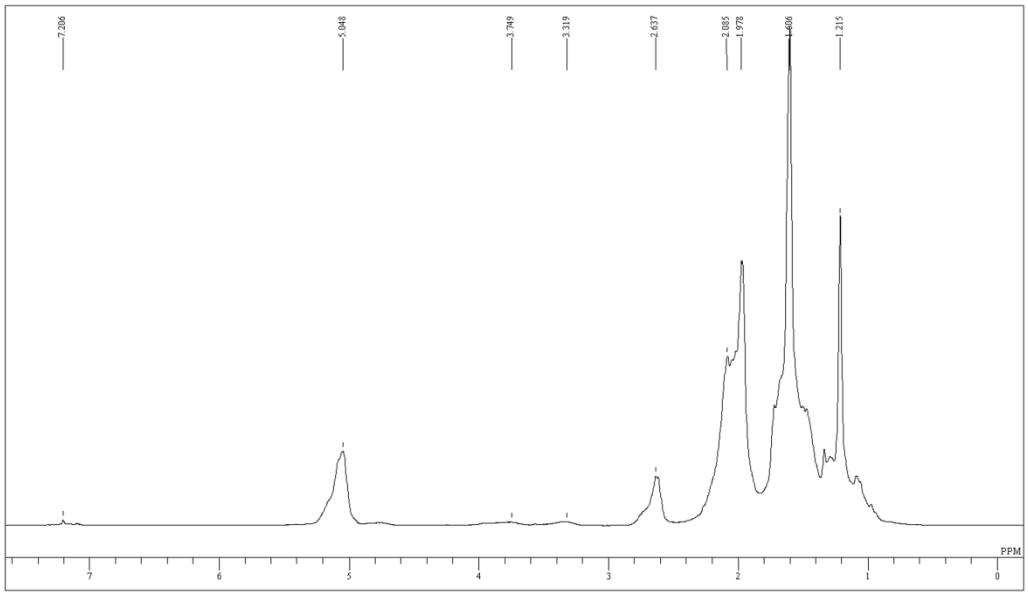

Acid-Modified ENR for 7 hours sample

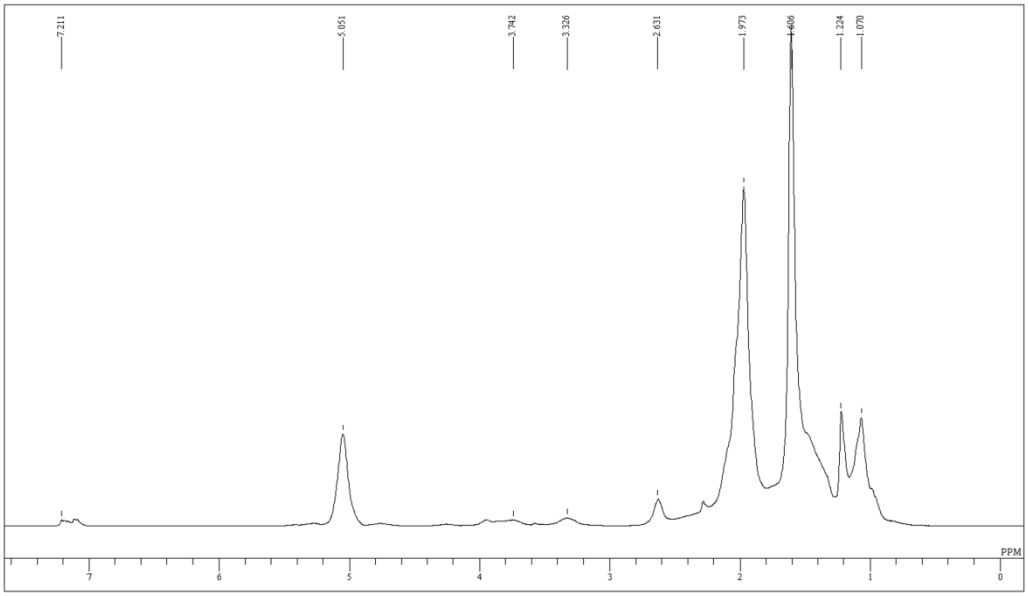

Acid-Modified ENR for 16 hours sample

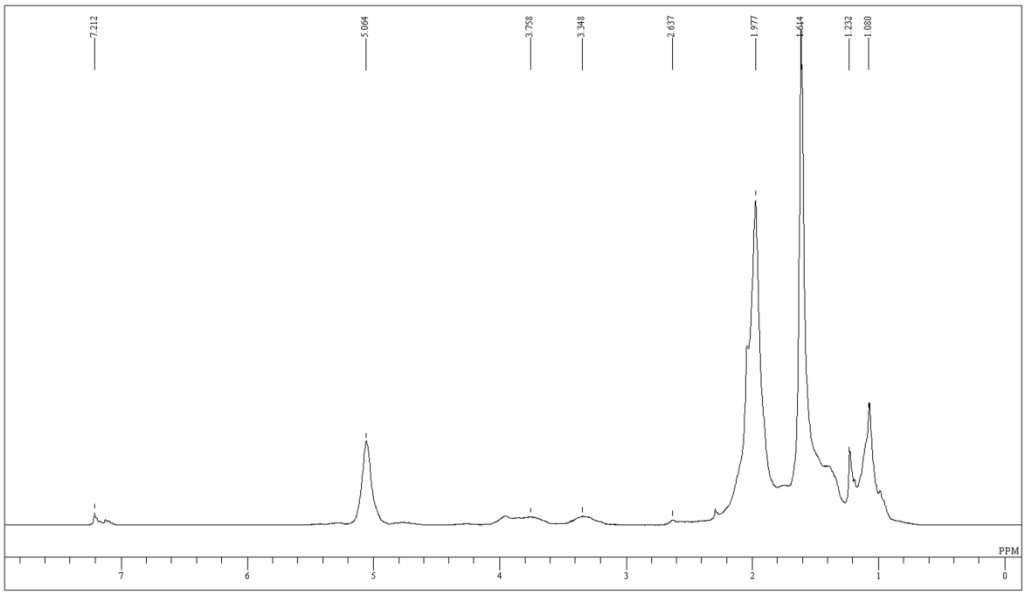

Acid-Modified ENR for 18 hours sample

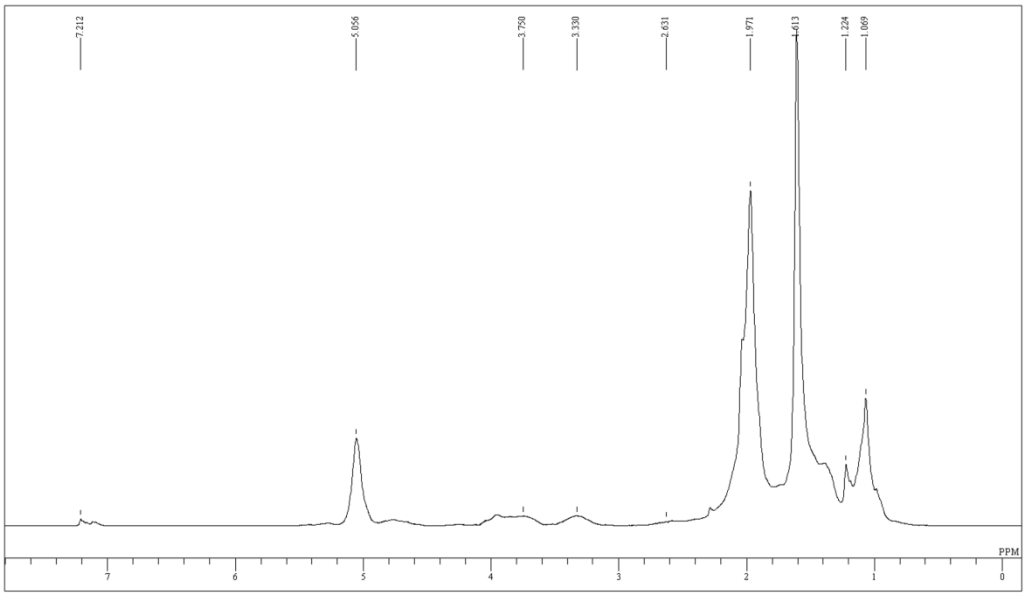

Thermal gravimetric analysis

ENR50 (initial sample)

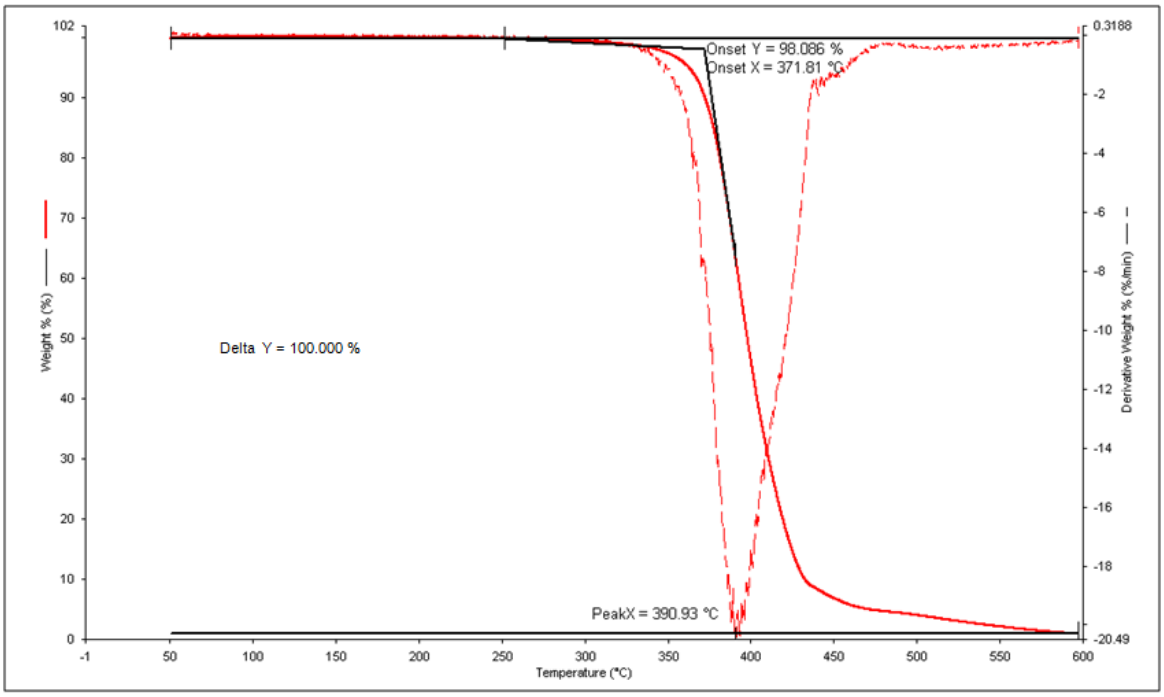

30-min acetic acid-modified ENR50 sample

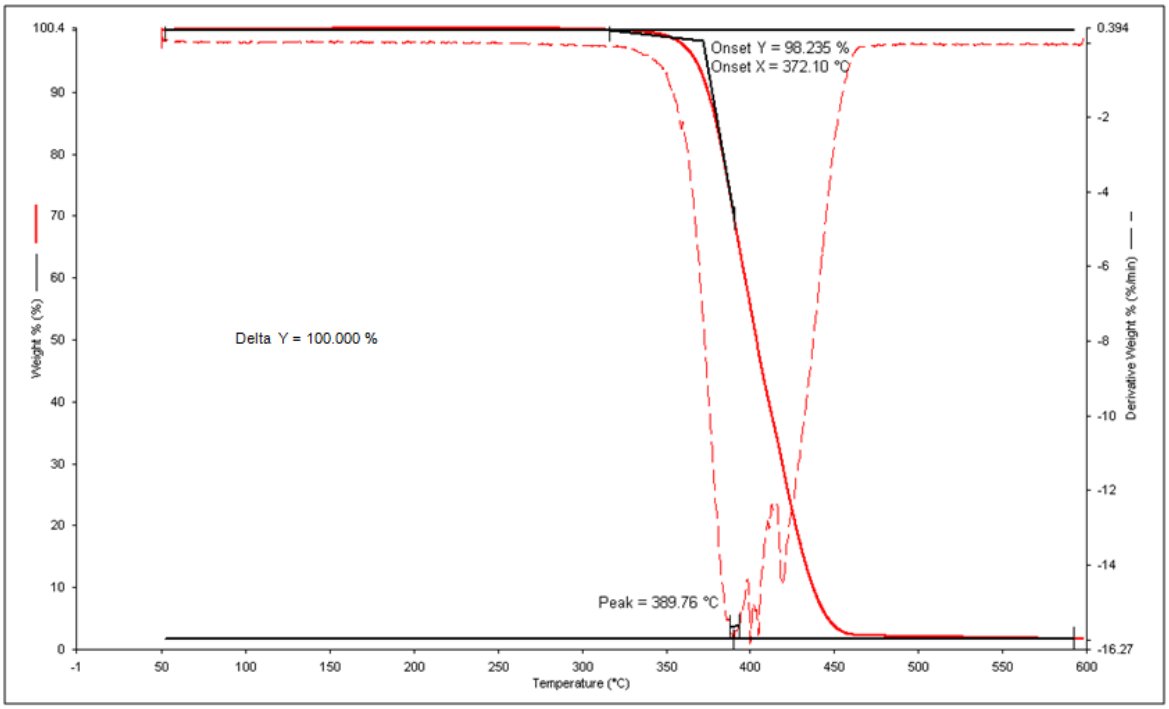

2-h acetic acid-modified ENR50 sample

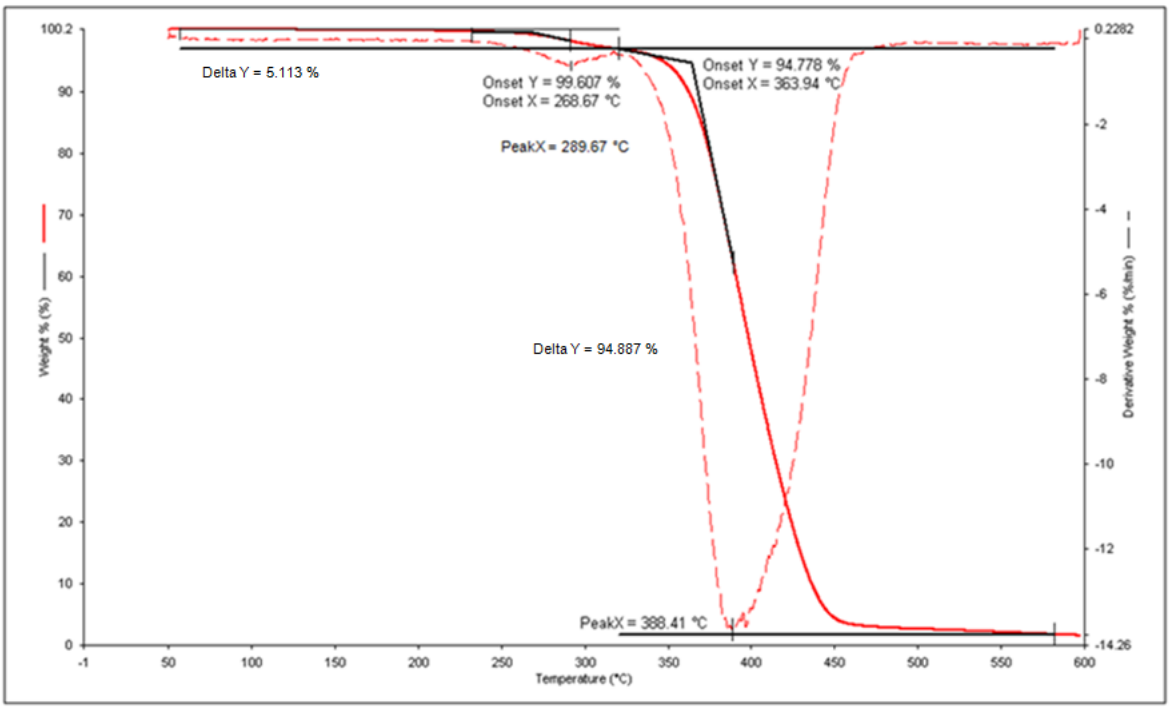

7-h acetic acid-modified ENR50 sample

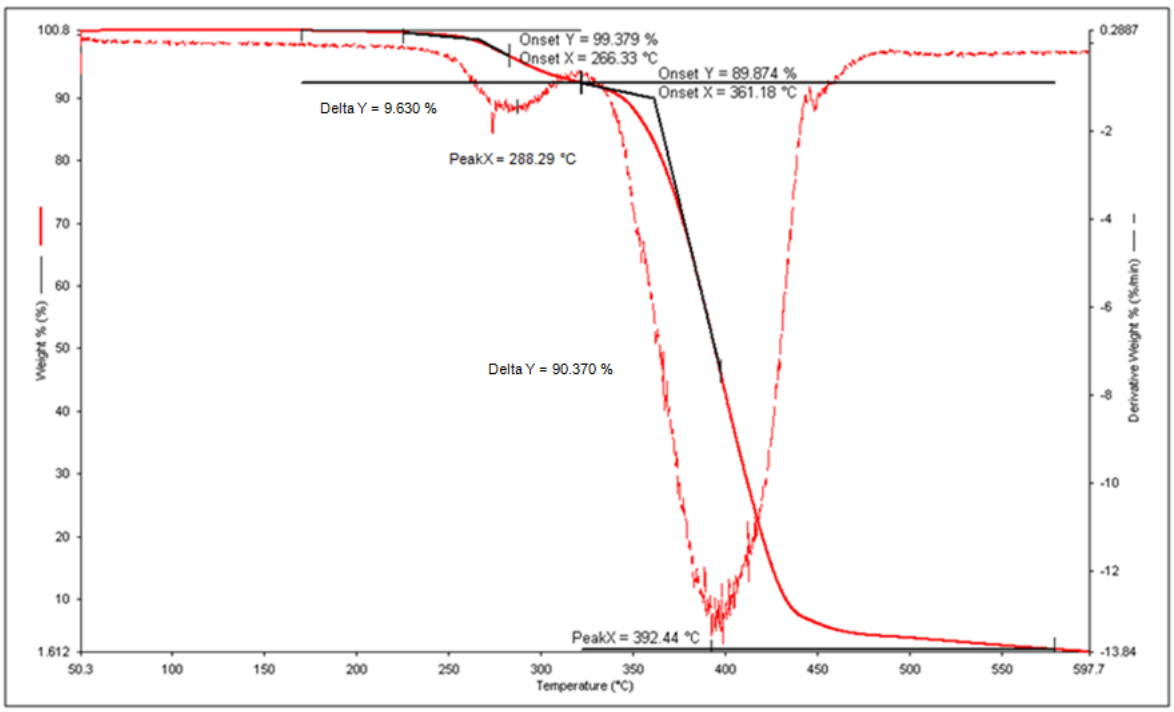

16-h acetic acid-modified ENR50 sample

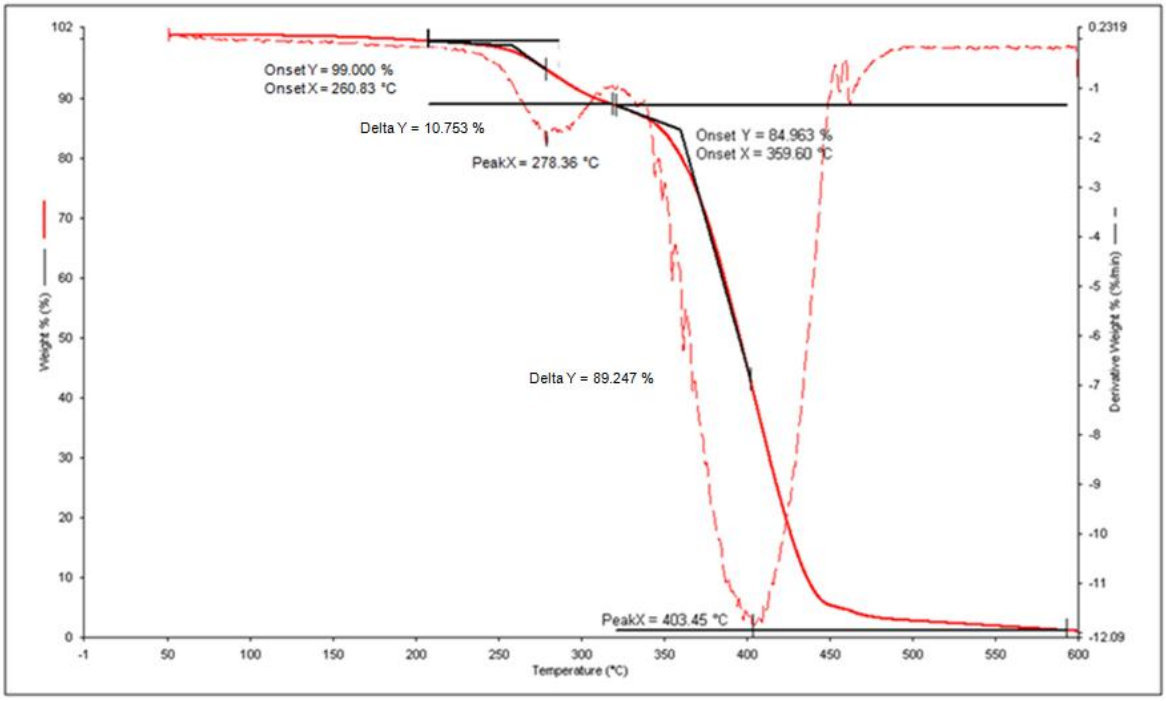

18-h acetic acid-modified ENR50 sample

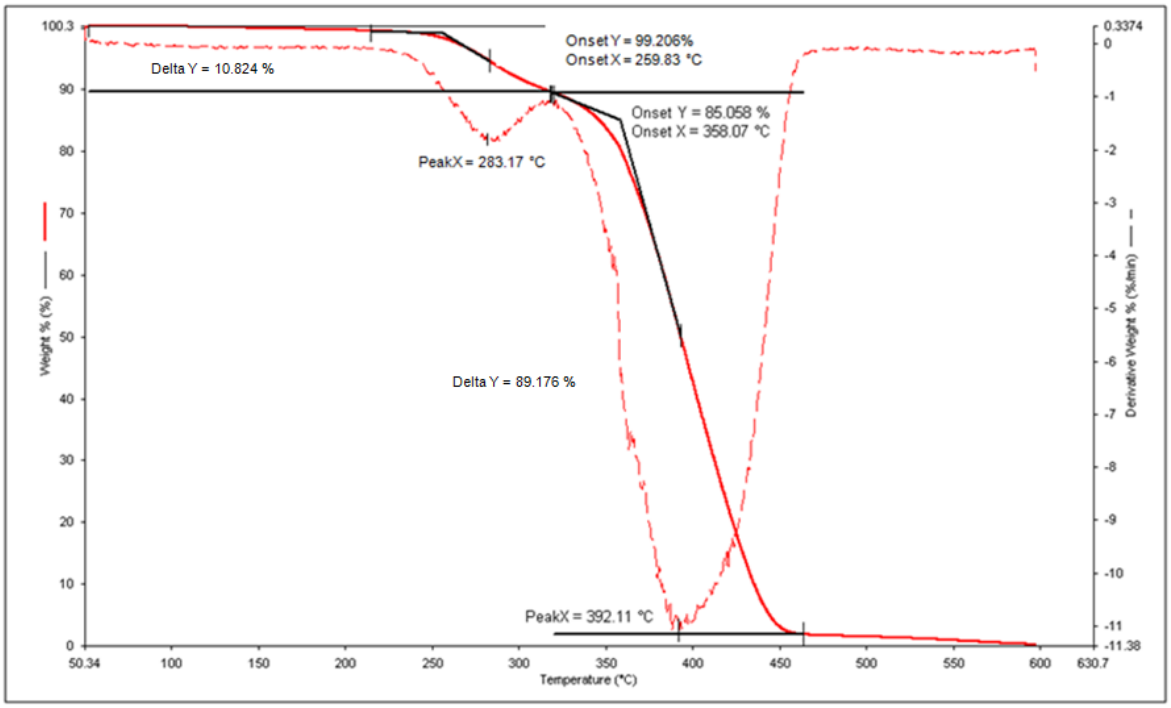

Decomposition temperature for various reaction time acetic acid-modified ENR50 samples

Amount of weight loss (%)	Decomposition temperature for acetic acid-modified ENR50 sample (℃)					
	0 h	0.5 h	2 h	7 h	16 h	18 h
1	322	352	275	264	238	243
2	346	358	295	273	256	261
3	357	361	316	280	265	268
4	364	363	337	287	271	277
5	366	365	347	294	283	280
6	368	367	351	301	285	283
7	369	371	355	311	289	292
8	370	372	357	328	294	296
9	372	373	360	336	300	307
10	374	375	362	343	306	316

Differential scanning calorimetry

ENR50 (Initial sample)

1st reading

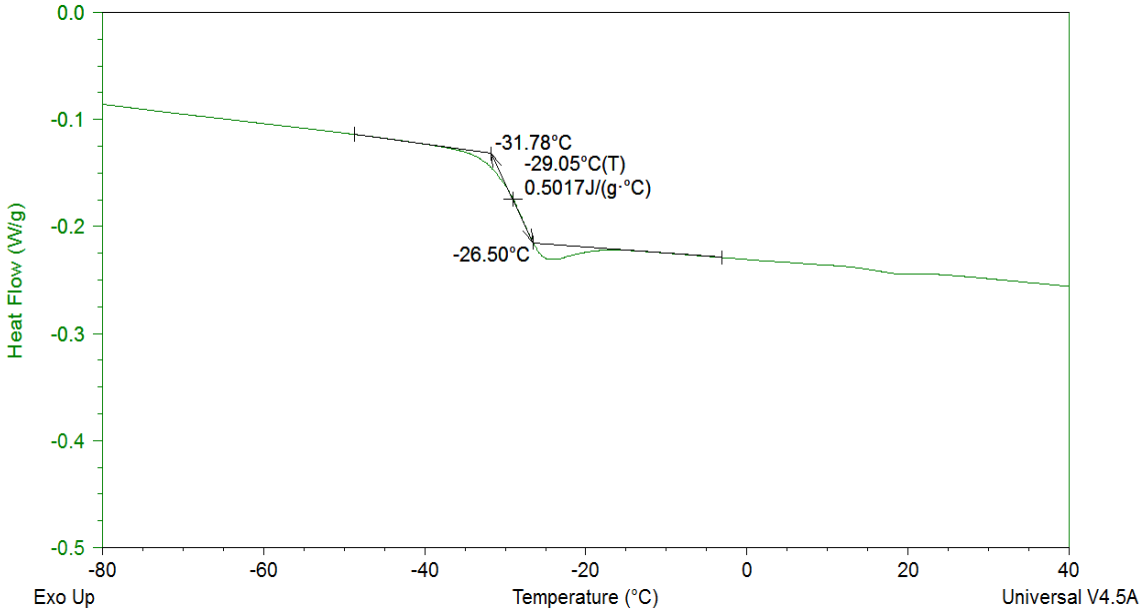

2nd reading

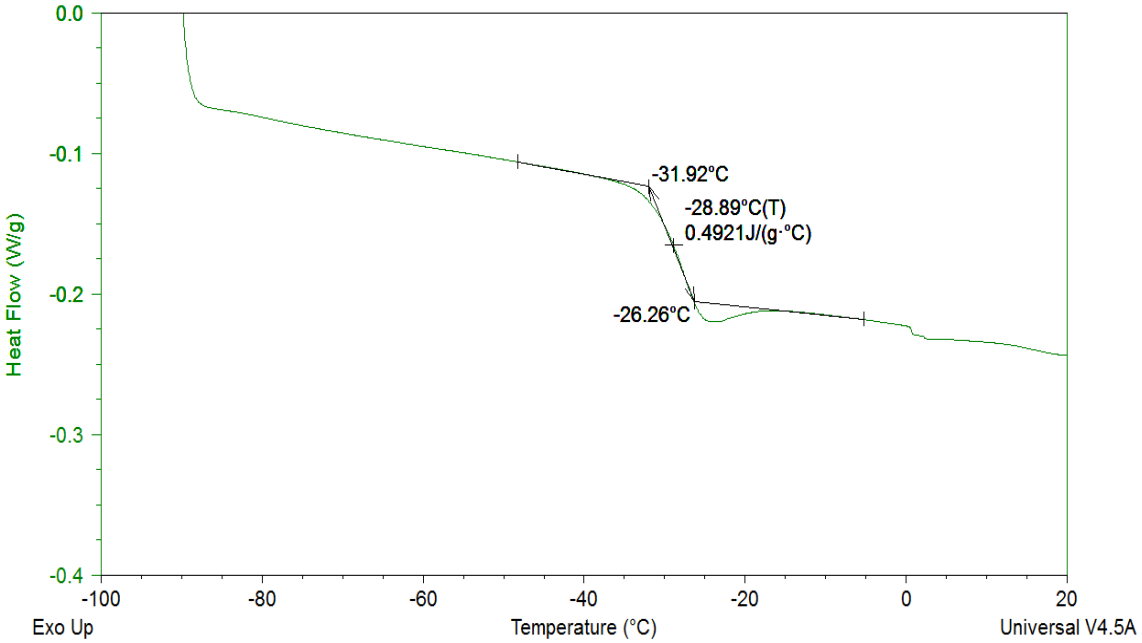

18-h acetic acid-modified ENR50 sample

1st reading

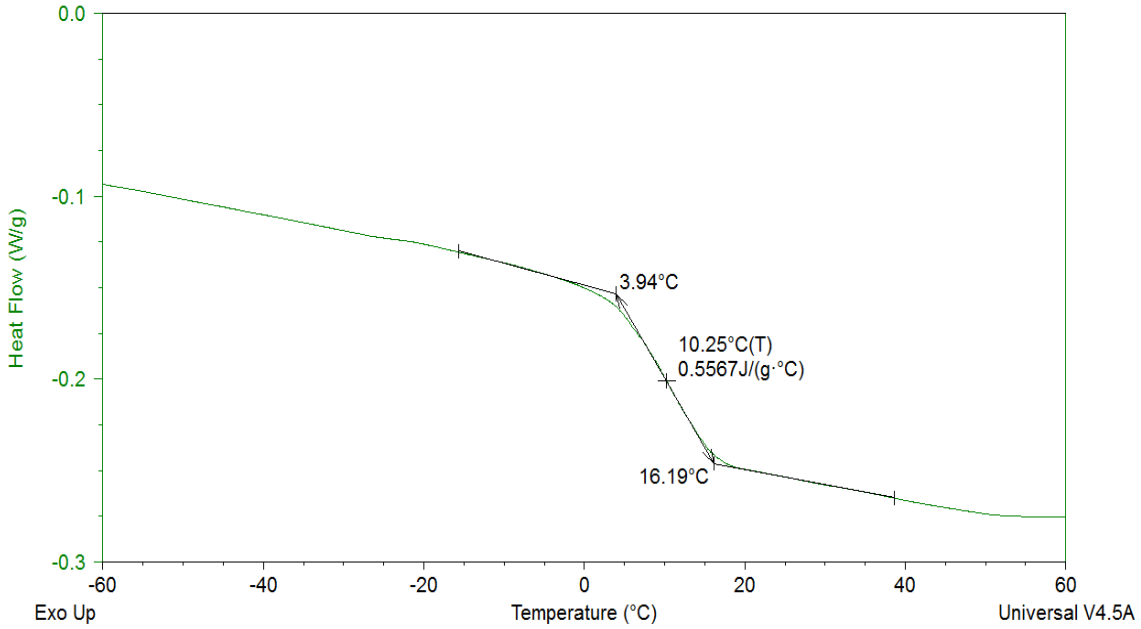

2nd reading

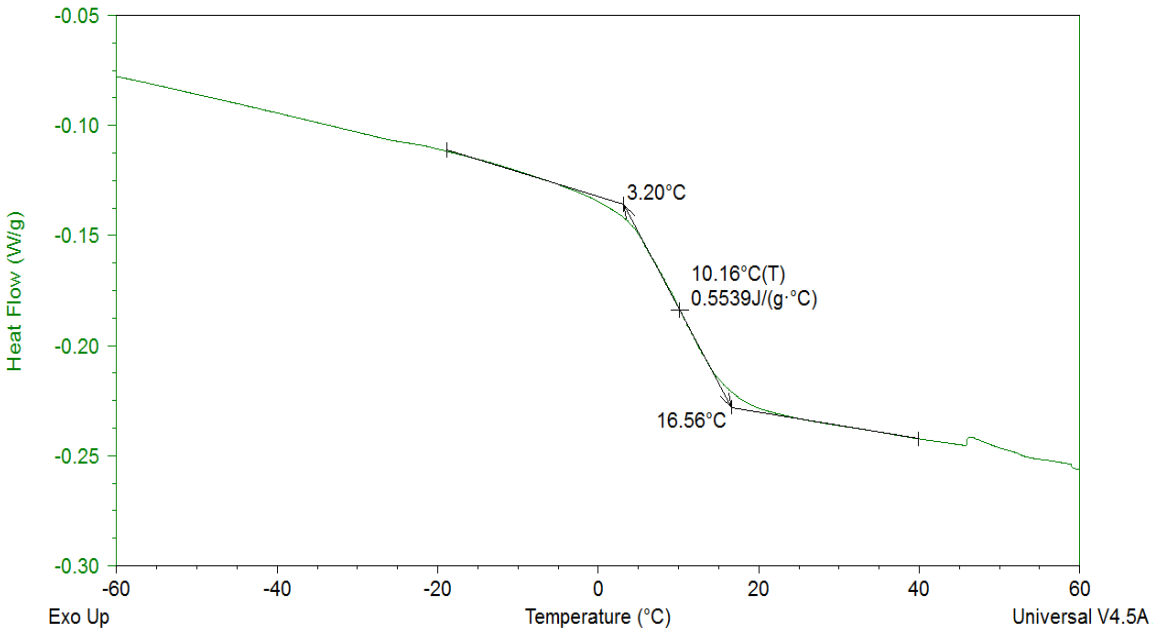

APPENDIX 2

Characterization of PEO, M_η=100K

Differential scanning calorimetry

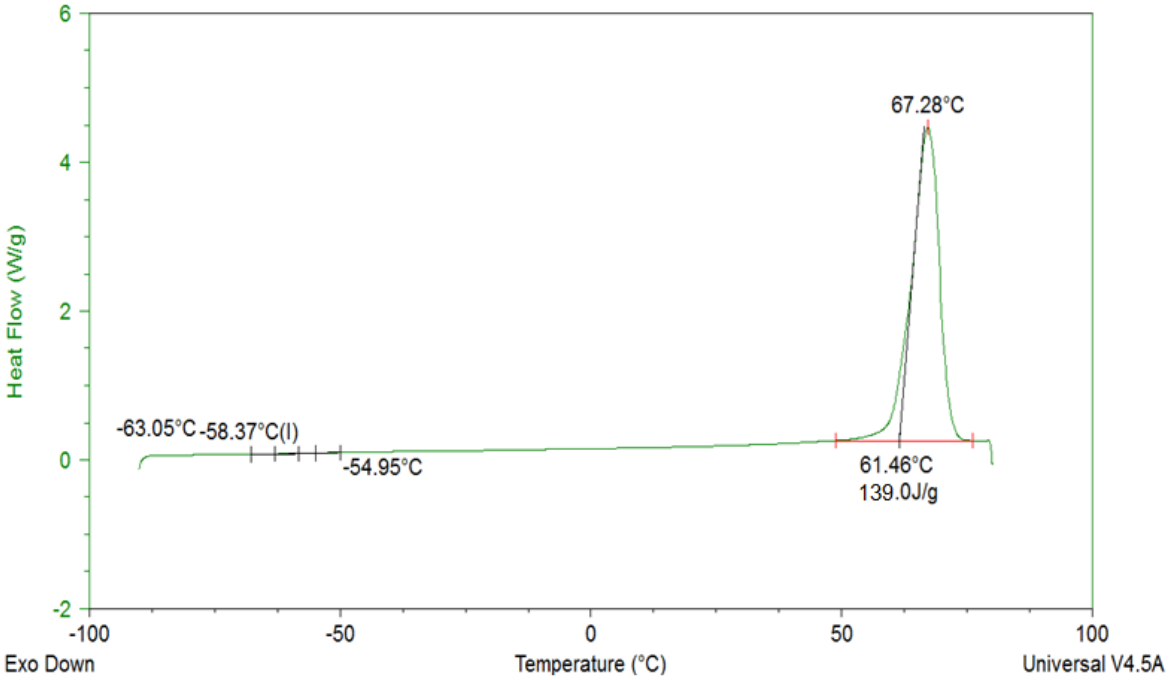

APPENDIX 3

Compatibility of 18-h acetic acid-modified ENR50 and PEO blends

FTIR spectroscopy

Acid-modified ENR/PEO 0/100

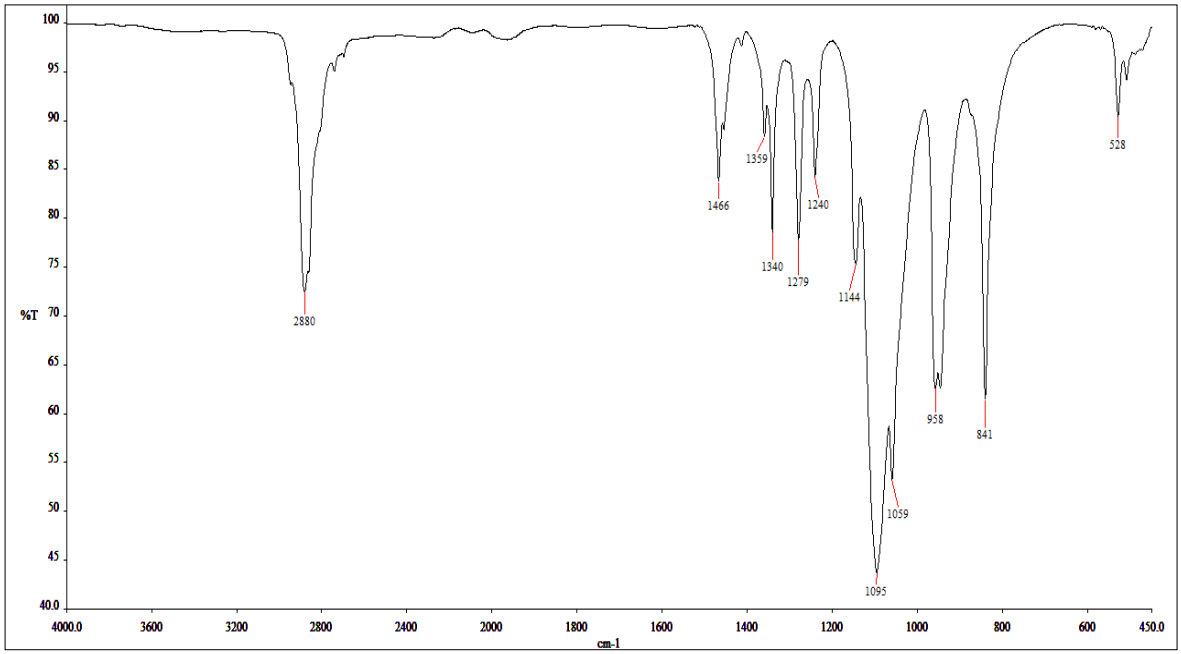

Acid-modified ENR/PEO 25/75

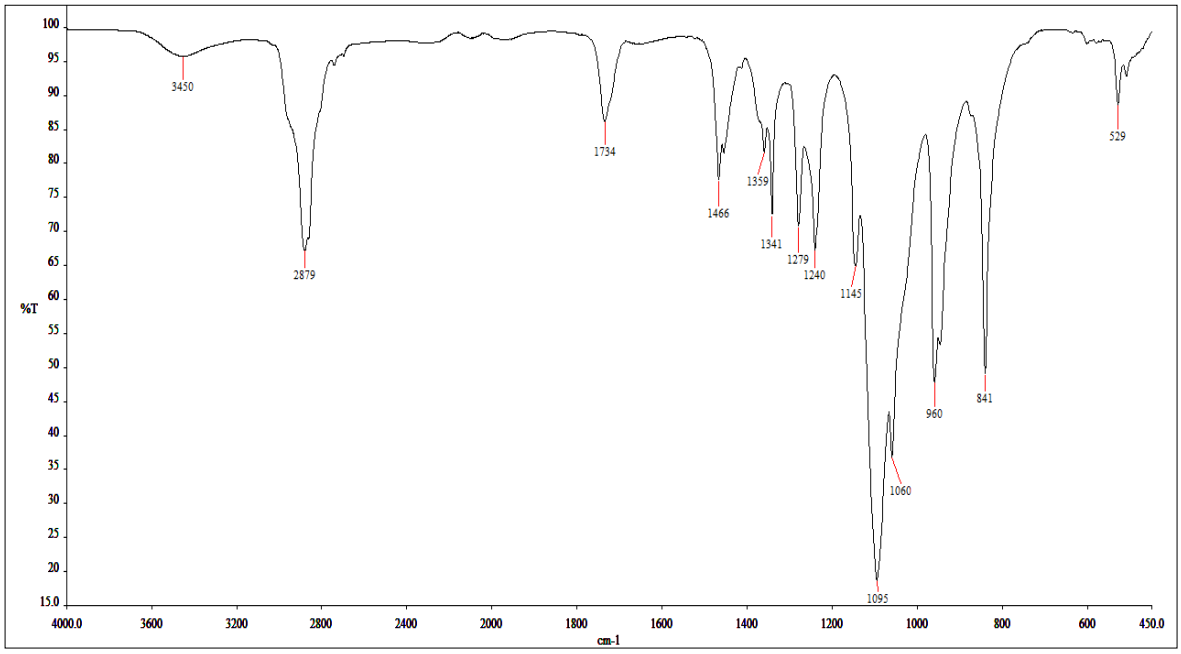

Acid-modified ENR/PEO 50/50

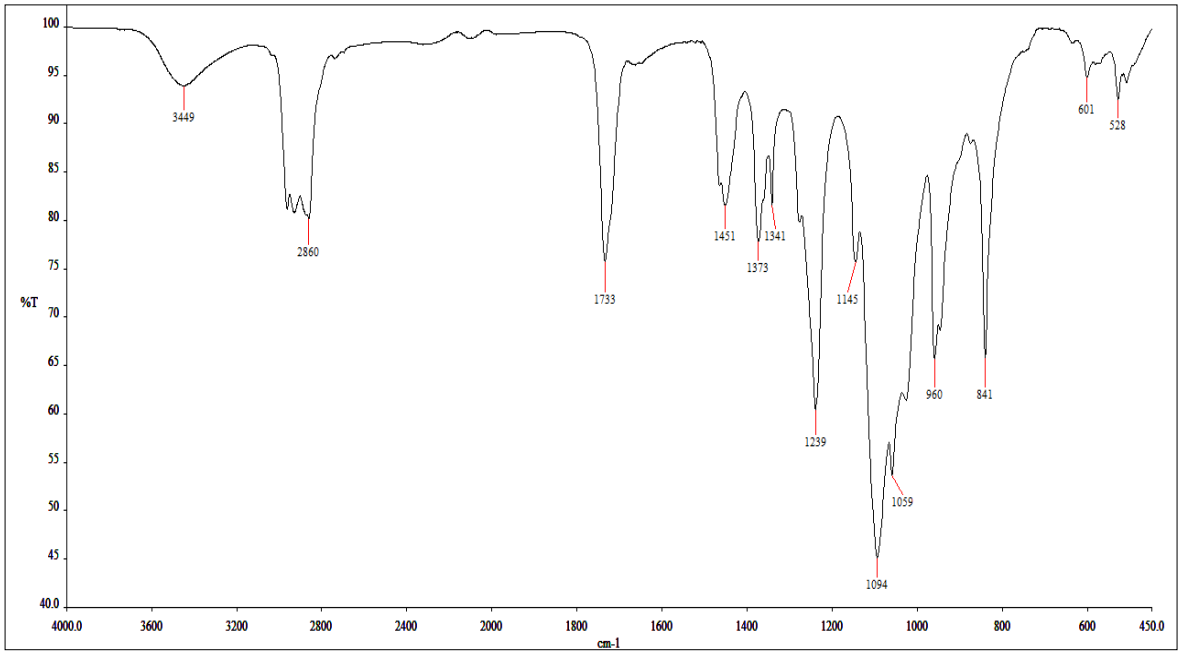

Acid-Modified ENR/PEO 75/25

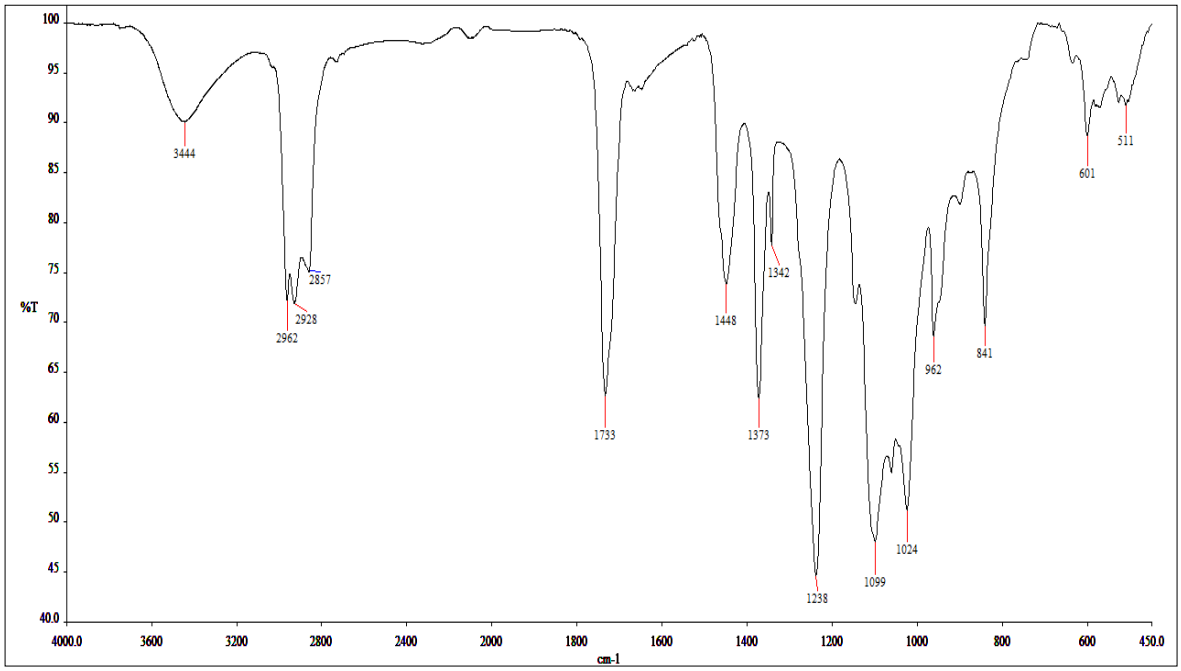

Acid-modified ENR/PEO 100/0

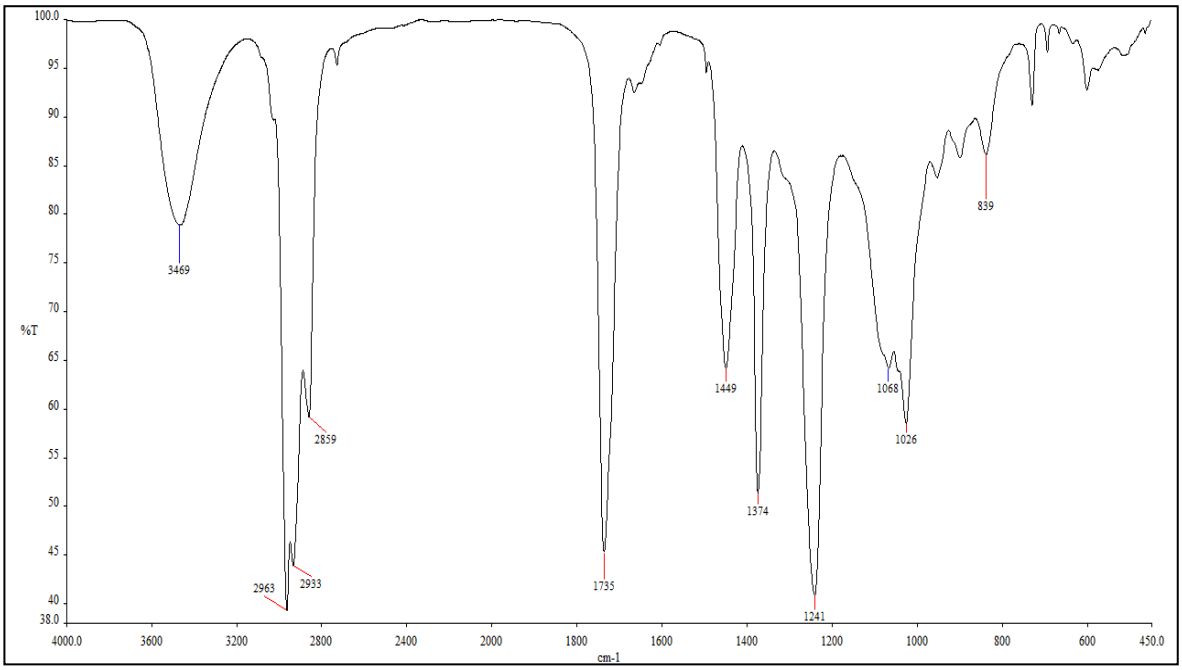

Thermal gravimetric analysis

Acetic acid-modified ENR50/PEO 0/100

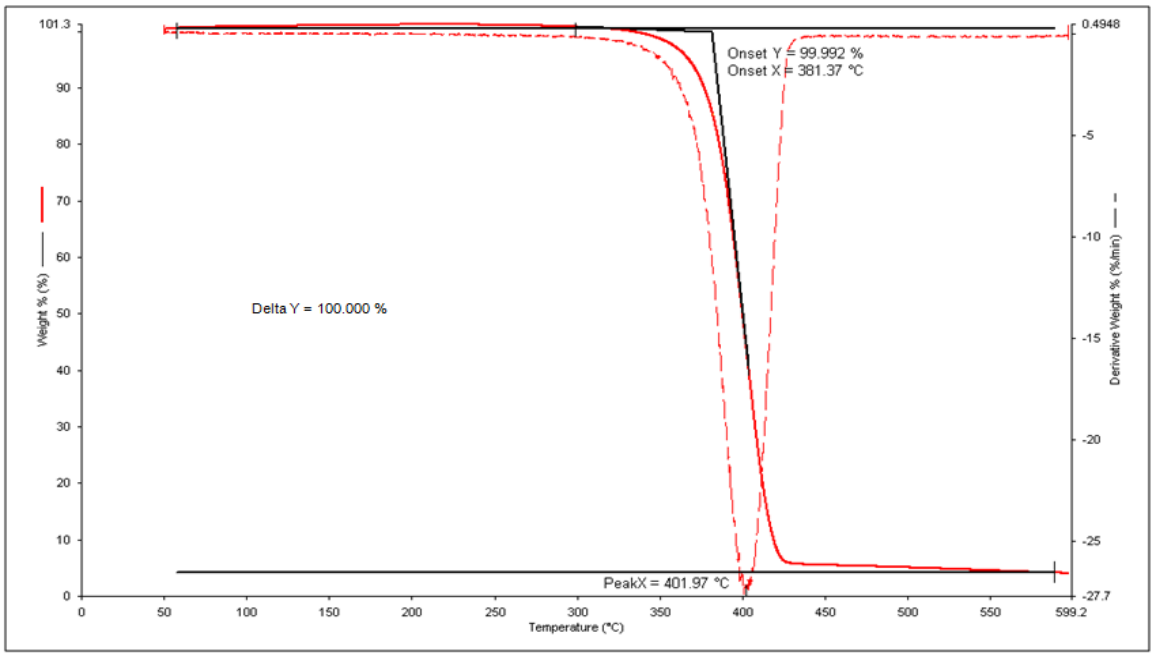

Acetic acid-modified ENR50/PEO 25/75

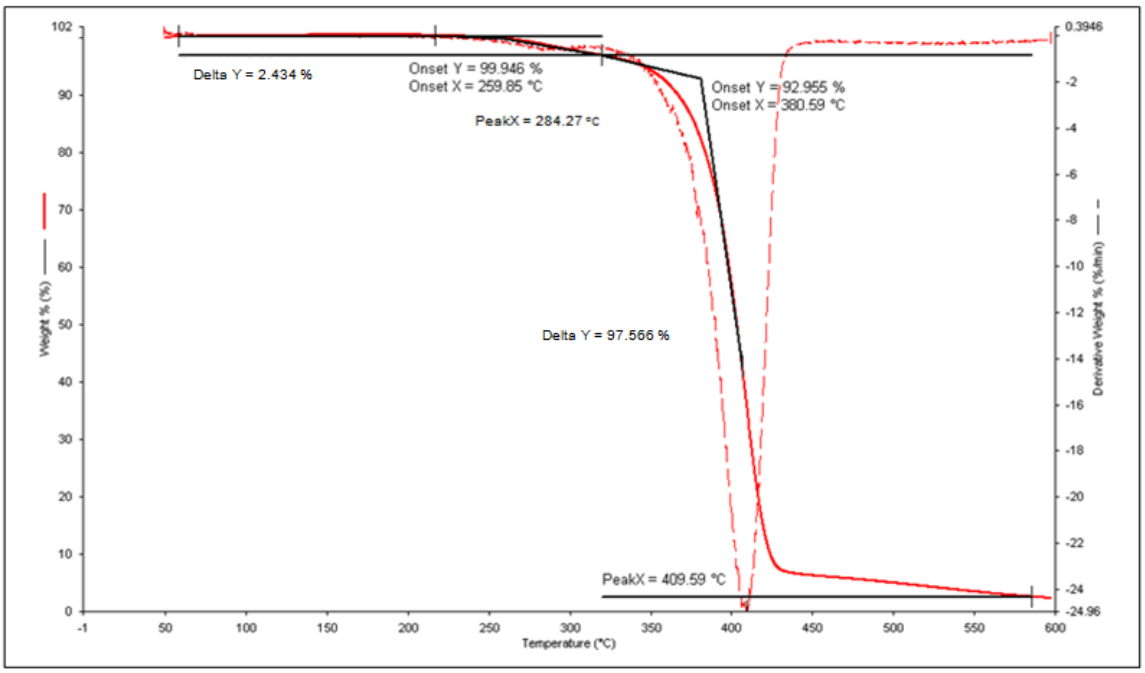

Acetic acid-modified ENR50/PEO 50/50

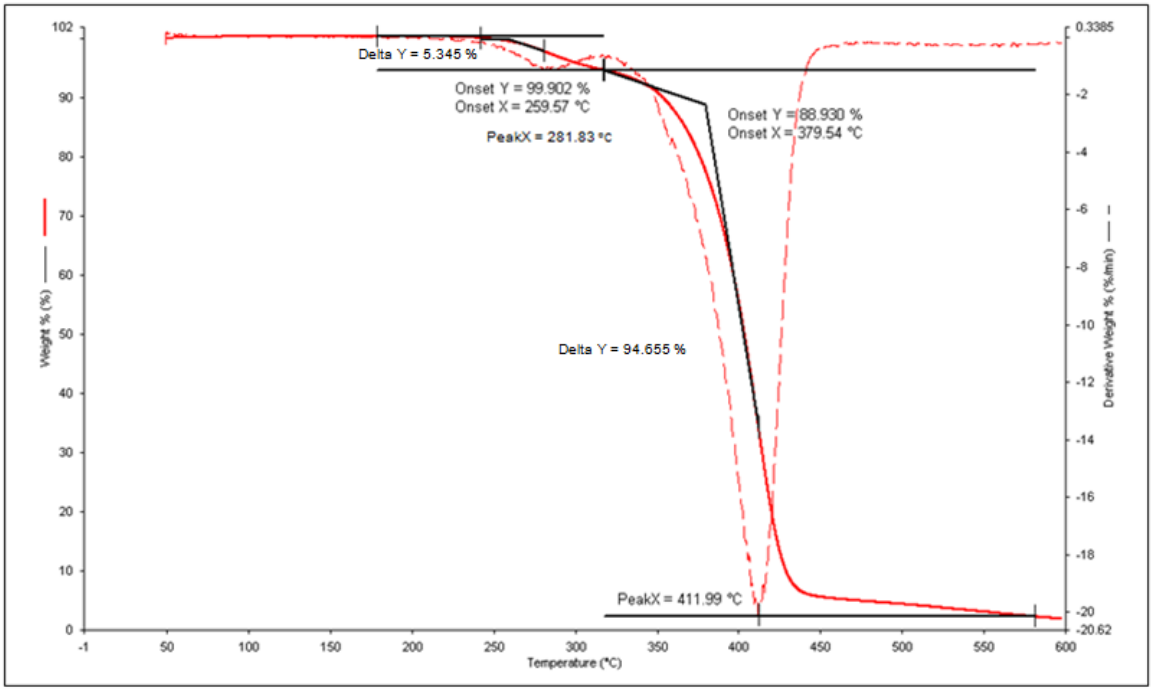

Acetic acid-modified ENR50/PEO 75/25

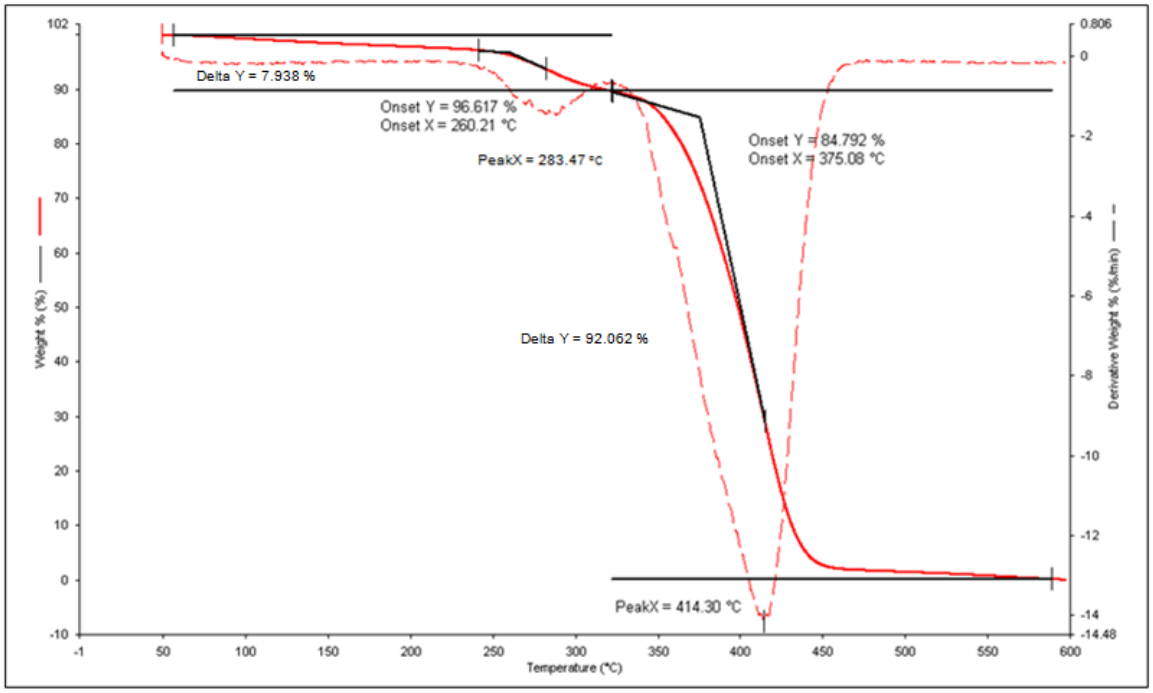

Acetic acid-modified ENR50/PEO 100/0

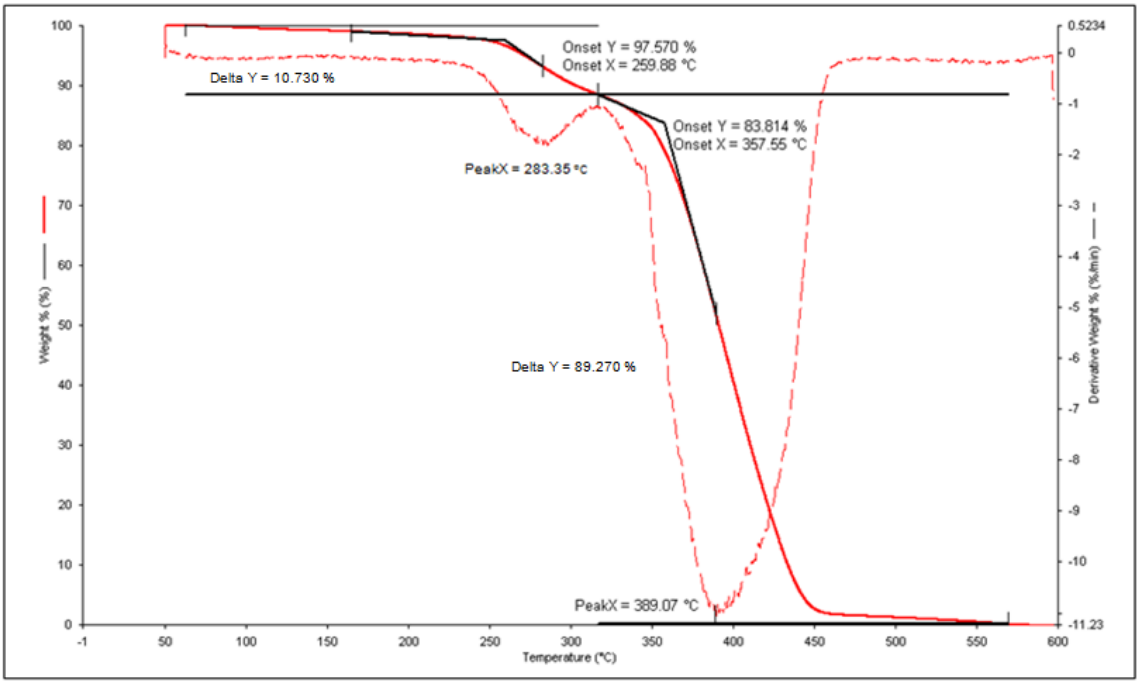

Differential scanning calorimetry

Acetic acid-modified ENR50/PEO 0/100

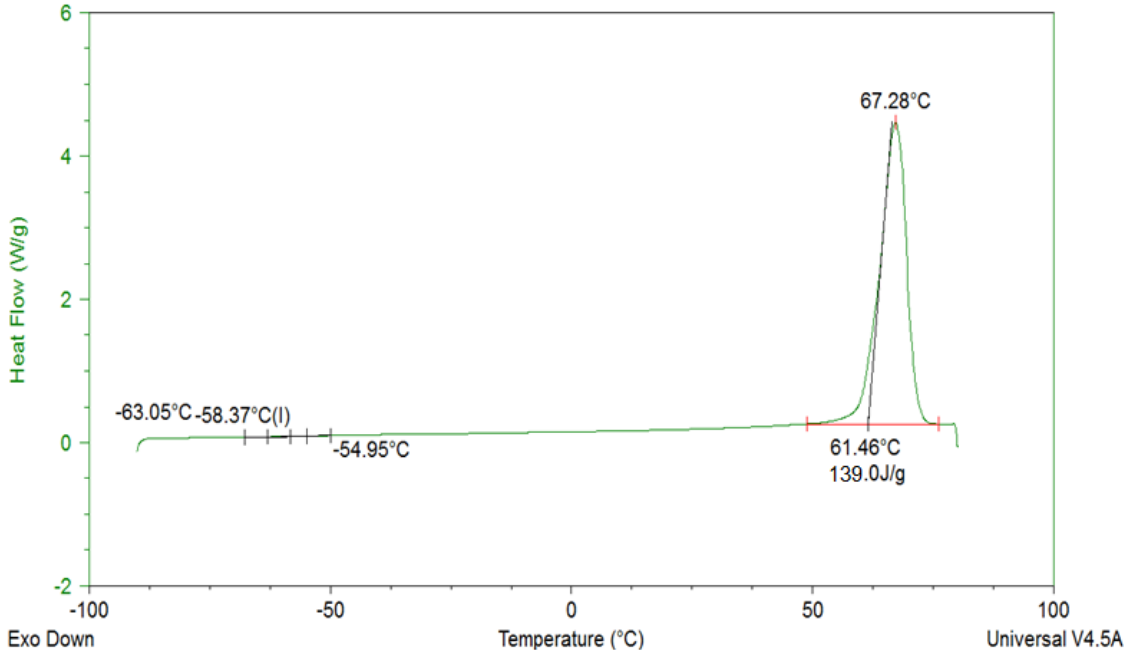

Acetic acid-modified ENR50/PEO 25/75

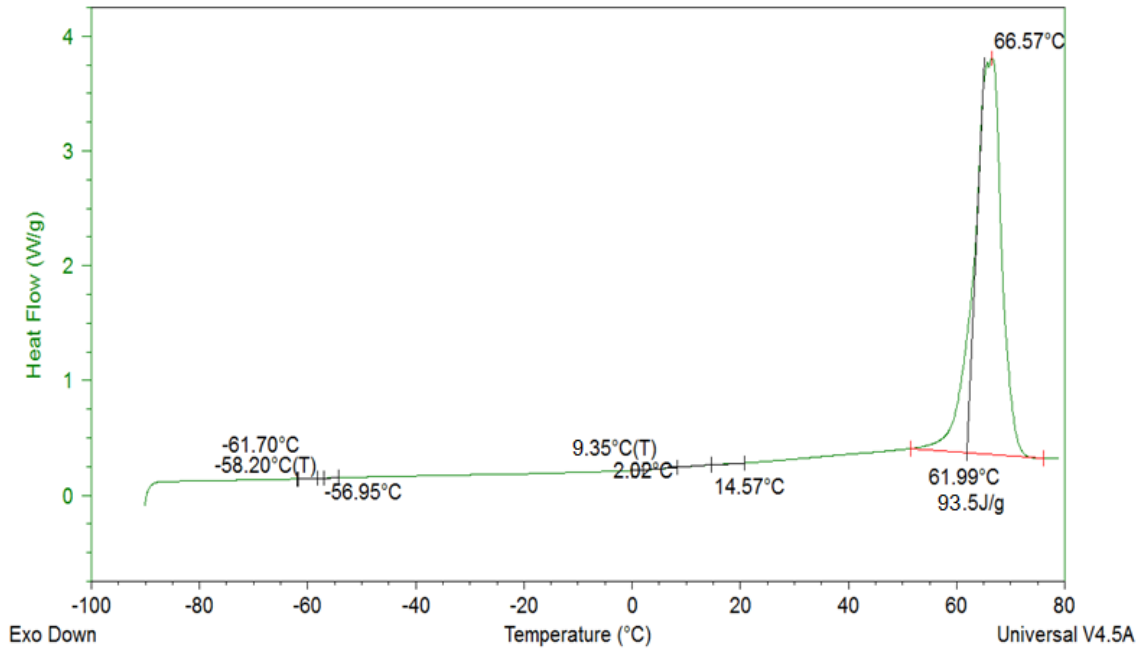

Acetic acid-modified ENR50/PEO 50/50

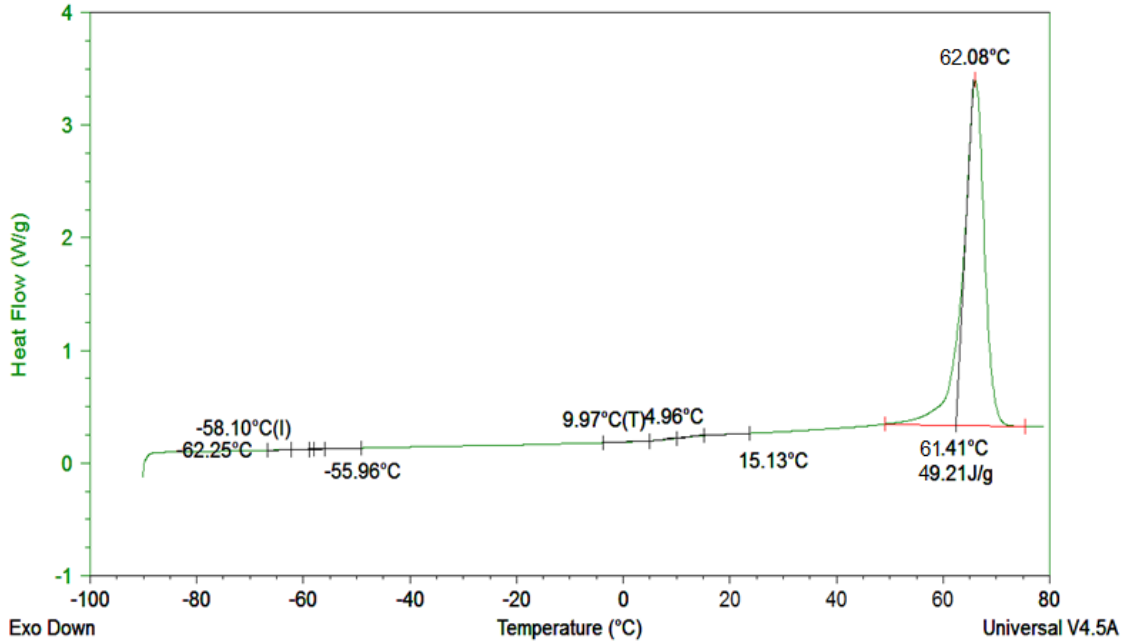

Acetic acid-modified ENR50/PEO 75/25

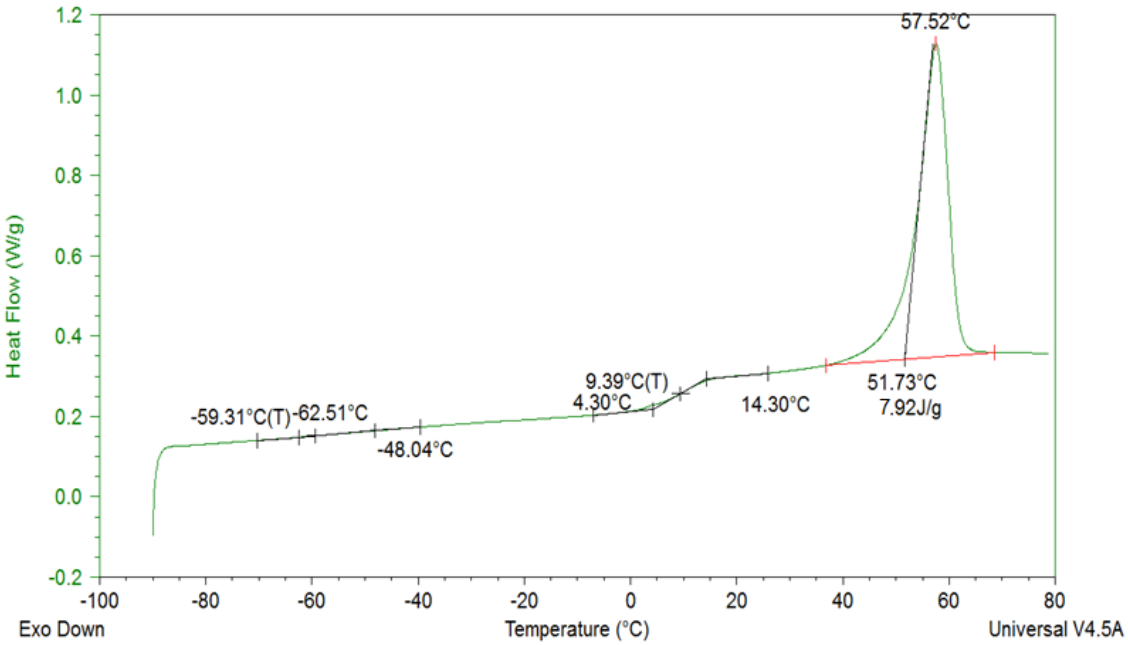

Acetic acid-modified ENR50/PEO 100/0

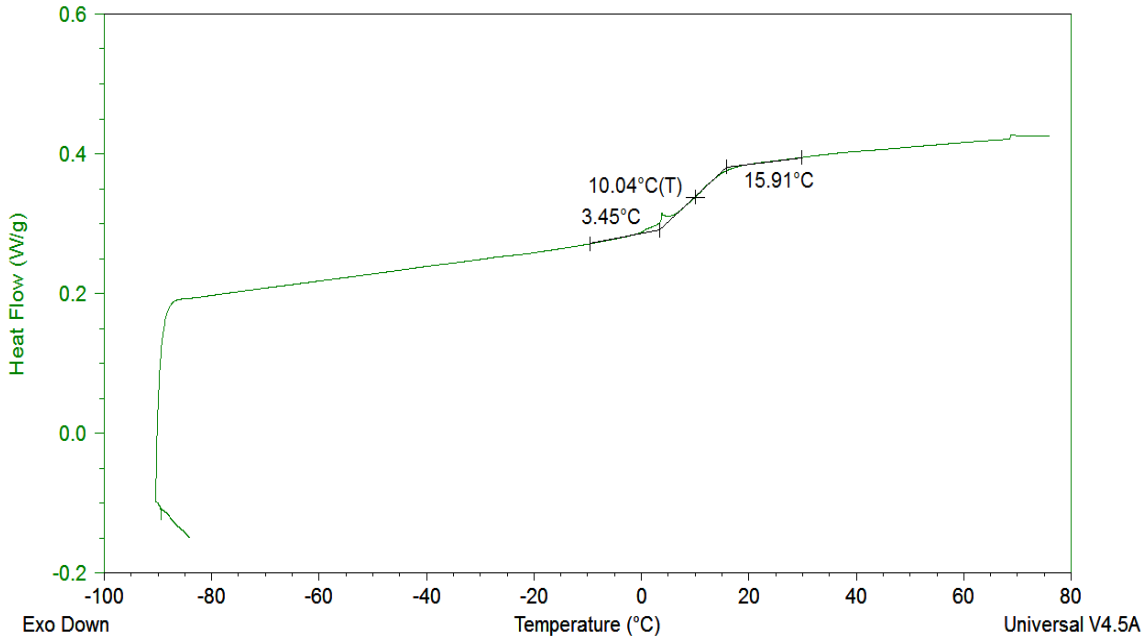

Impedance spectroscopy analysis

Conductivity, σ					
Acetic acid-modified ENR50/PEO ratio	1st Reading (S cm^{-1})	2nd Reading (S cm^{-1})	3rd Reading (S cm^{-1})	4th Reading (S cm^{-1})	Average (S cm^{-1})
25/75	3.07×10^{-8}	5.94×10^{-9}	1.50×10^{-8}	8.40×10^{-9}	1.50×10^{-8}
50/50	5.37×10^{-9}	5.66×10^{-9}	6.31×10^{-9}	8.02×10^{-9}	6.34×10^{-9}
75/25	2.51×10^{-9}	9.13×10^{-9}	3.64×10^{-9}	3.78×10^{-9}	4.77×10^{-9}
ENR50/PEO/$LiClO_4$ ratio	1st Reading (S cm^{-1})	2nd Reading (S cm^{-1})	3rd Reading (S cm^{-1})	4th Reading (S cm^{-1})	Average (S cm^{-1})
25/75/12	2.48×10^{-5}	2.64×10^{-5}	2.41×10^{-5}	2.69×10^{-5}	2.56×10^{-5}
50/50/12	1.04×10^{-6}	1.84×10^{-6}	1.51×10^{-6}	2.01×10^{-6}	1.60×10^{-6}
75/25/12	2.06×10^{-7}	2.81×10^{-7}	2.08×10^{-7}	3.18×10^{-7}	2.53×10^{-7}
Acetic acid-modified ENR50/PEO/$LiClO_4$ ratio	1st Reading (S cm^{-1})	2nd Reading (S cm^{-1})	3rd Reading (S cm^{-1})	4th Reading (S cm^{-1})	Average (S cm^{-1})
25/75/12	1.03×10^{-4}	1.04×10^{-4}	1.10×10^{-4}	1.10×10^{-4}	1.07×10^{-4}
50/50/12	3.21×10^{-5}	3.44×10^{-5}	3.59×10^{-5}	3.54×10^{-5}	3.45×10^{-5}
75/25/12	2.14×10^{-6}	2.26×10^{-6}	2.36×10^{-6}	2.52×10^{-6}	2.32×10^{-6}

CALCULATION OF RADIAL GROWTH RATE, *G* BY USING POLARIZING OPTICAL MICROSCOPE

SYSTEM: ACETIC ACID-MODIFIED ENR50/PEO BLENDS

REMARKS:

1. First picture was taken once the temperature reached at the selected crystallization temperature during the cooling process.
2. About 15 micrographs have been captured, but only about 9 pictures were chosen for measurement of radius for the spherulites.
3. Time interval for each micrograph ranged from 1-15 seconds.

Abbreviations used:

d = diameter (μm)
$\bar{d}$ = mean of diameter (μm)
s = standard deviation (μm)
R = radius (μm)
n = no. of pictures
c = correlation coefficient
s_x = standard deviation for time (μm)
s_y = standard deviation for radius (μm)
G = growth rate (μm/s)
ΔG = error of growth rate (μm/s)

EXPERIMENT: Isothermal crystallization at T_c= **49 °C** for acetic acid-modified ENR50/PEO 0/100

	TIME INTERVAL, *t* (s)														
	1	2	3	4	5	6	7	8	9	10	11	12	13	14	15
d (μm)	107.09	114.46	123.82	130.52	139.88	148.58	154.36	162.03	169.04	176.08	183.65	190.54	198.09	205.73	212.29
	101.81	105.01	109.42	113.63	117.64	121.85	125.62	129.85	133.32	137.89	141.28	145.93	149.36	152.92	157.85
	102.37	106.26	110.45	114.31	120.95	126.39	129.42	135.64	141.98	147.23	153.89	159.11	165.28	169.86	174.86
	103.64	109.55	116.55	124.10	134.89	146.46	152.28	159.20	167.74	176.16	188.06	200.82	211.67	217.17	228.84
$\bar{d}$ (μm)	103.72	108.82	115.06	120.64	128.34	135.82	140.42	146.68	153.02	159.34	166.72	174.1	181.1	186.42	193.46
s (μm)	2.37	4.22	6.63	8.14	10.73	13.66	15.00	16.30	18.10	19.75	22.76	25.84	28.76	30.08	32.76
R (μm)	51.86	54.41	57.53	60.32	64.17	67.91	70.21	73.34	76.51	79.67	83.36	87.05	90.55	93.21	96.73

CALCULATION OF RADIAL GROWTH RATE, Δ*G* (μm/s)

Graph: Plot of R (μm) vs time (s). Therefore, G is the slope for this graph where,

n =9
c =0.999
c^2 =0.998
$\sqrt{1-c^2}$ = 0.045
s_x=2.74 s
s_y =8.60 μm
$\sqrt{n-2}$ = 2.65
$\sqrt{\sum_{i=1}^{n} x_i^2}$ =16.88 s
G (μm/s) = 3.14
ΔG (μm/s) =0.13

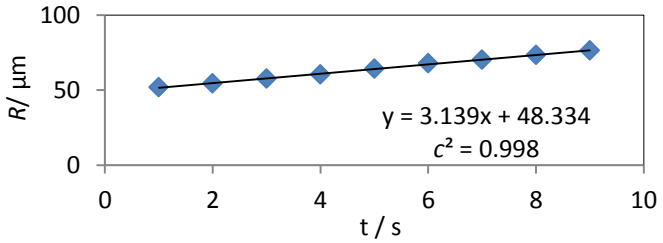

Radius of PEO growing spherulites as a function of time for acetic acid-modified ENR50/PEO 0/100 at T_c = 49 °C.

***G* = 3.1 ±0.1 μm/s**

EXPERIMENT: Isothermal crystallization at T_c = **49 °C** for acetic acid-modified ENR50/PEO 25/75

	TIME INTERVAL, *t* (s)									
	2	4	6	8	10	12	14	16	18	20
d (μm)	133.86	141.56	147.92	153.94	159.97	166.35	170.68	175.62	180.72	187.41
	112.31	114.93	121.17	124.13	130.37	132.74	137.26	141.20	146.13	147.77
	127.71	131.34	141.24	148.50	158.42	167.64	171.81	177.54	188.95	193.06
	105.94	130.94	134.23	139.49	144.86	150.68	154.63	161.21	164.29	168.45
$\bar{d}$ (μm)	119.96	129.69	136.14	141.52	148.41	154.35	158.60	163.89	170.02	174.17
s (μm)	13.02	11.00	11.44	13.03	13.81	16.34	16.24	16.79	18.94	20.51
R (μm)	59.98	64.85	68.07	70.76	74.20	77.18	79.30	81.95	85.01	87.09

CALCULATION OF RADIAL GROWTH RATE, Δ*G* (μm/s)

Graph: Plot of *R* (μm) vs time (s). Therefore, *G* is the slope for this graph

where,

n = 9

c = 0.996

c^2 = 0.992

$\sqrt{1-c^2}$ = 0.089

s_x=5.48 s

s_y =8.26 μm

$\sqrt{n-2}$=2.65

$\sqrt{\sum_{i=1}^{n} x_i^2}$=33.76 s

G (μm/s) =1.50

ΔG (μm/s) =0.12 = 0.1

***G* = 1.5 ±0.1 μm/s**

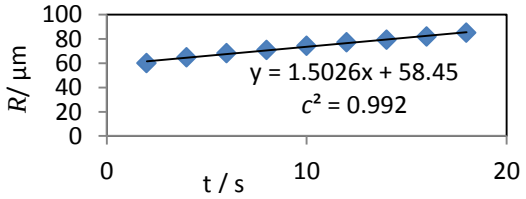

Radius of PEO growing spherulites as a function of time for acetic acid-modified ENR50/PEO 25/75 at T_c = 49 °C.

EXPERIMENT: Isothermal crystallization at T_c= **49 °C** for acetic acid-modified ENR50/PEO 50/50

	TIME INTERVAL, *t* (s)											
	15	30	45	60	75	90	105	120	135	150	165	180
d (μm)	133.23	184.56	229.27	278.26	297.78	351.06	383.91	426.53	467.21	516.58	562.44	581.29
	117.68	162.83	183.41	236.94	261.54	319.73	347.59	398.41	428.95	478.02	537.82	546.83
	128.79	184.27	216.30	270.33	295.62	346.44	372.04	425.96	461.84	502.41	557.29	571.94
	119.45	164.96	192.26	246.83	265.89	347.89	378.16	427.62	469.72	512.63	560.37	589.80
$\bar{d}$ (μm)	124.79	174.16	205.31	258.09	280.21	341.28	370.43	419.63	456.93	502.41	554.48	572.47
s (μm)	7.45	11.88	21.17	19.41	19.15	14.50	15.98	14.16	18.94	17.32	11.31	18.58
R (μm)	62.39	87.08	102.66	129.05	140.10	170.64	185.21	209.82	228.47	251.21	277.24	286.23

CALCULATION OF RADIAL GROWTH RATE, Δ*G* (μm/s)

Graph: Plot of *R* (μm) vs time (s). Therefore, *G* is the slope for this graph

where,

n = 9

c = 0.9983

c^2 = 0.9966

$\sqrt{1-c^2}$ = 0.058

s_x = 41.08 s

s_y = 56.66 μm

$\sqrt{n-2}$ = 2.65

$\sqrt{\sum_{i=1}^{n} x_i^2}$ = 253.23 s

G (μm/s) = 1.377

ΔG (μm/s) = 0.071

G = 1.38 ± 0.07 μm/s

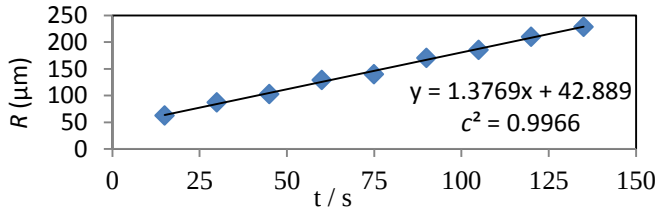

Radius of PEO growing spherulites as a function of time for acetic acid-modified ENR50/PEO 50/50 at T_c = 49 °C.